ALMA MATER STUDIORUM - UNIVERSITÀ DI BOLOGNA

FACOLTA' DI INGEGNERIA

CORSO DI LAUREA IN INGEGNERIA ENERGETICA

DIPARTIMENTO DI INGEGNERIA ELETTRICA

TESI DI LAUREA

In

TECNOLOGIE ELETTRICHE INNOVATIVE

SPACE CHARGE AND DIELECTRIC RESPONSE MEASUREMENTS TO ASSESS INSULATION AGING OF LOW-VOLTAGE CABLES USED IN NUCLEAR POWER PLANTS

CANDIDATO
Marco Bernabè

RELATORE
Dott. Ing. Davide Fabiani

CONTRORELATORE
Prof. Ing. Andrea Cavallini

CORRELATORI
Ing. Fabrizio Palmieri
Ing. Luca Verardi

Anno Accademico 2011/12

Sessione II

A thing of beauty is a joy for ever:
Its loveliness increases; it will never
Pass into nothingness; but still will keep
A bower quiet for us, and a sleep
Full of sweet dreams, and health, and quiet breathing.
Therefore, on every morrow, are we wreathing
A flowery band to bind us to the earth,
Spite of despondence, of the inhuman dearth
Of noble natures, of the gloomy days,
Of all the unhealthy and o'er-darkened ways
Made for our searching: yes, in spite of all,
Some shape of beauty moves away the pall
From our dark spirits. Such the sun, the moon,
Trees old, and young, sprouting a shady boon
For simple sheep; and such are daffodils
With the green world they live in; and clear rills
That for themselves a cooling covert make
'Gainst the hot season; the mid forest brake,
Rich with a sprinkling of fair musk-rose blooms:
And such too is the grandeur of the dooms
We have imagined for the mighty dead;
All lovely tales that we have heard or read –
An endless fountain of immortal drink,
Pouring unto us from the heaven's brink.

Nor do we merely feel these essences
For one short hour; no, even as the trees
That whisper round a temple become soon
Dear as the temple's self, so does the moon,
The passion poesy, glories infinite,
Haunt us till they become a cheering light
Unto our souls, and bound to us so fast,
That, whether there be shine, or gloom o'ercast,
They alway must be with us, or we die.

(JOHN KEATS, Endymion, 1817)

Summary

The current design life of nuclear power plant (NPP) could potentially be extended to 80 years. During this extended plant life, all safety and operationally relevant Instrumentation & Control (I&C) systems are required to meet their designed performance requirements to ensure safe and reliable operation of the NPP, both during normal operation and subsequent to design base events. This in turn requires an adequate and documented qualification and aging management program.

It is known that electrical insulation of I&C cables used in safety related circuits can degrade during their life, due to the aging effect of environmental stresses, such as temperature, radiation, vibration, etc., particularly if located in the containment area of the NPP. Thus several condition monitoring techniques are required to assess the state of the insulation. Such techniques can be used to establish a residual lifetime, based on the relationship between condition indicators and ageing stresses, hence, to support a preventive and effective maintenance program.

The object of this thesis is to investigate potential electrical aging indicators (diagnostic markers) testing various I&C cable insulations subjected to an accelerated multi-stress (thermal and radiation) aging.

After a brief introduction (Chapter 1), the state of art knowledge on degradation of polymeric cable materials is presented (Chapter 2). Chapter 3 shows the experimental setup available at DIE-LIT laboratory (University of Bologna) relevant to space charge measurements and dielectric response. Chemical composition of the samples, their accelerated aging and treatment are discussed in Chapter 4 and 5. Finally, Chapters from 6 to 9 concern experimental results on two main different kinds of cable with emphasis on possible chemical-physical explanations. The results of the electrical tests will be compared with those of the mechanical ones, thus possible correlations between them as well as aging markers will be investigated.

This work is part of the 7th framework European project ADVANCE (Ageing Diagnostics and Prognostics of low-voltage I&C cables).

Index of contents

Chapter 1

1 Introduction

1.1 Concept and objectives

Extending the lifetime of a Nuclear Power Plants (NPPs) to 60+ years is one of the most important concerns in the global nuclear industry. As electric cables are one of the long life items that have not been considered for replacement during the design life of NPPs (typically 40 years), assessing their degradation state and predicting their remaining lifetime are very critical issues. The polymers used for the insulation and jacket materials of electric cables are susceptible to aging and degradation mechanisms caused by exposure to many of the stressors encountered in nuclear power plant service environments. Therefore, premature cable aging (especially for those cables with prolonged exposure to harsh environments) could lead to unavailability of equipment important to safety or could cause plant transients and shutdowns [23].

The integrity and function of power and instrumentation and control (I&C) cables are monitored indirectly through the performance of in-service testing of safety-related systems and components. These tests can demonstrate the function of the cables under test conditions. However, they do not provide assurance that they will continue to perform successfully when they are called upon to operate fully loaded for extended periods as they would under normal

service operating conditions or under accident conditions (design basis event (DBE) conditions) [43].

Therefore, methods of monitoring cables condition have long been researched in an attempt to identify an effective technique that can be used to determine the existing cables condition, as well as predict their future performance. Condition monitoring (CM) techniques are considered an important aspect of managing cable aging. They also play an important role in the validation of the physical and chemical degradation models providing useful experimental data from the field. Related to the advance of new CM techniques is the development of acceptance criteria that can be used to make decisions regarding the acceptability of the condition of cables currently installed in nuclear plants. While a CM parameter may provide an indication of cables aging degradation, specific acceptance criteria are needed to determine if the current condition, which may include degradation from "hot spots" and localized anomalies, is acceptable for continued service. In many cases, CM parameters provide a measure of cables physical condition, such as material hardness. However, these measurements must be correlated to the cable electrical performance in order to provide useful information on the cable acceptability for continued service. Therefore, correlation of the physical properties to electrical properties is crucial.

Since large I&C cable replacements could be prohibitively expensive in terms of plant unavailability, effective in situ condition monitoring techniques together with the establishment of appropriate acceptance criteria will support utilities decision making in order to avoid unnecessary cables replacements.

An European project with duration of 36 months has been proposed. This project aims at:

- Adapting, optimizing and assessing promising electrical condition monitoring techniques for nuclear cables that are non-destructive and can be used in the field to determine the current condition of installed cables over the entire length;

- Using of condition monitoring techniques to predict remaining useful life, including the establishment of acceptance criteria and correlation of physical cables properties to electrical properties;
- Correlating condition indicators of cables near the end of life with accident (DBE) survivability;
- Investigating new cables design and formulation adapted to full-length electrical CM techniques to provide fundamental knowledge for the next generation of cables for future NPPs with improved diagnostic.

At nuclear power plants (NPPs) two basic types of thermal and radiation aging of cables are of concern: bulk (global) aging, where the degradation is distributed over the cable length, and local aging (hot spots), where a localized heat or radiation source, such as a hot pipe is close to a cable tray or conduit. Usually long cable circuits may pass through several different operating environments over the length of their routing throughout the plant.

Portions of a cable circuit may pass through areas experiencing more harsh environmental conditions, such as high temperature, high radiation, high humidity as well as increased exposure to durst, dirt and sometimes to corrosive contaminants. There has been concern that such local adverse environmental stressors can cause excessive aging and degradation in the exposed sections of a cable that could significantly shorten its effective service life and cause unexpected early failures [23].

To simulate global and local ageing, accelerated cable ageing (thermal and irradiation) will be performed in order to quantify the ability of electrical in-situ CM techniques of being able to detect various degrees of local and bulk degradation. Accelerated ageing will be performed on a representative selection of cables already installed in NPP. The objective is to measure and correlate the values of condition indicators given by promising electrical in-situ CM techniques to those obtained with other more conventional, mechanical for instance, CM methods. Moreover, to understand and correlate the evolution of electrical properties with the physical/chemical degradation mechanisms of polymers for different kinds of cable materials and composition and to

establish appropriate acceptance criteria. The electrical properties of cables insulators will be monitored and characterized mainly by dielectric spectroscopy, polarization/depolarization current analysis, space charge distribution.

The aim of these investigations is to provide the base knowledge for the next generation of cables with improved diagnostic capability. Since many reactors will be constructed in the near future, the availability and the use of cables with improved diagnostic capability will allow a very effective condition monitoring thus making this initial cable choice very valuable at a later time.

1.2 Cable aging, diagnostic properties and CM methods

Thermal stress and irradiation will both cause oxidation and chain scission in polymers. Both chain scission and oxidation will give rise to new chemical species and free radicals, affecting the dielectric response of the material.

Furthermore, both physical and chemical trapping sites will be created at the surface and in the bulk of the insulation system. Whenever these phenomena are spread over a significant fraction of the cable, they will give rise to changes in the dielectric response of the complete cable as well as to the presence of space charge. At the latest stages of aging, cracks use to appear.

The most useful CM method would provide information on those diagnostic properties that can be used to determine the current ability of a cable system to perform within specified acceptance criteria, as well as to make predictions about its future functional performance and accident survivability. To predict future performance, it is desirable to have a trendable indicator and a well-defined end point. A trend curve can then be used to estimate the time remaining before the end point is reached.

Aging characterization methods have concentrated especially on mechanical and chemical properties, that are mainly assessed in laboratory (not in-situ). The impact of multi-stress ageing (thermal and radiation stress mainly) on low voltage cable insulations used in nuclear power plants has been investigated

widely in the past, particularly resorting to measurements of chemical/physical and mechanical properties in general.

However, literature regarding the effect of aging on electrical properties of low voltage insulation is still lacking. Most of the diagnostic tools and dielectric characterization techniques have been developed and optimized for HV and MV cables. The main difficulty is to interpret the results of the measurements and to make a correlation with the degree of cable aging. The long-term relation between physical/chemical degradation mechanisms and the electrical properties variations have not been studied in detail for LV cable materials.

In order to interpret the electric CM techniques measurements and to define appropriate acceptance criteria (endpoints), the approach that will be used in this work will consist in applying (and adapting) those non-destructive diagnostic techniques on different kinds of cable materials:

- Pulsed Electro Acoustic (PEA) technique for space charge assessment, estimating the amount of traps created and their depth distribution (affecting mobility of carriers within the dielectric);
- wide-frequency dielectric spectroscopy by dielectric analyzer tool;
- low-frequency dielectric spectroscopy by polarization/depolarization current measurements (in the time and frequency domain).

These techniques have been developed mainly for HV and MV. The assumption is that the effect of radiation and thermal stresses could be revealed by the aforesaid techniques, independently of the voltage level applied to the insulation.

An investigation about the possibility of separating the effects of thermal aging and cumulative dose will be conducted. Then, strategies to combine the results from PEA analyses with those concerning dielectric response will be carried out.

A connection between these electrical measurements and polymer changes will be established through chemical-physical analyses and mechanical analyses to understand how diagnostic markers are influenced by the amount of internal

polymer degradation[1]. This will form the basis to define critical values of the diagnostic markers, beyond which operation of the cable is still possible but not advisable. It could also help understanding the time behavior of diagnostic markers as a function of the extent of degradation during time.

In the next steps of the project the results obtained on these cables artificially aged in laboratory will then be compared to those from naturally aged cables in nuclear power plants. The same type of cables types and materials will be preferred. These measurements will be performed with the electrical CM techniques that have shown the best performances for local and global ageing detection. Field tests could verify the presence of cable local and global degradation and, thanks to the comparison with laboratory tests, assess the degree of degradation and estimate the remaining lifetime. Field test will also verify aging models obtained from the ageing simulation experiments. Furthermore, this chemical-physical analyses will provide insights on the effect of aging on the ability of cables to resist fire propagation.

Besides the study of old cable already installed in NPPs, investigations will be carried out on future cables design and formulation to provide fundamental knowledge for the next generation of cables for future NPPs with improved diagnostic capability. Two fundamental research approaches exist for future cables. The first one consists in making cables that last longer, while the second one consists in making cables that are easy to diagnose, enhance the answer to the cable monitoring solicitation in order to get a better follow-up of the aging. These two approaches are complementary. The idea is to have a cable that has a predictable and measurable ageing-dependent electrical response when tested with electrical CM techniques. Electrical CM techniques have the advantage of allowing a quick and full-length cable assessment from one location and of being able to localize mismatches of electrical parameters.

[1] Today the most used reference indicator to assess the degradation state of the polymer insulation is the elongation-at-break (EaB). Although currently there is no standardized acceptance criterion for the minimum EaB for a cable material that will define the end of its useful service life for normal, mild or harsh environments, a conservative value of ≥50 percent has usually been used as an acceptance criterion. This mechanical CM technique has the main disadvantage of being destructive and of requiring relatively large amounts of cable for the tests, thus making it inadequate for in-situ CM [43].

Therefore having cables supporting safety critical functions that are easy to diagnose and whose remaining lifetime is easy to predict will allow a very effective condition monitoring in future plants. To our knowledge, this second approach has never been explored for low-voltage cables.

Chapter 2

2 Theoretical background

This chapter focuses on the sources of polymer degradation (i.e. temperature, radiation, oxidation, moisture content) and deals with effects of these elements on the cables materials representing the state of art of knowledge about these phenomena.

2.1 Degradation of polymeric cable materials in Nuclear Power Plant

The environmental service conditions in a NPP will induce chemical and/or physical changes to polymeric materials, which may cause changes/degradation in the functional characteristics of cable. Materials evolve with time because they are not in a stable thermodynamic state. For electrical cable, the most relevant components that will suffer significant degradation are the polymeric insulation and jacket materials. Each manufacturer use its own formulation for fillers, stabilizers and additives, therefore cables from different manufacturers can show significant variation of behavior during aging.

The degradation of the polymer chains is the most important mechanical aging mechanism because it has a direct influence on the service behavior of the material. Such phenomena are:

- Scission of macromolecular chains: the breaking of one chain creates two new ones. It is often the result of the scission of alkoxyl or

peroxide groups. The effect is usually a mechanical weakening of the polymer.

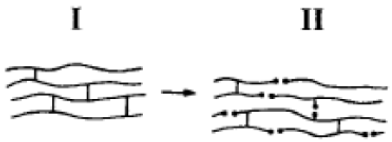

- Cross-linking reaction: it is the formation of a covalent bonding between two adjacent chains. With the increase of the density of those bonds, the material's stiffness usually increases too, as consequence of the formation of a three-dimensional network. Prolonged cross-linking causes embrittlement.

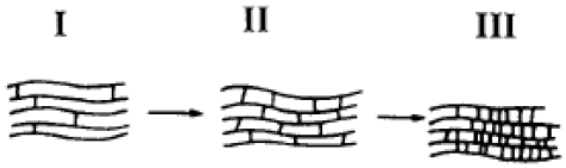

- Change of side groups: the cyclisation and change of side groups lead to instauration and gas evolution.

The predominance of these phenomena is linked to the position of the bonding rupture on the polymer chain. The mechanical degradation of the polymer chains has a direct impact on the integrity of the dielectric and can lead to its physical breakdown.

There is a number of aging stressors which are important in the degradation that occurs in NPPs. These are briefly discussed below.

2.1.1 Effect of temperature

Polymers in NPP are mostly degraded by thermal oxidation in the presence of oxygen, as a result of chain scission or cross-linking among chains and the accumulation of oxidative products. For some polymer materials, the migration of additives and plasticizers can also be significant. Besides natural thermal aging, caused by ambient room temperature which leads to a slow degradation of organic materials, a local high temperature (hot spot) can quickly cause an

important damage. In this work, we no longer speak about hot spots and, dealing with I&C low voltage cables, we will not even speak about Joule's effect induced by high current density (self-heating).

As said above the rate of degradation is accelerated by an increase in temperature. For accelerated thermal ageing, the relation between the rate constant for degradation (k) and aging temperature (T) is determined by the hypothesis of Arrhenius equation (Eq. 2.1).

$$k = A\mathrm{e}^{\left(-\frac{E_A}{RT}\right)} \tag{2.1}$$

where E_A is the activation energy, A is the frequency factor, and R is the gas constant. As a rough approximation, the degradation rate will increase by approximately 2 times for a 10°C rise in temperature, for the values of activation energy that have typically been used in the past for cable materials. The kinetics of thermal degradation depends on several factors like the nature of the material, the intensity of the heating, the distance to the source, the presence of heat protections (shielding, ventilation).

The degradation rates obtained at different elevated temperature are plotted using the Arrhenius equation and extrapolated to a lower temperature to predict the lifetime in service. The main problem with this application of the Arrhenius theory is that the activation energy of degradation can change over the temperature frame and over the composition of the insulating material (e.g. it cannot be applied across a physical transition of the material, it cannot be applied if the same reaction doesn't occur at the higher temperature as occurs at the service temperature or even if the degradation mechanism changes). Knowledge of the cable service temperature and of the properties of the materials used to make the cable is fundamental. If measured values of E_A at these temperatures are not available, it is recommended that a value of 63 kJ/mol is used for temperatures below 100 ºC.

However, the inaccuracy inherent to the application of the Arrhenius formula increases with the increase of the aging rate.

A logarithmic plot of this equation versus 1/T gives a straight line with a slope corresponding to the activation energy (Figure 2.1).

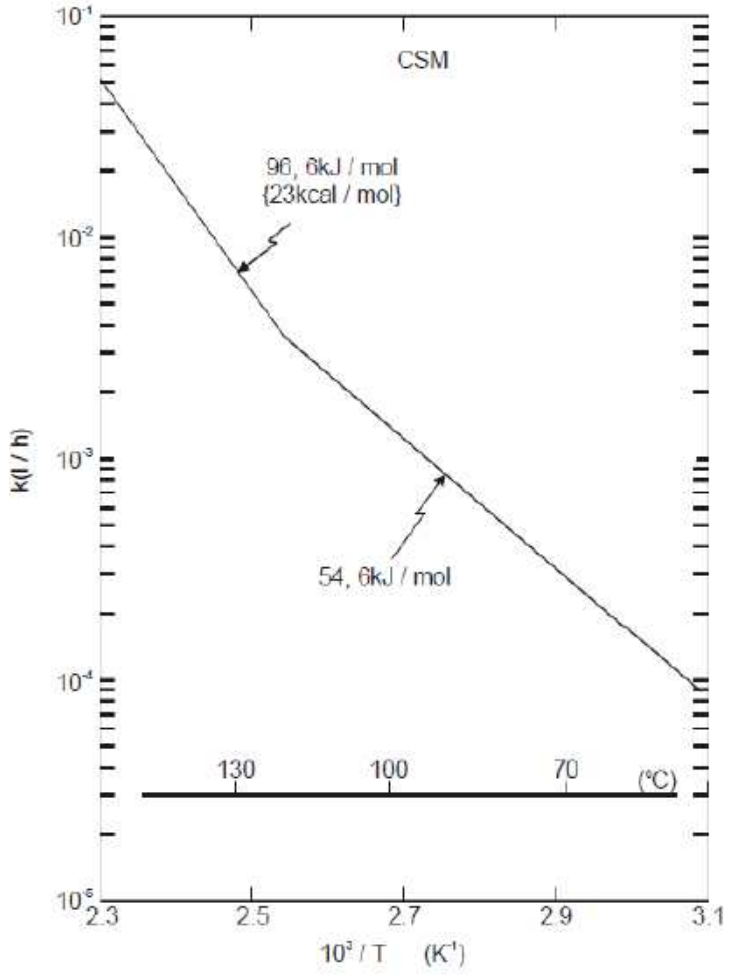

Figure 2.1 Example of Arrhenius plot for thermal degradation rate for CSPE. [23]

2.1.2 Effect of radiation

Gamma and neutron radiation are the most significant stressor for cable service life during normal operation of a NPP, especially in the presence of oxygen. During accident, beta radiation may also play an important role if the cable is not protected by a conduit, so environmental conditions are fundamental. The effect of radiation degradation consists mainly of oxidative degradation. In general, the cable properties degrade with increasing absorbed dose but many polymers are also sensitive to the radiation dose rate. The rate of degradation can be a very complicated function of absorbed dose and is usually non-linear.

The polymers are more sensitive to ionizing radiation than metals and ceramics because of the nature of the bonding. Common polymers are made of long

hydrogenated carbon chains and, in many polymers, some of the side hydrogen atoms are substituted by groups. When subjected to ionizing radiation, ions can be created in the bulk of the material and, when a free electron is captured, the de-excitation of the specie generates chemical radicals. They can be of variable reactivity, and reactions may propagate along the chain or to a side chain. Otherwise, mobile electrons can be induced by the radiation and be trapped in sites of low potential energy. This leads to temporary changes in the electrical performances. The production of free radicals under irradiation can result in chain scission or cross-linking processes that cause an irreversible evolution of the mechanical, chemical and electrical properties of the material. For example, a change of dissipation factor or permittivity can modify the behavior of resonant circuits and deteriorate his reliable functioning. There may also be post-irradiation evolution of the material because free radicals can decay slowly. Most of the protection additives for the material against radiation focuses on the trapping of the free radicals through the use of antioxidant molecules. Another family of stabilizers works on the deactivation of excited sites. By eliminating the number of excited sites, they also decrease the kinetics of the formation of free radicals.

Note that dose rate effects can be important factors in the degradation of cables in NPP. In several polymer materials, the dose required to reach a certain level of degradation (DED[2]) is significantly lower when the dose rate applied is low. For irradiation in vacuum or inert gas environments, it is usually assumed that there is no dose rate effect of the properties changes of the polymers. If the rate of energy absorption is greater than the rate of dissipation, this will no more be true because there will be a significant heating of the material. This increase of temperature will accelerate the chemical reactions but also modify the mobility of the polymer chains and thus increase the physical mechanisms like diffusion (especially near the glass transition temperature). Consider that during irradiation of polymers, different gases can evolve from the material.

[2] DED is the radiation dose required to reach a specific level of degradation, e.g. an elongation at break of 100% absolute

2.1.3 Combined effect of temperature and irradiation

Temperature and radiation have synergistic effects [2][3]. Depending on the conditions, there will be a predominant degradation process which will predict the behaviour of the material. A predominance chart showing the dominant process in function of the dose rate and the temperature can be used (Figure 2.2):

- Zone I : Thermooxydation controlled by oxygen diffusion
- Zone II : Thermooxydation non-controlled by oxygen diffusion
- Zone III : Radiooxydation non-controlled by oxygen diffusion
- Zone IV : Radiooxydation controlled by oxygen diffusion
- Curve B : Limit between thermooxydation and radiooxydation
- Curve C : Limit between oxygen controlled and non-controlled radiooxydation

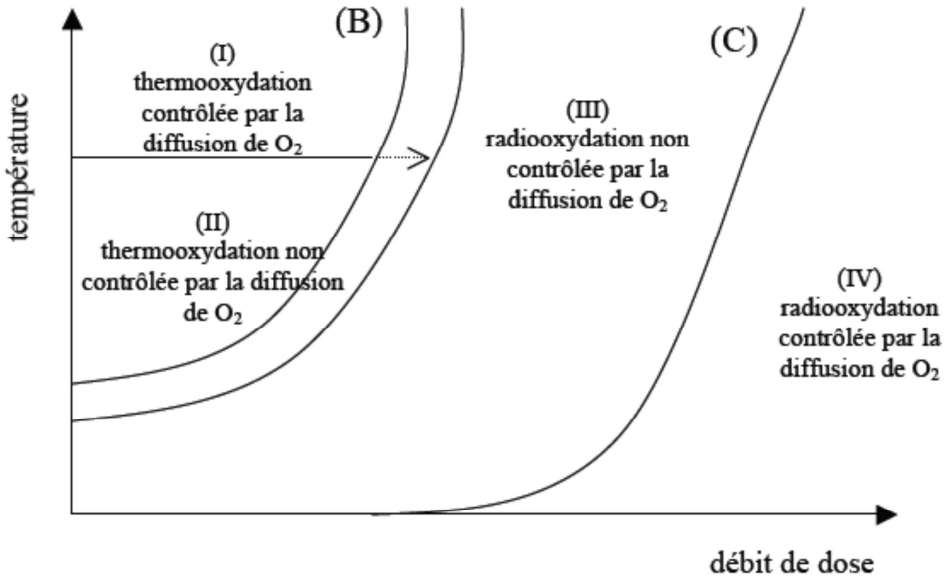

Figure 2.2 Predominance diagram for the mechanism of degradation.[2]

Using this kind of chart, it is possible to predict a critical limit value for the irradiation dose rate after which the oxidation of the polymer is no more homogeneous due to oxygen diffusion, in that case oxidation will occur at the surface of the polymer and cross-linking at the centre.

2.1.4 Effect of oxygen concentration

Oxidation in the presence of air is often the main degradation mechanism [21]. The initiation of this phenomenon can either be temperature or radiation but the combination of both is synergistic. Two distinct processes must be taken into account to study the evolution of the material properties affected by oxygen-caused degradation.

- The creation of the free radical chain reaction underlying the oxidation
- The oxygen diffusion effects

Concerning the oxygen diffusion, this effect is controlled by the permeation coefficient of the polymer and the material thickness. Oxygen diffusion can become rate determinant if the oxygen present in the material bulk is consumed by reaction with free radicals (generated by the irradiation) faster than oxygen can be replaced from the atmosphere by diffusion. If this effect is important, the degradation of the material becomes heterogeneous: high oxidation takes place at the surface of the cable and less oxidation (or no oxidation) occurs in the bulk. At lower irradiation rates, the oxygen has more time to diffuse through the material and the oxidized zone is deeper. This phenomenon is the major explanation of the dose rate sensitivity of polymers showing larger damage for a given absorbed dose if the irradiation rate is low.

An estimate of the sample thickness L at which diffusion limited oxidation is insignificant can be made using the following equation:

$$L \propto 2\left(\frac{p \cdot P_{ox}}{\varphi}\right)^{0.5} \tag{2.2}$$

where p is the partial pressure of oxygen surrounding the sample, P_{ox} is the oxygen permeation rate and φ is the oxygen consumption rate in the material [32]. The consumption rate and the permeability will also be functions of temperature and/or radiation dose rate. It is of most concern when carrying out accelerated testing on thick samples, e.g. whole cables, for both thermal and radiation ageing. If this condition is satisfied, then the integrated oxidation through the thickness will be at least 95% of the homogeneous value.

The use of antioxidants is widely common in cable manufacturing. It has been proved that antioxidants provide significant radiation stability. It has also been shown that antioxidants which are effective for thermal stability are effective for radiation stability too. The protection of antioxidant is not linear, even if the stabilization against radiation ageing increases at large doses as the amount of antioxidant is increased. Studies have shown that a minimum concentration in antioxidant is required to have a significant protection of the material. On the other hand, an excess content of antioxidant does not contribute to reducing more the degradation rate. We must remember that if the ageing temperature is higher than a specific threshold, the antioxidant can evaporate from the polymer matrix resulting in a decrease of the concentration and an accelerated degradation.

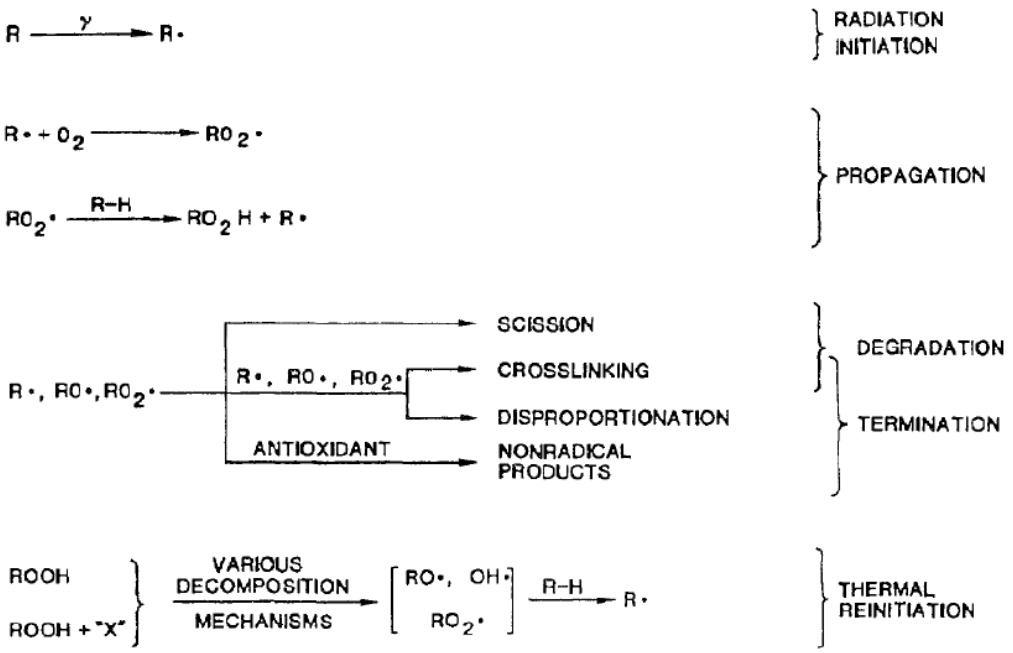

Figure 2.3 Different steps in oxidation. [22]

2.1.5 Other effects

There are several other sources of degradation occurring in NPPs environment. Moisture, for example, is another stressor for polymer materials. In some configurations, electric cables can be exposed to high humidity that can penetrates the cable jacket or the wires insulation and modify not only the mechanical properties but also the electric ones; a possible degradation mechanism is the ageing due to water trees. Electrical stress, mechanical stress (including vibration), ozone attack or chemical contamination must also be taken into account. Finally, post-irradiation degradation can occur due to the gradual decay of various reactants like remaining radicals.

Table 2-1 lists the parameters involved, the degradation mechanisms generated by aging and their effects on cable insulations.

Table 2-1 Ageing mechanisms of cable insulation.

Possible ageing mechanisms of cable insulation system		
Ageing factor	**Ageing mechanisms**	**Effects**
Thermal		
High temperature Temperature cycling	- Chemical reaction - Incompatibility of materials - Thermal expansion - Diffusion - Anneal locked-in mechanical stresses - Melting/flow of insulation	- Hardening, softening, loss of mechanical strength, embrittlement - Increased tanδ Shrinkage, loss of adhesion, separation, delamination at interfaces - Swelling - Loss of liquids, gases - Conductor penetration - Rotation of cable - Formation of soft spots, wrinkles - Increased migration of components
Low temperature	- Cracking - Thermal contraction	- Shrinkage, loss of adhesion, separation, delamination at interfaces - Loss/ingress of liquids, gases - Movement of joints, termination
Electrical		
Voltage, ac, dc, impulse	- Partial discharges (PD) - Electrical treeing (ET) - Water treeing (WT) - Dielectric losses and capacitance - Charge injection - Intrinsic breakdown	- Erosion of insulation, ET - PD - Increased losses and ET - Increased temperature, thermal ageing, thermal runaway - Immediate failure
Current	- Overheating	- Increased temperature, thermal ageing, thermal runaway
Mechanical		
Tensile, compressive, shear stresses, fatigue, cyclic bending, vibration	- Yielding of materials - Cracking - Rupture	- Mechanical rupture - Loss of adhesion, separation, delamination at interfaces - Loss/ingress of liquids, gases
Environmental		
Water/humidity Liquids/gases Contamination	- Dielectric losses and capacitance - Electrical tracking - Water treeing - Corrosion	- Increased temperature, thermal ageing, thermal runaway - Increased losses and ET - Flashover
Radiation	-Increase chemical reaction rate	Hardening, softening, loss of mechanical strength, embrittlement

Chapter 3

3 Experimental setup and procedure

This chapter concerns CM tools supplied at DIE-LIT laboratory (University of Bologna) relating space charge measurements and dielectric response.
CM techniques have the aim of evaluating the condition of the different samples during the aging testing process.

3.1 Pulse Electroacoustic Method (PEA)

The PEA method is a non-destructive technique for profiling space charge accumulation in polymeric materials [31]. A sequence of high-voltage pulses of very short time length (5-30 ns) at repetition frequencies in the range 0.050-10 kHz is applied to the insulation specimen subjected to a DC field. Each pulse produces an electric force displacing internal charges and generating pulsed acoustic pressure waves in correspondence of each charge layer in excess with respect to neutrality. The resultant pressure pulse is detected by a piezoelectric transducer, where the acoustic signal waves are transformed to electrical signals, so that the charge distribution in the specimen under test can be obtained from the output voltage of the transducer. The output signal is amplified and visualized by a digital oscilloscope.

The analysis of space-charge profiles is restricted to one dimension: this assumption imposes to consider that space charge density, electric field distribution and acoustic wave propagation can vary only along the specimen thickness (z-coordinate).

3.1.1 Experimental setup

Two PEA cell systems are available at UNIBO: one designed for cables and another one designed for flat specimens, i.e. peelings from cable sheaths.
The operating principle is obviously the same. In this paragraph we will describe the experimental setup for the cable system.

A complete PEA Cable system (Figure 3.1) is composed by:

- a high voltage DC generator
- a voltage pulse generator
- the PEA cell
- a digital oscilloscope
- a personal computer
- a GPIB card to interface computer and oscilloscope.

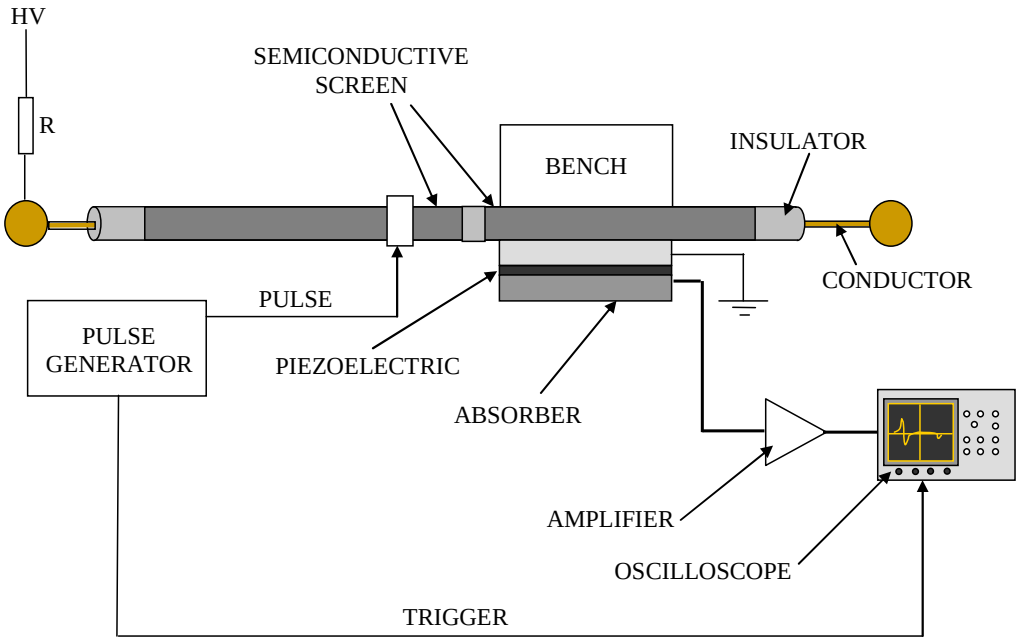

Figure 3.1 Scheme of a complete PEA Cable system.

The pulse is directly connected to the semiconductive screen, in this case the cable itself is used like decoupling capacitor. The trigger signal for the oscilloscope is directly provided by the pulse generator unit. At the back of the piezoelectric transducer, an absorber is present to eliminate reflections of the acoustic waves. The electrode has also the function of delaying the acoustic wave until its arrival at the piezoelectric sensor. The delay is necessary due to the interference of the electromagnetic noise caused by the firing of the electrical pulse.

When performing the measurements, a thin layer of silicon oil is used as acoustic coupling between the sample and the electrodes.

The setup can operate at temperature between 15°C and 40°C and at atmospheric pressure, max applicable voltage is limited only by the Electric Strength of the cable. Spatial resolution Δz for samples is about 40 µm and sensibility with respect to inner charge is 0.1 C/m^3. Sensitivity is established on basis of the noise in the output signal.

The equivalent circuit is reported in Figure 3.2.

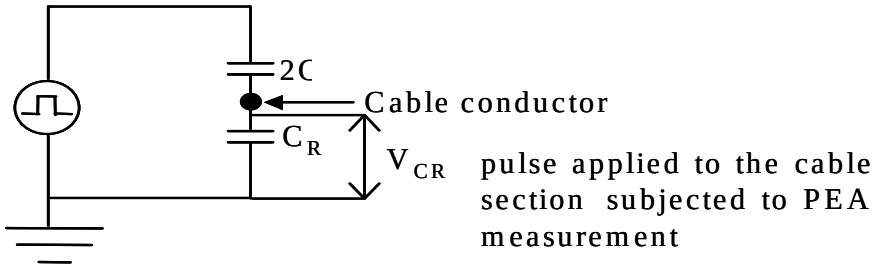

Figure 3.2 Equivalent circuit of PEA Cable system.

3.1.2 Acquisition software and signal processing

The acquisition program, Labview based, can acquire, at prefixed times, the signal acquired by the oscilloscope. This is obtained through files .dat which contain the value of voltage corresponding to each point recorded by the scope. Moreover a file fin.dat, where the information about the test condition and the

specimen are reported, is created; this file is needed to use by the processing software.

An example of the response from the preamplifier of a flat specimen sample without internal space charge subjected to HVDC is presented in Figure 3.3.

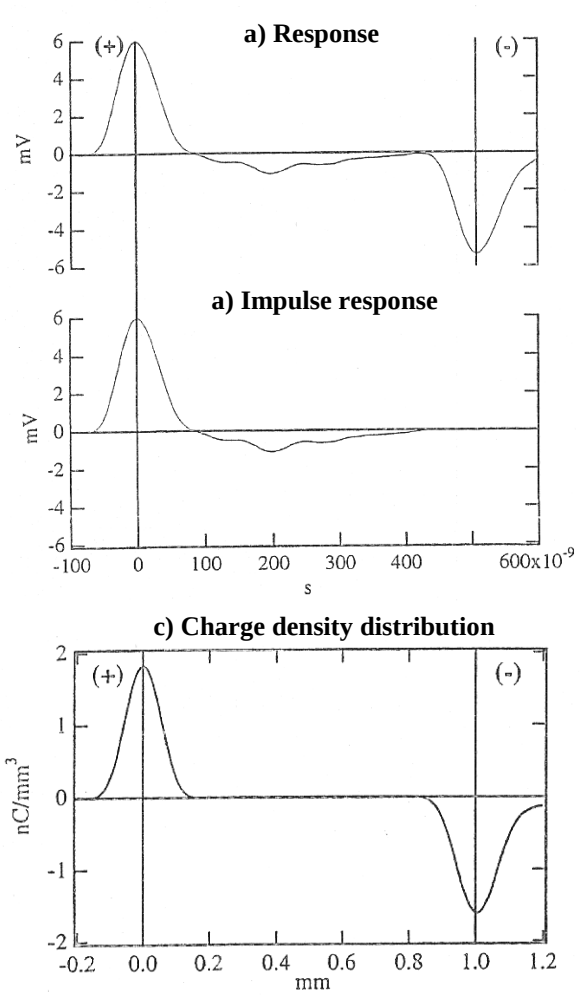

Figure 3.3 a) response from the preamplifier of a flat specimen sample without internal space charge; b) impulse response of the pulse-transducer system; c) deconvolved and calibrated charge density distribution for a flat specimen sample without internal space charge.

With the response from the measuring subtracted, the voltage peaks in the figure are due to induced charge on the electrodes. As there is no space charge in the sample yet, there should be no signal from the middle region of the sample. There is, however, due to the response of the pulse-transducer system. So the impulse response of the measuring system must be established and this

is done by calibration. The actual charge profile is obtained by deconvolving the obtained response with the impulse response. This is done by converting the waves into the frequency domain by use a FFT (Fast Fourier Transform). Note that the high frequency noise is magnified by the deconvolution process, thus a filter is used. The deconvolved response containing the information about the charge distribution is then converted back by Inverse FFT. Let's spend some word about calibration: with no internal space charge and with the impulse response subtracted, the induced charge on the electrodes is given by:

$$\sigma_s = \varepsilon E = \varepsilon \frac{V}{d} \tag{3.1}$$

Where E and V are the applied DC electrical field and voltage, respectively, and d is the thickness of the sample. The obtained value is used to calibrate the deconvolved charge distribution, making it possible to plot the charge profile in real units of charge density, C/m^3. A charge distribution is proportional to $v_s \Delta t_s$, where v_s is the acoustic wave velocity and Δt_s is the sampling interval. Thus, calibration is obtained by multiplying the output from the deconvolution by the constant:

$$k = \frac{\sigma_s}{v_s \Delta t_s} \tag{3.2}$$

The scale factor is determined for each sample and account for all the parameters.

3.1.3 Measured quantities and aging markers

Systems for space charge measurements are able to provide profiles of charge (see Figure 3.4) and electric field gradient, under applied field, at any poling time.

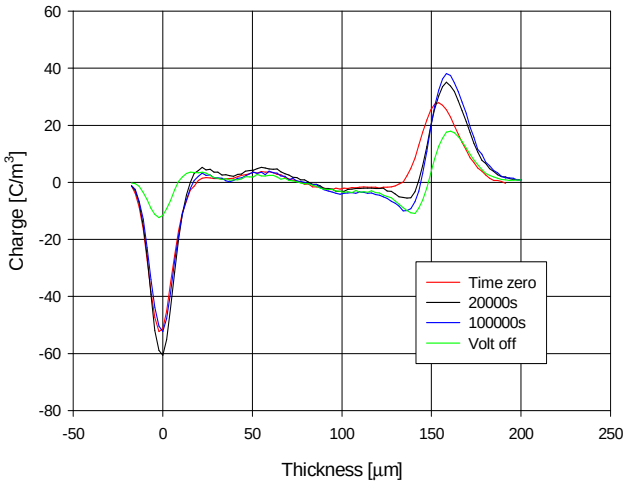

Figure 3.4 Examples of space charge profiles recorded during space charge measurements.

Space charge measurements often are carried out according to a polarization/depolarization procedure. The polarization-depolarization procedure generally carried out for the measurement of space charges by the PEA method consists of the application of a poling field, E_P (Laplace field), for a given time, t_P, followed by depolarization for a subsequent time t_D. Depolarization is realized removing voltage and grounding both electrodes. The volume density of space charge at every position x, between the electrodes ($x_0 < x < x_L$, L being insulation thickness), is measured for the whole time $t \in (t_P + t_D)$, thus yielding the space charge profiles, $q(x,t;E_P)$. When depolarization starts (i.e., poling voltage is removed and electrodes short-circuited), charge within the insulation decreases with time due to both depletion from the insulation (resulting in a current that flows in the external circuit) and recombination. Under the assumption that recombination can be neglected, charge leaves the specimen, once the depolarization procedure begins, within times correlated to the depth of traps where charge was stored during polarization and to the transit time.

Typical outputs of the measurements are patterns providing charge intensity and polarity through a color scale, as a function of time and insulation

thickness. Quantities proposed in literature to summarize the huge amount of data coming from patterns e.g.:

- charge profile and maximum charge
- electric field profile and maximum field at the electrodes
- charge mobility

are functions of poling time and field, and so they change with the test parameters.

The mean value of net (positive plus negative) charge density accumulated within the specimen at a certain time t, $q(t;E_P)$, can be calculated integrating the absolute value of $q(x,t;E_P)$ over insulation thickness, as follows 153[24]:

$$q(t;E_P) = \frac{1}{(x_l - x_0)} \int_{x_0}^{x_l} \left| q(x,t;E_P) \right| dx \tag{3.3}$$

where x_0 and x_l are the electrode positions, t is the time at which the measurement is done, E_P is the poling field, $q(x,t;E_P)$ is the charge profile. In order to calculate the value of $q(t;E_P)$, reference can be made properly with charge profiles observed during depolarization. In the following, $q(t;E_P)$ and $q(x,t;E_P)$ will be referred as $q(t)$ and $q(x,t)$ respectively, for the sake of brevity, but keeping in mind that they are actually relevant to a given poling field E_P.

Plotting the values of $q(t)$ thus obtained in relative value with respect to $q_0=q(t_0)$, where t_0, is a reference transit time (generally *1* to *10 s* after volt-off), as a function of the depolarization time, the so-called depolarization characteristic can be obtained (Figure 3.5).

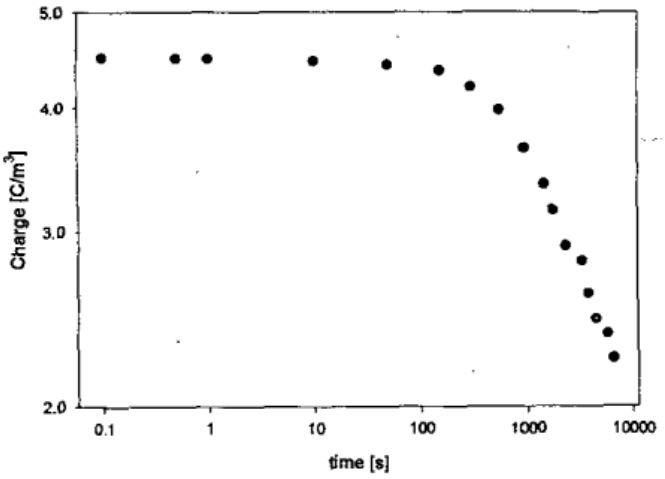

Figure 3.5 Example of depolarization characteristic.

From the depolarization characteristic the slope of the regression line that fits experimental points can be extracted. The larger the slope, the higher the rate of stored charge decrease. Being related to the time needed to deplete charge from a specimen after voltage removal, the slope must be dependent on the trap-controlled mobility, i.e. the mobility of entrapped charges in the absence of external electrical field.

An estimate of average (thus apparent) trap-controlled mobility could be derived, in principle, through appropriate processing of charge *vs* time depolarization characteristic. Trap depth could be estimated the same way. Apparent trap-controlled mobility is only a very rough approximation of the mobility as usually defined, but, even if affected by significant approximation, can be useful for material characterization and aging diagnosis.

For this purpose, depolarization characteristic will be fitted through a simple MATLAB script, and mobility will be easily extracted. The expression of apparent trap-controlled mobility $\mu(t)$ used is the following [25]:

$$\mu(t) \propto \frac{2\varepsilon}{q^2(t)} \frac{dq(t)}{dt} \tag{3.4}$$

where *q(t)* is the charge density that can be calculated at any depolarization time, d*q(t)*/d*t* is the slope of the depolarization curve at time *t*, ε is an average estimate coming from specific measurements of permittivity carried out on the specimens tested by dielectric spectroscopy. This expression is reached making two assumptions:

- charge relaxation is only due to leakage current while recombination is disregarded
- charge densities are replaced by their average values (prevailing charge is unipolar and located close to electrodes)
- the transit time is negligible with respect to time spent within deep traps[3].

The threshold characteristic (Figure 3.6 Example of variation of the inner charge absolute value with electric field. The red arrow indicates the space charge accumulation threshold.), obtained plotting q_0 as a function of poling field, is another source of interesting quantities, i.e. the threshold for space charge accumulation, E_T, and the rate of space charge accumulation (as a function of field), b, which is the slope of the space charge accumulation threshold characteristic. E_T and b are quantities characteristic of a material, independent of the test field and time, provided that the measurements are performed such that the space charge accumulation process reaches quasi-steady-state conditions. They depend, however, on the temperature, the environment and the kind of electrode-insulator interface, even if the threshold does seem to be affected significantly by the nature of the electrode.

[3] The initial transient is missing for mobility evaluation, due to the unavoidable delay for data acquisition from the beginning of depolarization. Thus mobility estimation for free or shallow-trapped charges, associated with the very beginning of charge decay, is practically unfeasible by the technique described.

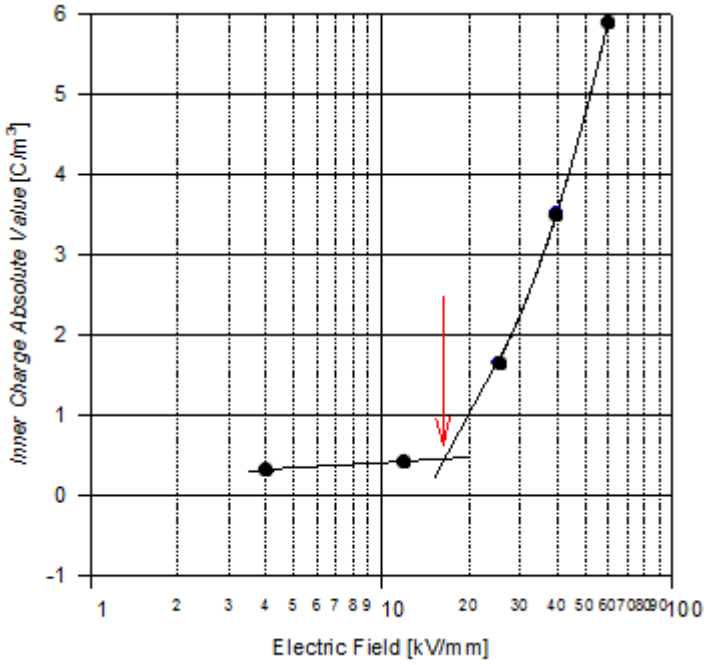

Figure 3.6 Example of variation of the inner charge absolute value with electric field. The red arrow indicates the space charge accumulation threshold.

3.2 Dielectric spectroscopy, low frequencies (10^{-6} ÷ 1 Hz): CHARGE/DISCHARGE CURRENT MEASUREMENTS

Charging/discharging current measurements are an useful tool to investigate the dielectric response and the conductivity of polymeric materials commonly used in cable insulations manufacture.

Experimental results from this CM method will not be presented in this thesis. However, data are now being processed and some anticipation concerning this analysis will be reported.

The measurements are constituted by two phases:

- the first consists of imposing a DC voltage on the insulating material and acquire the value of the current as a function of time;
- once completed the charge test, the current has reached a steady value. The second phase consists in switching off the voltage generator and

instantly short-circuit the specimen, recording the value of the discharging current until it reaches zero.

The value of the dielectric response can be calculated using the Fourier Fast Transform (FFT) or Kramers-Kroning (K-K) transforms, obtaining the complex susceptibility (χ' and χ'').

3.2.1 Experimental setup

The experimental setup of the C/D current system circuit (Figure 3.7) is composed by:

- a high voltage DC generator
- an electromer
- the test cell
- a personal computer
- a GPIB card.

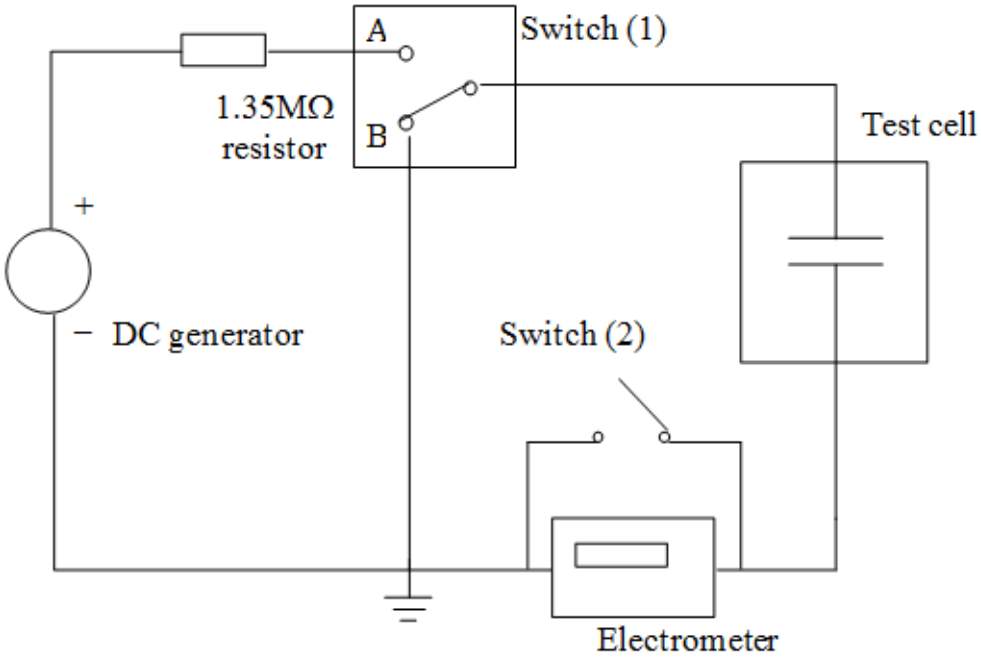

Figure 3.7 Scheme of the experimental setup for charging/discharging current measurements.

During the charge phase the DC generator supply the voltage to the specimen (switch (1) in position A). Once the current has reached a steady value, the specimen is short-circuited (switch 1 in position B) and the discharging phase begins. The current is measured by a programmable electrometer connected to a PC with a GPIB. The resistor protects the electrometer: its high value guarantees the protection of the electrometer in case of specimen breakdown, and does not influence the results. The switch (2) allows to disconnect the electrometer during the first instants of discharge, and protect it from the DC generator voltage.
Specimen and electrodes are placed inside a metal container which screens electromagnetic interferences.

3.2.2 Acquisition software

Data acquisition is provided. It allows to program the sampling intervals, in order to increase the acquisition frequency during the first instants. The software visualizes the current-time characteristic, in order to set the end point of the charge phase when the current steady state is reached.

3.2.3 Measured quantities

In order to carry out the time domain analysis, studying the dielectric response g(t) ,we use the Laplace's transform. A schematic representation of this method applied to dielectrics is the following:

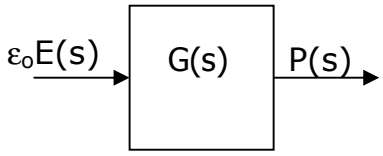

where G(s) = L[g(t)] represent the dielectric system, $\varepsilon_o E(s)$ is the solicitation, P(s) is the dielectric response, i.e. the polarization caused by the electric field. Making three assumptions:

- g(t) = 0 for t<0, system initially at rest;
- g(t) = 0 for t→∞, no permanent polarization;
- linear system (effects superposition allowed),

we have:

$$P(s) = \varepsilon_0 E(s) G(s) \tag{3.5}$$

whose inverse transform gives the expression of P(t):

$$\mathrm{P(t)} = \varepsilon_0 \ \mathrm{E(t)} * \mathrm{g(t)} = \varepsilon_0 \int_0^t \mathrm{E(t-}\tau\mathrm{)g(}\tau\mathrm{)d}\tau \tag{3.6}$$

As everybody knows, the charge current density can be expressed as

$$\mathrm{J_c} = \mathrm{J_s} + \frac{\partial\, \mathrm{D(t)}}{\partial\ \mathrm{t}} = \gamma \mathrm{E} \ + \frac{\partial\, (\varepsilon_0 \mathrm{E(t)} + \mathrm{P(t)})}{\partial\ \mathrm{t}} \tag{3.7}$$

where the first term $\mathrm{J_s}$ is the conduction current, and the second term $\frac{\partial \mathrm{D(t)}}{\partial \mathrm{t}}$ is the displacement current. The function describing $\mathrm{E(t)}$ is the Heaviside step function u(t), so

$$\mathrm{E(t)} = Eu(t) \tag{3.8}$$

and the expression of the displacement current becomes

$$\mathrm{J_p} = \varepsilon_0 \cdot \ \mathrm{E} \cdot \delta(\mathrm{t}) + \varepsilon_0 \cdot \ \mathrm{E} \cdot \mathrm{g(t)} \tag{3.9}$$

where $\delta(\mathrm{t})$ is the Dirac delta. The displacement current becomes zero at the end of the charging phase, so the value of the conductibility is given simply by the relation

$$\gamma = \frac{J_c}{E} \tag{3.10}$$

Once reached the steady current condition, we short-circuit the specimen (E = 0). This is equal to supply an input to the system, with expression

$$\mathrm{x(t)} = -Eu(t) \tag{3.11}$$

which raises a depolarization current $\mathrm{J_d}$. Applying the Laplace's transform we obtain

$$J_d(t) = -\varepsilon_0 E \left[\delta(t) + g(t)\right] \tag{3.12}$$

Which, for t>0, gives the expression of the dielectric response

$$g(t) = -\frac{J_d(t)}{\varepsilon_0 E} \tag{3.13}$$

An example of profiles obtained with a charging/discharging current measurement is shown in Figure 3.8. As an alternative to time domain analysis

we do the frequency domain analysis, using Fourier's transform. It allows to transform a generic[4] function g(t):

$$F[g(t)] = G(j\omega) = \int_0^{+\infty} g(t)\exp(-j\omega t)dt \tag{3.14}$$

to give the frequency spectrum G(jω).

Starting from the expression of the inverse transform $P(t) = L^{-1}[P(s)]$,

$$P(t) = \varepsilon_o \int_0^t E(\tau)g(t-\tau)d\tau \tag{3.15}$$

and applying Fourier's transform we obtain

$$P(\omega) = \varepsilon_o E(\omega)\chi(\omega) \tag{3.16}$$

where $\chi(\omega) = F[g(t)]$ is a complex number. The real part represent the polarization in phase with the field, the imaginary part is quadrature component.

$$\begin{aligned}\chi(\omega) = \chi'(\omega) - j\chi''(\omega) &= \int_0^{+\infty} g(t)\exp(-j\omega t)dt = \\ &= \int_0^{+\infty} g(t)(\cos(\omega t) - j\sin(\omega t))dt = \\ &= \int_0^{+\infty} g(t)\cos(\omega t)\,dt - j\int_0^{+\infty} g(t)\sin(\omega t)\,dt\end{aligned} \tag{3.17}$$

[4] The integral of the function $\int_0^{\infty} g(t)dt$ must be finite.

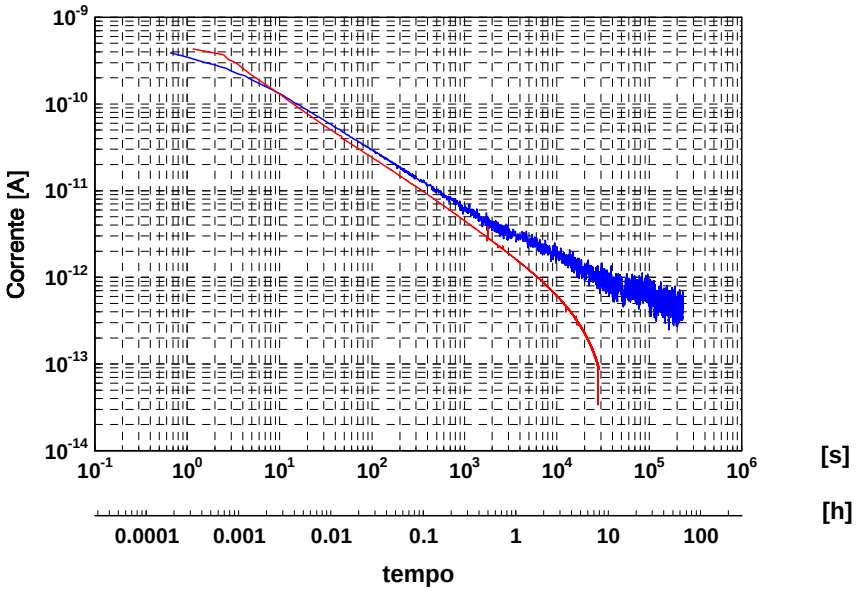

Figure 3.8 Example of charging current profile (blue) and discharging current profile ($-J_d$).

When ω=0 the imaginary part of the complex susceptibility χ(ω) is equal to zero and the real part must be finite.

$$\chi'(0) = \int_0^{\infty} g(t)dt \qquad \chi''(0) = 0 \tag{3.18}$$

Once the expression of χ(ω) is known, we can do the inverse transform obtaining the dielectric response:

$$\begin{aligned} g(t) = F^{-1}[\chi(\omega)] &= \frac{2}{\pi}\int_0^{+\infty} \chi'(\omega)\cos(\omega t)d\omega = \\ &= \frac{2}{\pi}\int_0^{+\infty} \chi''(\omega)\sin(\omega t)d\omega \end{aligned} \tag{3.19}$$

We can now define a complex permittivity, starting from

$$\begin{aligned} D(\omega) &= \dot{\varepsilon}(\omega)E(\omega) = \varepsilon_o E(\omega) + P(\omega) = \\ &= \varepsilon_o E(\omega) + \varepsilon_o E(\omega)\chi(\omega) = \\ &= \varepsilon_o E(\omega)\left[1 + \chi'(\omega) - j\chi''(\omega)\right] \end{aligned} \tag{3.20}$$

we obtain

$$\dot{\varepsilon} = \varepsilon' - j\varepsilon'' = \varepsilon_o(1 + \chi' - j\chi'') \rightarrow \chi' = \frac{\varepsilon' - \varepsilon_o}{\varepsilon_o}, \chi'' = \frac{\varepsilon''}{\varepsilon_o} \tag{3.21}$$

3.3 Broadband dielectric spectroscopy, $10^{-3} \div 10^{6}$ Hz): DIELECTRIC ANALYZER

Dielectric spectroscopy (sometimes called impedance spectroscopy) measures the dielectric properties of a medium as a function of frequency [27]. It is based on the interaction of an external field with the electric dipole moment of the specimen, i.e. electrical polarization. The main parameter which accounts for polarization is the complex permittivity ε. Real and imaginary part of permittivity, ε' and ε", in the frequency range 10^{-3} - 10^{6}, can be evaluated by accurately measuring the impedance of the specimen as a function of frequency. Dielectric spectroscopy can be performed on every kind of insulation system (solid and liquid). In particular this tool can be easily adapted for different insulation systems, e.g. thick power cables, thin I&C cables, shielded/unshielded cables, flat specimens, etc.

3.3.1 Experimental setup

The dielectric analyzer is made up of two major components (see Figure 3.9):

- a frequency response analyzer with a sine wave and DC-bias generator and two AC voltage input channels. Each input channel measures the AC voltage amplitude of an applied sine wave. In addition, the phase shift between the sine waves applied to the both inputs is detected. More detailed, each channel measures the amplitude and phase angle of the harmonic base wave component of a signal applied to the input. The harmonic base wave component is measured at the frequency of the AC sine wave generator. Most other signal components are suppressed. In addition, higher harmonics may be measured.
- A dielectric (or impedance) converter with a wide dynamic range current to voltage converter and a set of precision reference capacitors.

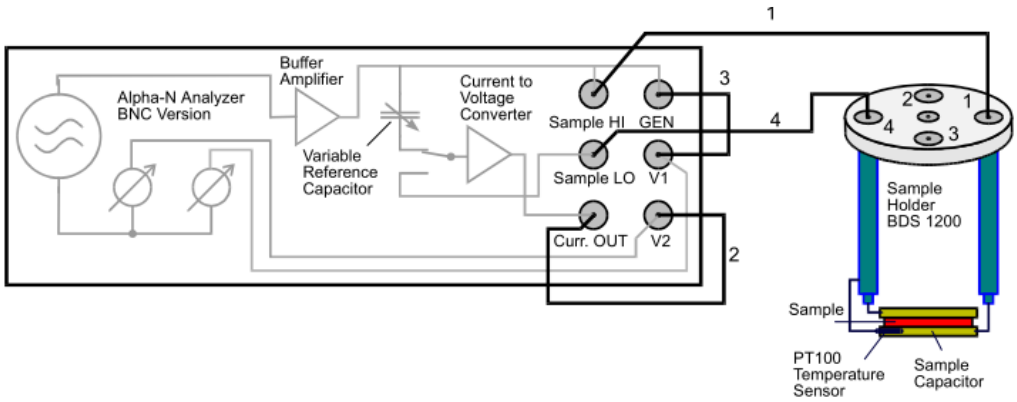

Figure 3.9 Dielectric analyzer with sample holder.

The principle of an electric material measurement is shown in Figure 3.10. The sample material is usually mounted in a sample cell between two electrodes forming a sample capacitor. For cable testing we connect the high voltage electrode to the conductor and the low voltage electrode to a wire mesh surrounding the cable.

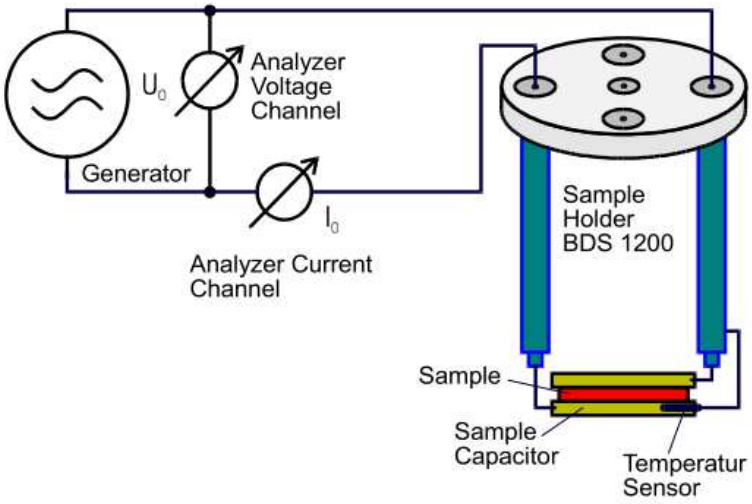

Figure 3.10 Scheme illustrating the principle of the measurement.

3.3.2 Measured quantities

A voltage V_0 with fixed frequency $\omega/2\pi$ is applied to the sample capacitor. V_0 causes a current I_0 at the same frequency in the sample. In addition, there will generally be a phase shift between current and voltage describe by the phase angle φ. Analyzing the material electric properties (permittivity and conductivity), the ratio V_0/ I_0 and the phase angle are determined for a specified geometry. Using the complex notation:

$$V(t) = V_0 \sin(\omega t) = \mathrm{Re}(U^* \exp(i\omega t)) \tag{3.22}$$

$$I(t) = I_0 \sin(\omega t + \phi) = \mathrm{Re}(I^* \exp(i\omega t)) \tag{3.23}$$

with $U = U^*$, and $I^* = I' + jI''$, $I_0 = \sqrt{I'^2 + I''^2}$, $\tan(\varphi) = \frac{I''}{I'}$.

For a sample with linear electromagnetic response, the measured impedance of the sample capacitor

$$Z^* = Z' + jZ'' = \frac{V^*}{I^*} \tag{3.24}$$

is connected with the dielectric function of the sample material by

$$\varepsilon^*(\omega) = \varepsilon' - j\varepsilon'' = \frac{-j}{\omega Z^*(\omega)} \frac{1}{C_0} \tag{3.25}$$

where C_0 is the capacity of the empty sample capacitor.

3.3.3 Measurement temperature's choice

The choice of the optimum temperature at which execute the test is fundamental. It is well-known that chemical and physical changes which can occur upon aging of polymers will affect the complex dielectric constant as well other dielectric properties at low frequencies and high temperatures [19]. Typical curves for an EVA based polymer cable, aged for 400 hours at 0.85 kGy/h and 85°C, representing the real part of the permittivity, the imaginary part of the permittivity and the dissipation factor respectively, are shown in Figure 3.11, Figure 3.12 and Figure 3.13, respectively. Figures illustrate the strong dependence of all dielectric properties on temperature at low frequencies: as the measurement temperature is increased, tan δ increases rapidly reaching the value 0.57 at 60°C for the frequency of 0.01 Hz (note that the correspondent value at room temperature of 25°C is 0.27). A similar behavior is shown by the real and the imaginary part of permittivity, even if changes are appreciable starting from different values of frequency.

A peculiar behavior of the test performed at room temperature can be highlighted: both imaginary part of permittivity and dissipation factor show polarization peaks (the first at 1 Hz and the second one, broader, at 400 Hz). Those polarization peaks disappear if measurement temperature is increased. At higher temperature, thus, the behavior of electric response is more regular, which enables a better correlation of electric properties with aging.

In order to investigate the dependence of dielectric response on temperature, a test at low temperature (about 15°C) has been carried out: the real part of permittivity is well below all the other curves (see Fig. 3.11) while the imaginary (Fig. 3.12) has two slight peaks, less wide and shifted toward the high frequencies compared to those at RT, the first centered at 100 Hz and the second at 200000 Hz respectively.

Therefore, the most likely conclusion that can be made is that the polarization peaks could be due to a real material relaxation phenomena of the insulation enhanced at room temperature.

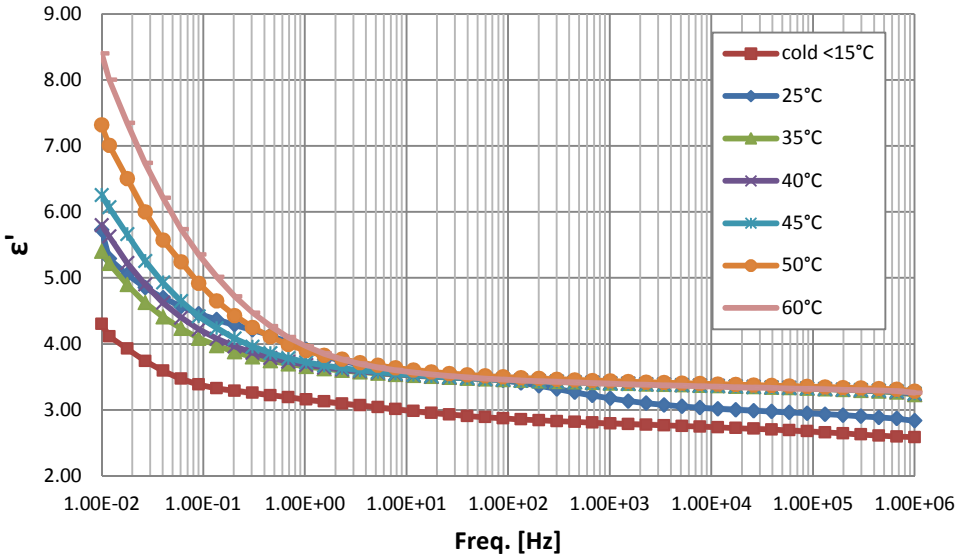

Figure 3.11 Real part of the permittivity for an EVA based polymer cable, aged for 400 hours at 0.85 kGy/h and 85°C.

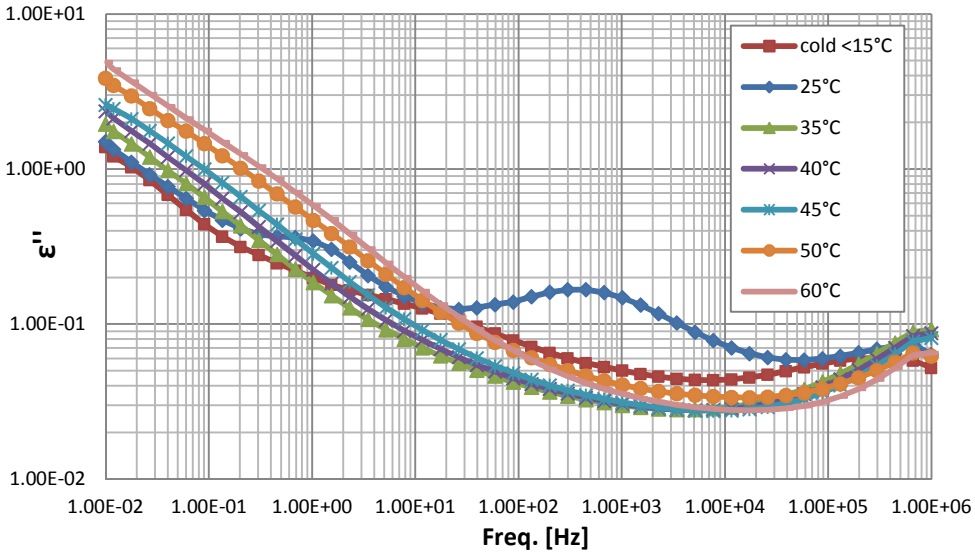

Figure 3.12 Imaginary part of the permittivity for an EVA based polymer cable, aged for 400 hours at 0.85 kGy/h and 85°C.

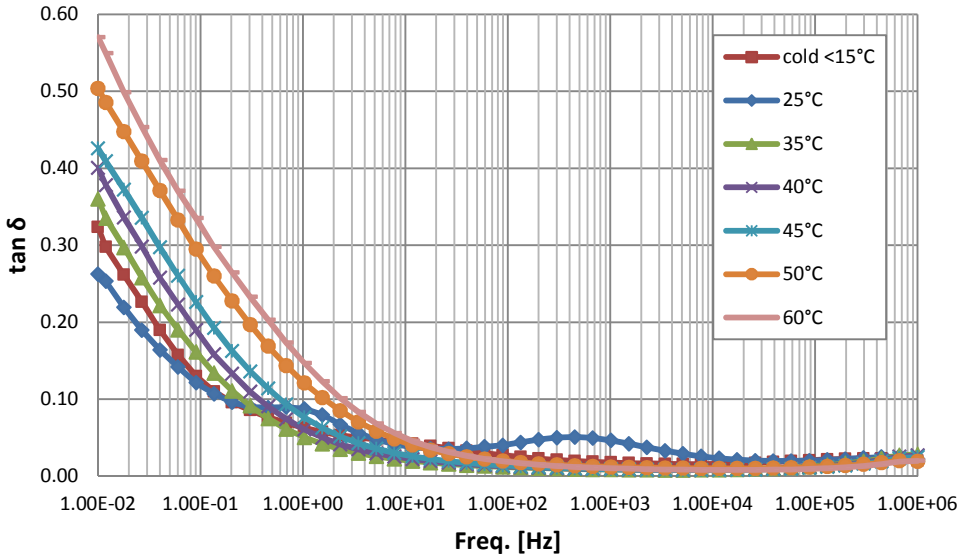

Figure 3.13 Dissipation factor tan δ for an EVA based polymer cable, aged for 400 hours at 0.85 kGy/h and 85°C.

Another possible explanation could be linked to the bad contact between conductor and insulation (commonly present in these kinds of cables) or between the insulation and the outer screen, which could provide another contribution to this phenomenon. Loose contacts could lead, in fact, to artifact signals in the dielectric response of the specimens. For this purpose partial discharge measurements on these specimens were performed in order to search for voids or delaminations between conductor and insulation at different temperatures. Figures 3.14 and 3.15 show partial discharge patterns (amplitude; phase) for the same cable tested by DS. Measurement temperatures were 25°C and 50°C, respectively. Tests were conducted at 4.3 kV. As can be seen in both cases internal partial discharges occur. However, even if inception voltage (PDIV) is the same, at 50°C partial discharges show much smaller amplitude, indicating, thus, that voids/delaminations get smaller and smaller with temperature increase. Hence, at higher temperature, DS signal could improve significantly.

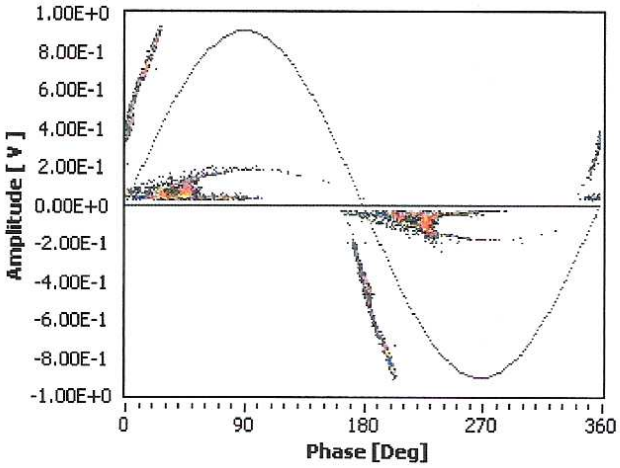

Figure 3.14 Partial Discharge Pattern at 25°C for an EVA based polymer cable, aged for 400 hours at 0.85 kGy/h and 85°C, PDIV=3.3 kV, measurement at 4.3 kV.

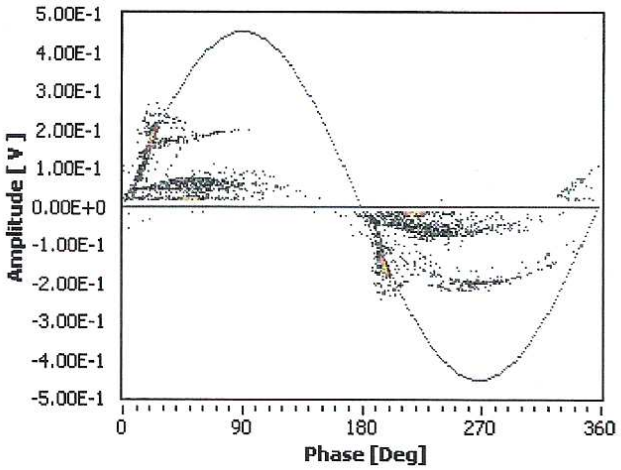

Figure 3.15 Partial Discharge Pattern at 50°C for an EVA based polymer cable, aged for 400 hours at 0.85 kGy/h and 85°C, PDIV=3.2 kV, measurement at 4.3 kV.

Concluding, in order to have comparable data and a better correlation with the aging time, a measurement temperature of 50°C has been chosen for time-domain dielectric spectroscopy technique in this thesis work.

Chapter 4

4 Samples description and composition

A complex composition of insulations and sheaths in the electrical cables determines aging effects. Except a dominant polymeric constituent, there are usually at least several other components influencing radical processes that lead eventually to the gradual deterioration of insulation and sheath features and to the shortening of cables service life-time.

4.1 Overview of cable composition

Compounding ingredients of insulations and sheaths are protected as intellectual property, thus a chemical nature of the additives and their concentrations are not revealed. Consequently, provided information is usually incomplete and non-specific. Additionally, identification and quantification of components and additives are complex and frequently do not lead to the satisfactory results. The effectiveness of chemical analysis of insulation and sheath is limited due to complex character of the specimens. The analytical problems arise from the following factors:

- Investigation of the material comprising dozens of components is incomplete and often impossible due to lack of information about constituents (and consequently references).

- The particular chemical groups might be a part of various organic compounds.
- Analysis of elements might lead to ambiguous conclusions. E.g. sulphur might be included in the antioxidant molecules, in curing agents or in polymeric macromolecules

If quantitative and qualitative chemical analyses are fully applicable then the manufacturing technology and material formulas used by particular producers would be revealed and available. A composition of each insulation and sheath remains unrecognized as each producer usually develops an original procedure and unique selected set of components. Thus, an understanding of the chemical mechanisms involved in the degradation/aging processes is limited due to lack of complete knowledge about the cables composition.

Additionally, there is not a comprehensive protocol for the analysis of plastic materials. Therefore, it is necessary to apply several experimental methods giving complementary knowledge on the wide range of components used for the production of cables.

Methodology of the reported studies was selected in order to gain as much as possible knowledge about the most important components of the insulation and sheath materials influencing aging processes.

Chemical structure of the polymeric macromolecules was confirmed by thermogravimetric analysis (TGA) and High performance liquid chromatography (FTIR) . Additionally, radicals generated in the materials were investigated by electron spin resonance spectroscopy (ESR). Analysis of the polymer additives was performed by High-performance liquid chromatography (HPLC) and Gas chromatography–mass spectrometry (GC-MS). Elementary analysis was carried out using neutron activation analysis (NAA) with the use of a nuclear reactor, Inductively coupled plasma mass spectrometry (ICP-MS), Ion chromatography (IC) and atomic absorption spectrometry (AAS).

The main elements of insulations and sheaths commonly used in NPPs are listed in the following paragraphs.

4.1.1 Polymer

The polymers used for manufacturing jackets and insulations are ultimately susceptible to chemical degradation under exposure to various conditions commonly encountered in NPP environments. Initiation of the process predominantly depends on the strength of the carbon-carbon bond in backbone as well as pendant and functional groups which are determined by the chemical structure of the polymer. It is generally accepted that the aging induced by various stressors such as ionizing and UV radiation, thermal factors and others, is determined by the comparable radical mechanisms. Scission is favored in polymers that are branched or have many side groups. During aging, tertiary alkoxy or carbon radicals are generated which undergo beta scission, unimolecular cleavage to lower molecular weight fragments or others. Morphology of polymer is a very important factor determining yield and nature of radical processes. In general, amorphous phase facilitates radical combination and crosslinking, whereas crystalline phase stabilizes unpaired spins (residual radicals) that in multistage processes are oxidized.

4.1.2 Flame retardants

Next abundant components are flame retardant which contribution might achieve more than 50%. Due to their hygroscopicity they may greatly affect electrical properties, especially if reactions involving flame retardant materials are activated by radiation. Flame retardant wire and cable materials are divided into non-halogen flame retardant and halogen-containing flame retardant materials.

General classification:

- Inorganic flame retardants include metal hydroxides like aluminum hydroxide and magnesium hydroxide. Other compounds like e.g. zinc borate are used to a much lesser extent.
- Phosphorus based flame retardants: this category comprises mainly organic and inorganic phosphorus compounds with different oxidation states.

- Nitrogen based flame retardants are typically melamine and melamine derivatives used in combination with phosphorus based flame retardants.

Brominated flame retardants are represented by a wide range of brominated components added to materials to inhibit their ignition and to slow their rate of combustion.

The fillers, usually Al(OH)3 or Mg(OH)2, with high specific surface area might efficiently diminish level of radicals generated by stressors due to transfer of paramagnetic centers onto dispersed phase. Additionally, due to a large content of flame retardants in the material they efficiently contribute in heat and radiation energy dissipation diminishing their effects on plastics.

4.1.3 Antioxidants

Antioxidants are materials that can interfere with any of the stages in the oxidation process. For maximum antioxidant effectiveness, inhibiting the oxidative process at more than one step, combination of two types of antioxidants is usually very effective. They play a role of radical trap and a hydroperoxide decomposer thus can frequently provide better protection against oxidative aging than either type of antioxidant alone. Hindered amines and phenols are examples of alkoxy and peroxy radical trap antioxidants. During aging antioxidants are "consumed" and no longer protect the polymer. Combinations of phenolic antioxidants with phosphites and thiosynergists are often used. The phosphite antioxidant reacting with hydroperoxide becomes oxidized to phosphate while the peroxide is reduced to alcohol or other harmless functional group. In addition, peroxide decomposing antioxidants are thought to be capable of reacting with the consumed phenolic antioxidant to regenerate its protective action. This is the way in which a combination of two antioxidants can provide longer service than either one alone.

During end use polymers might be in contact with metals (copper) which can very efficient catalyze an oxidative degradation. Therefore, deactivators able to complex metals and inhibit their chemical activity are used. These are usually

phenolic antioxidants containing functional groups that coordinate metallic ions.

4.1.4 Lubricant

Chemically lubricants are metal stearates, fatty acids, acid esters or alcohols, esters, paraffin waxes, amides or a combination of these components. They are added to reduce the shear rate during processing particularly if inorganic fillers are being add.

4.1.5 Plasticizers

Plasticizers are added to improve flexibility and softness of wires and cables. They are chemically and thermally stable; their addition also enhances the stability and reduces the degradation of the host polymers. They are of various chemical types, some being used in specified products only. Phthalates, such as di(2-ethylhexyl)phthalate, trimellitates, benzoates and terephthalates are examples of monomeric plasticizers. However, many other different components are used as plasticizers.

4.1.6 Colorants

Color of wires and cables is obtained by using organic or inorganic pigments, or dyes that are available in the form of powder or liquid as well as a concentrate or coloured resin. In order to obtain suitable color usually mixture of several colorants is required. Many inorganic colorants comprises titanium dioxide or iron oxide.

4.1.7 Others

Except above specified components, other additives are also available, e.g. stabilizers, initiators, curing agents, etc. thus a chemical composition of insulations and sheaths is very complex and might comprise a lot of constituents of various nature and concentrations. Cable manufacturers might choose the suitable components from many products taking into consideration their character, compatibility, stability, dispersity, etc. Because of these reasons

a composition of insulation and sheath materials usually remains trade secret and is undisclosed by producers.

This thesis will focus on the study of two main types of low voltage I&C cables, whose structures and materials, resulting from chemical analysis, will be described below.

4.2 CSPE/EPR cable (S9)

The first cable tested is a LOCA Low Voltage Power Cable (0,6-1 kV). The insulation is made of EPR (Ethylene propylene rubber). EPR manufacture uses the same monomers as polyethene and polypropene, the ethylene and propylene monomers are randomly combined to yield a rubbery, stable polymer. Inner and outer sheaths are made of CSPE (chlorosulfonated polyethylene synthetic rubber), whose trademark is Hypalon. The cable was manufactured in 1996, then stored in shelter.

4.2.1 Cable construction data

Table 4-1 Cable construction data for S9 cable.

Construction			
Conductors	Number		3
	Diameter [mm]		7
	Cu/tin coated		no
Insulation of conductors	Number		1 per conductor
	Color		Black
	Thickness [mm]		1,2
	Type		EPR
Sheath	Inner (filler)	Type	Hypalon (CSPE)
		Thickness [mm]	2
	Outer	Type	Hypalon (CSPE)
		Thickness [mm]	2
Screening	Tape		2 glass steel tapes: - 1 above steel screen - 1 under steel screen
Other protectors	Type of screen		Steel
	Number of layers		2 layers (0.2 mm each): butt-gap and covering butt-gap

4.2.2 Cable structure

Figure 4.1 illustrates the cable section. We can distinguish the 3-conductor, each with its insulation, metallic and thermal screens and two sheaths. Note that a PET foil is interposed between the conductor and the insulation.

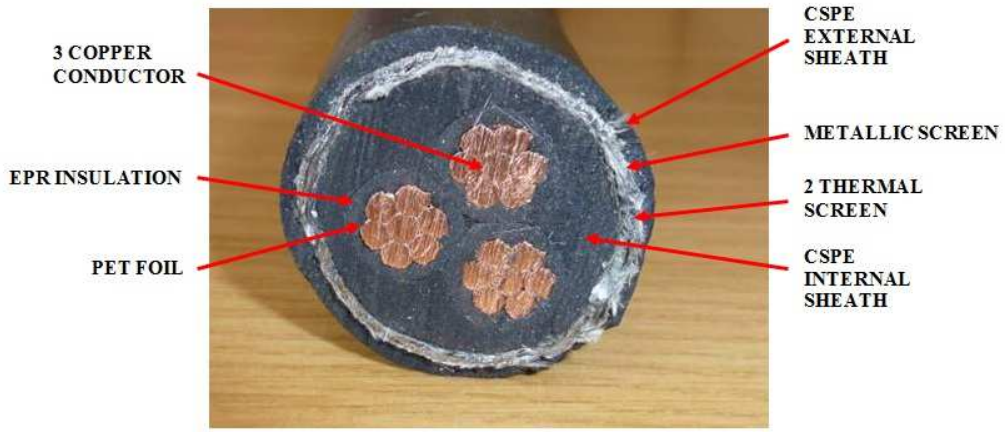

Figure 4.1 Section of S9 cable.

This cable will be submitted to accelerated ageing with 3 combinations DR-T (dose rate-temperature).

4.3 EPDM/EVA cable (S3)

The second cable tested is a power cable installed in the Doel Nuclear Power Station since 1985. Both insulation and sheaths are made of EPDM and EVA copolymer (ethylene-propylene-polyene terpolymer). The cable was stored for 25 years at room temperature.

4.3.1 Cable construction data

Table 4-2 Cable construction data for S3 cable.

Construction			
Conductors	Number		5
	Diameter [mm]		1.76
	Cu/tin coated		Cu
Insulation of conductors	Number		5
	Color		Yellow, Green, Black, Blue, Brown
	Thickness [mm]		1
	Type		EPDM/EVA
Sheath	Inner (filler)	Type	
		Thickness [mm]	
	Outer	Type	EPDM/EVA
		Thickness [mm]	2

4.3.2 Cable structure

Figure 4.2 Section of S3 cable. illustrates the cable section. We can distinguish five conductors, each with its insulation, the filler and the external sheath. Inner insulations present four different colours (black, blue, brown and yellow/green).

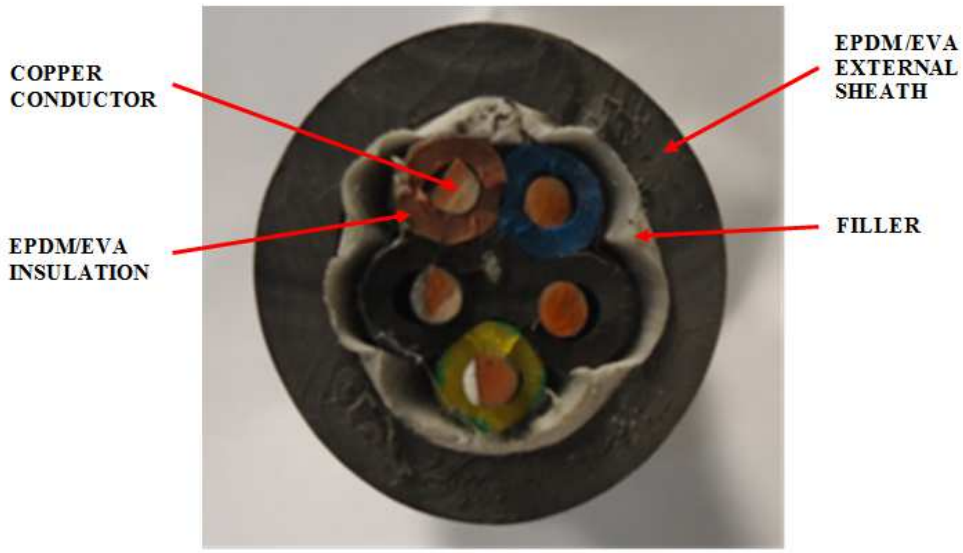

Figure 4.2 Section of S3 cable.

This cable will be aged with all 9 combinations DR-T (dose rate-temperature).

[In the follow chapters we will refer to S3 both for the cable in general and for the “black” insulation, as well as for the “black” cable sheath, S4 for the “blue” insulation, S5 for the “brown” insulation and finally S6 for the yellow-green one.]

Chapter 5

5 Samples aging and treatment

New cables from NPPs are submitted to several treatments before being tested through CM methods. The total cable length needed for each DR-T (dose rate-temperature) aging combination is 10 meters. After each aging time interval, 2 meters of cable has been cut out, its moisture content has been reduced and then it has been managed depending on CM test used.

5.1 The factorial experiment

For the multi-stress ageing of small cables samples it has been decided to carry out a factorial experiment which consists on a radiation aging treatment with different dose rate and different temperatures.

The experiments involve six radiation dose rates and two temperatures, 9 combinations DR-T in all. The chosen test temperatures vary between the working value measured at NPPs, typically near 55°C, up to 85°C. The chosen dose rates values aim at obtaining, in a reasonable time, a total absorbed dose between 10^5 Gy and 10^6 Gy. These values are typically reached in literature to age cable insulations tested with mechanical CM techniques. The scheduled total duration of tests is 1000 hours, for each combination DR-T. The electrical and mechanical properties have been measured every 200 hours. Test samples will be visually inspected to see if damage has occurred during aging.
Any aspect of interest during the inspections has been registered and evaluated.

Figure 5.1 shows hypothetical lifetime variation with dose rate and temperature.

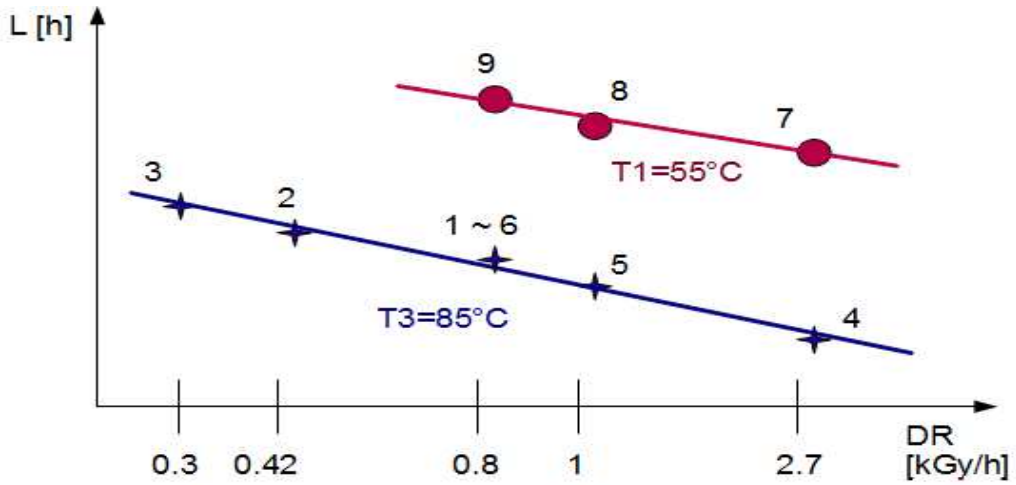

Figure 5.1 Diagram of the factorial test performed. Hypothetical lifetime variation with dose rate and temperature.

5.2 Aging procedure

Thermal and irradiation aging tests have been carried out simultaneously in order to take into account also synergistic effects.

The simultaneous action of elevated temperature and irradiation is performed in NRI irradiation facility ROZA (Řež, Czech Republic), which is a well-type ^{60}Co gamma ray source with the cobalt placed in the center of the irradiation shaft (Figure 5.2 Figure 5.3). The dose rate depends generally on the distance from the cobalt source. The dose rate gradient within the sample depends on the sample thickness and composition. To perform irradiation at elevated temperature, new thermobox had to be constructed before starting experiments. There are two circular heating elements in the bottom of the box. A fan distributes homogeneously the elevated air inside the thermobox which is closed using a top cover .

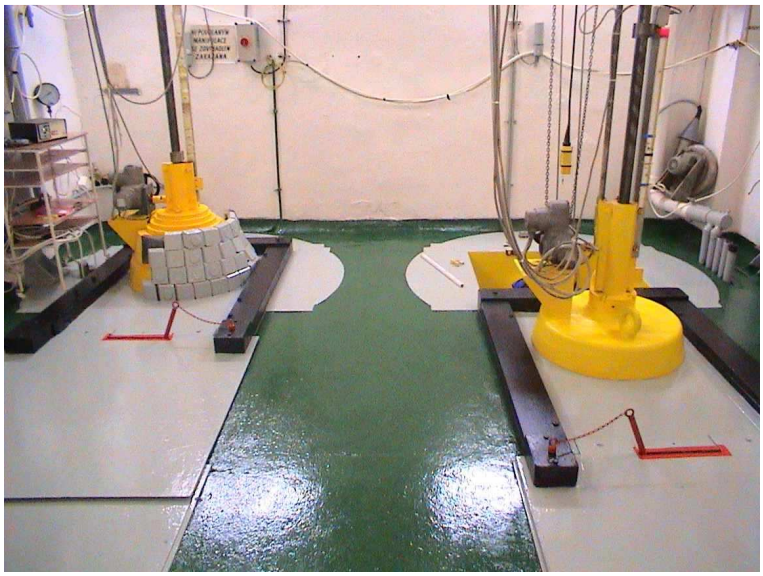

Figure 5.2 Gamma irradiators ROZA (right) and PRAZDROJ (left).

Figure 5.3 View into the irradiation shaft with cylinders with samples.

The tested samples are carefully fastened on 3 perforated stainless steel cylinders with the diameters 0.4 m, 0.6 m and 0.8 m. Figure 5.4 shows the samples on the cylinders. Cylinders are placed inside the thermobox, symmetrically around the guide tube for the cobalt source, and the thermobox is closed using a top cover. Continual fanning of the irradiation shaft ensures periodical change of fresh air inside the thermobox. The temperature was

recorded using a thermometer with 2 sensors. Dosimetry was based on the system alanine/ESR.

A 10 meter-long cable specimen was carefully fastened on each cylinder.

Figure 5.4 Samples on the cylinder, equipped with dosimeters and prepared for placing into the thermobox.

Average dose rates (DR) were:

- **DR1** = 0.86 kGy/h, cylinder Ø = 40cm
- **DR2** = 0.39 - 0.42 kGy/h, cylinder Ø = 60cm (depending on cable)
- **DR3** = 0.29 kGy/h, cylinder Ø = 80cm
- **DR4** = **DR7** = 2.74 kGy/h, cylinder Ø = 40cm
- **DR5** = **DR8** = 1.38 - 1.58 kGy/h, cylinder Ø = 60cm (depending on cable)
- **DR6** = **DR9** = 0.85 kGy/h, cylinder Ø = 80cm

Temperatures (T) were:

- **T1** = 85°C
- **T2** = 55°C

Depending on test number, we will refer to “first (1°) experiment” for DR1-DR2-DR3, “second experiment (2°)” for DR4-DR5-DR6 and “third experiment (3°)” for DR7-DR8-DR9.

5.3 Drying

After aging all cables have been subjected to a thermal treatment which is essential to reduce the disturb introduced by the content of water inside the sample. Thermal treatment used for the tests assumes leaving cables and flat specimens, placed in a glass vessel put under vacuum with silica gel grains on the bottom, in a thermostatic cell for 5 days at the temperature of 60°C. Silica gel grains are useful to absorb a major percent of humidity in a lower time.

5.4 Cutting

Electrical CM techniques implemented at UNIBO (Space charge density with PEA method, Dielectric Spectroscopy, Charging/Discharging Current) do not allow to test multipolar cables. Therefore cables conductors had to be separated and were cut depending on the type of test to perform.

5.4.1 Cables for DS

Cables for dielectric spectroscopy have been cut into 30 cm long segments. A 25 cm metallic mesh has been inserted around the cable in order to form a capacitor. Ends have been stripped to expose the conductor. (See Figure 5.5)

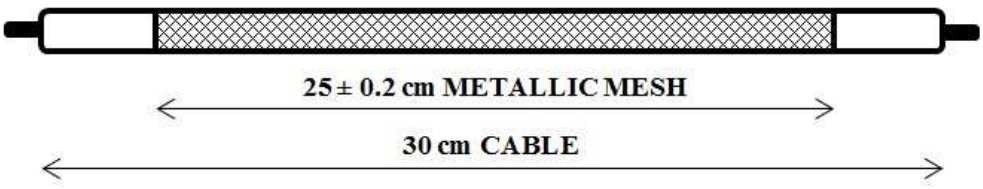

Figure 5.5 Cables preparation for dielectric spectroscopy.

5.4.2 Cables for PEA

Cables for pulsed electroacoustic method were cut into 75 cm long segments. A semiconductive screen is placed where high voltage pulse is applied. Its length must be at least equal to the length of piezoelectric transducer. (See Figure 5.6)

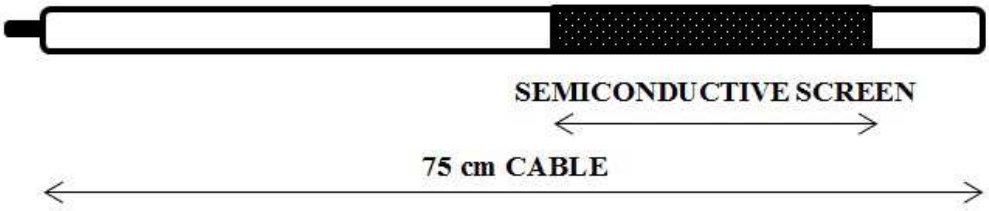

Figure 5.6 Cables preparation for pulsed electroacoustic method.

5.4.3 Flat specimens

Inner and outer insulations are difficult to test due to their geometry. Moreover, they are usually made of different materials; this could make the interpretation of results more difficult. In order to avoid these problems, outer insulations have been peeled to produce flat specimens (side 30 - 60 mm, thickness 0,1 – 0,5 mm, see Figure 5.7).

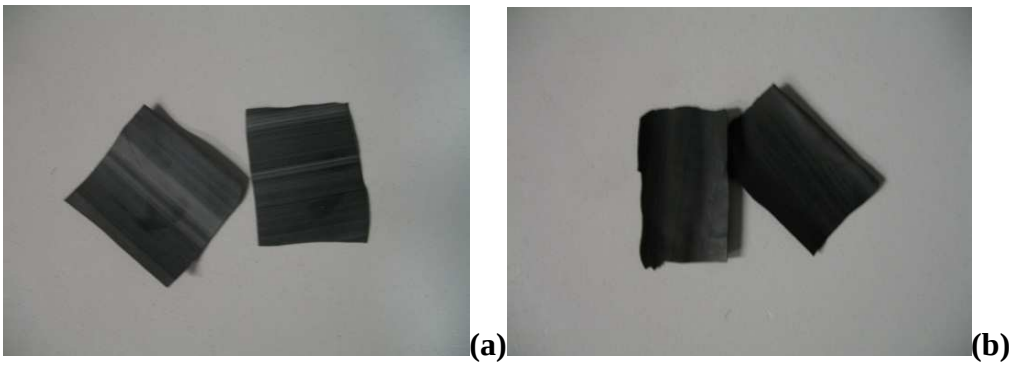

(a) **(b)**

Figure 5.7 Example of flat specimens (FS3 (a) and FS9 (b) outer sheaths).

5.5 Sample identification

Every cable has been clearly identified using tags or a permanent marking method. Labels are composed by one or two letters indicating the type of specimen, followed by three numbers: The first number indicates the cable name; the second number indicates the accelerated aging conditions; the third one indicates the aging time.

Identification codes to be used within the testing program are the following (Figure 5.8):

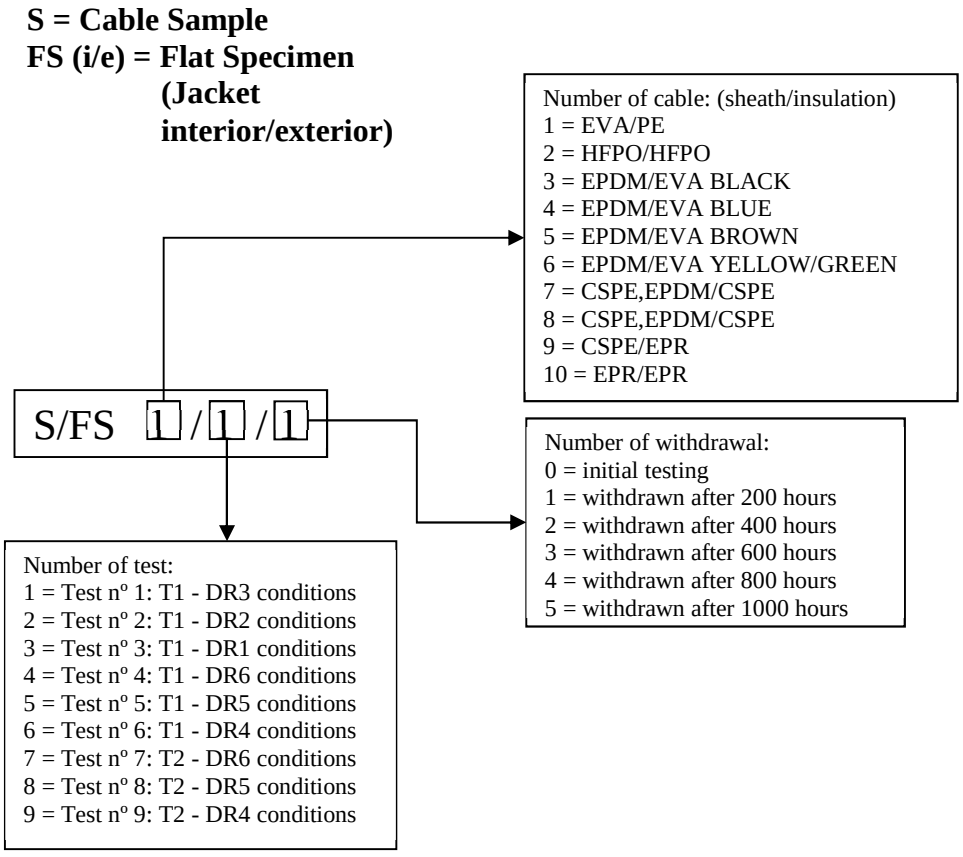

Figure 5.8 Sample codification.

Table 5-1 lists cables that will be tested in this thesis, their available length for CM methods before and after peeling, and the dose rate-temperatures combinations at which they will be aged.

Table 5-1 Cables for testing in this work.

Cable Name	Required Length [m]	Number of Conductors	Available length after peeling [m]	DR-T combinations
S/FS 3-4-5-6	**70**	**5 (4 different colours)**	**70**	**2,3,4,5,6,7,8,9**
S/FS 9	**30**	**1**	**30**	**2,5,8**

Chapter 6

6 Dielectric response in CSPE/EPR samples

This chapter deals with dielectric response measurements on S9 CSPE/EPR samples. In particular, EPR cable insulation will be tested using dielectric analyzer tool. Results of electrical and mechanical test will be discussed and possible correlations between them will be proposed.

An introduction is necessary. Fundamental investigations of the dielectric response leads to information about different molecular motions and relaxation processes. Polymer relaxations are associated with thermally activated jump processes involving molecular segments or even individual molecules. These phenomena are affected by the crystallinity degree. Most polymers exhibit more than one region of dielectric relaxations, called α, β, γ and δ motional processes in descending order of temperature and resulting in characteristic peaks of relaxation (for a complete discussion on the phenomena see [27]). A unique characteristic of dielectric spectroscopy is the wide frequency range over which polymers respond to an applied electric field. Frequency-domain response of an electric medium may be written in terms of complex dielectric permittivity $\varepsilon(\omega)$:

$$\varepsilon(\omega) = \varepsilon'(\omega) - i\varepsilon''(\omega) \tag{6.1}$$

where the real part consists of the contributions of free space – which is necessarily real, and of the real part of the susceptibility of the material medium itself. It is related to the energy stored reversibly in the material. The imaginary component is entirely due to the material medium which can be affected by several polarization mechanisms with consequent dissipation (or loss) of energy.

Note that dielectric permittivity is a complex function of at least two variables – frequency and temperature, although pressure may be another physical variable. A complete representation should therefore comprise two "three-dimensional" plots, one for the real part and one for the imaginary part as function of the other two variables (see Figure 6.1).

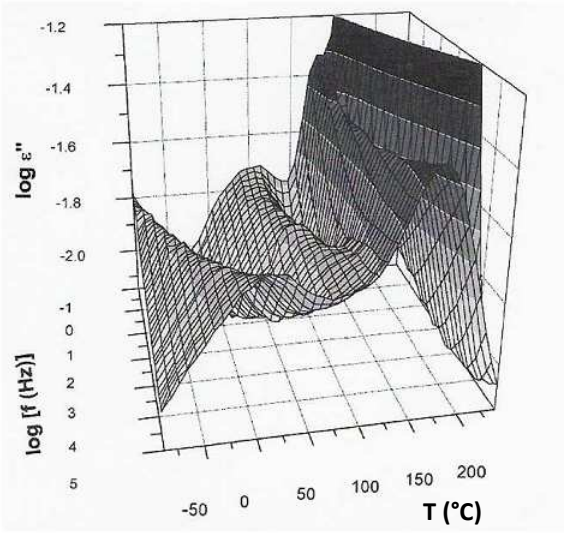

Figure 6.1 Example of a "three-dimensional" relaxation plot of the imaginary part of permittivity as function of frequency and temperature.[27]

In technical applications of dielectric relaxation spectroscopy the dissipation factor $\tan\delta = \frac{\varepsilon''}{\varepsilon'}$ is often discussed and evaluated where δ is the phase angle between applied voltage and resulting current.

As we stated above, fluctuations of the net dipole moment can be driven by several motional processes. Such motional processes can be fluctuations within a monomeric unit or rotational fluctuations of a short side chain. On a larger spatial scale the so called segmental motion which is responsible of the glass

transition becomes relevant. At a much higher length scale than a segment the molecular motion of the whole molecule characterized by the entanglement spacing or by the end-to-end vector of the chain takes place. This motional process is directly related to the viscoelastic properties of the material. Provided that the motional processes under consideration are related with a dipole orientation , a dielectric relaxation process is characterized by a peak of the imaginary part of permittivity and a step-like decrease of the real one versus frequency at isothermal condition (Figure 6.2).

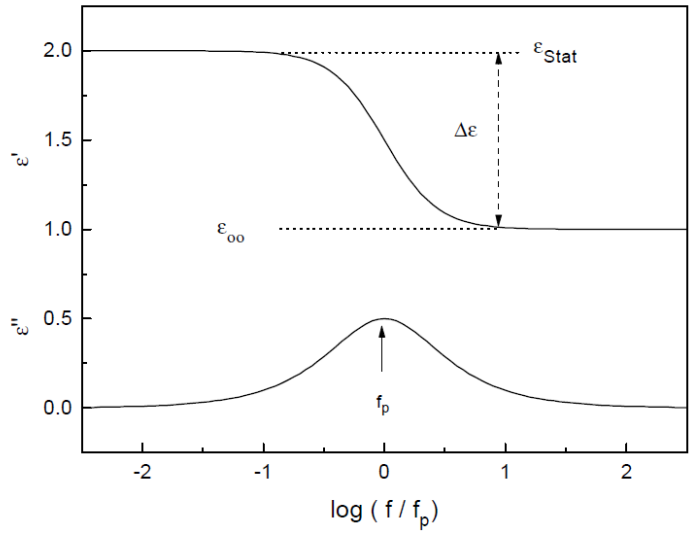

Figure 6.2 Principal behavior of the complex dielectric function in the frequency domain for a motional relaxation process [28].

6.1 Experimental results

The results from dielectric response measurements are summarized in Figures from Figure 6.3 to Figure 6.8. Frequency behavior of the real and imaginary part of relative permittivity are shown. The results refer to the three DR-T combinations at which this cable insulation has been aged (DR2, DR5 and DR8). Electrical properties are initially plotted in absolute values against the logarithm of frequency and then in relative values - to those measured on unaged specimens - as a function of aging time expressed in hours, for a fixed frequency. Values in absolute terms has been set to full scale in order to be able to highlight the differences. The scale of ε' is presented as linear while the scale of ε'' as logarithmic (due to its generally greater variations) because we are more interesting in evaluating the effects of aging rather than the essential link between the parts. Measurement were made at 50°C, this choice has been explained in §3.3.3, thus plots will be two-dimensional. Frequency ranged between 10^{-2}-10^{6} Hz with an input voltage of 3 V_{rms}. Characteristic parameters of cable S9 insulation for dielectric spectroscopy measurements are listed in Table 6-1 (equivalent diameter, thickness, area, reference capacitance).

Table 6-1 Cable S9 characteristic parameters for dielectric spectroscopy measurements

CABLE	Set	d [mm]	s [mm]	S [mm^2]	C_0 [F]
S9	S9XX	80.7	1.2	5115	3.77E-11

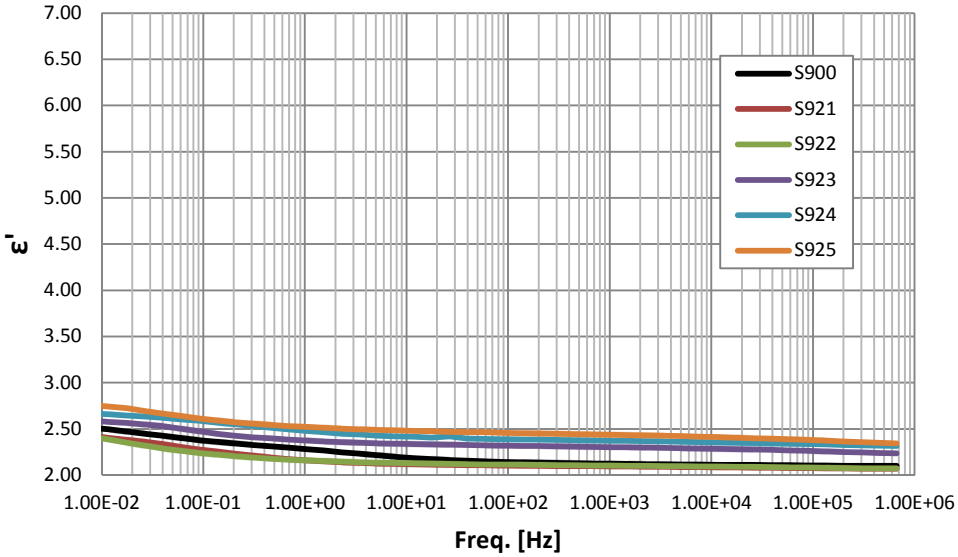

Figure 6.3 Real part of the permittivity for specimens S92x. DR2=0.39 kGy/h - T=85°C - Measurement temperature 50°C

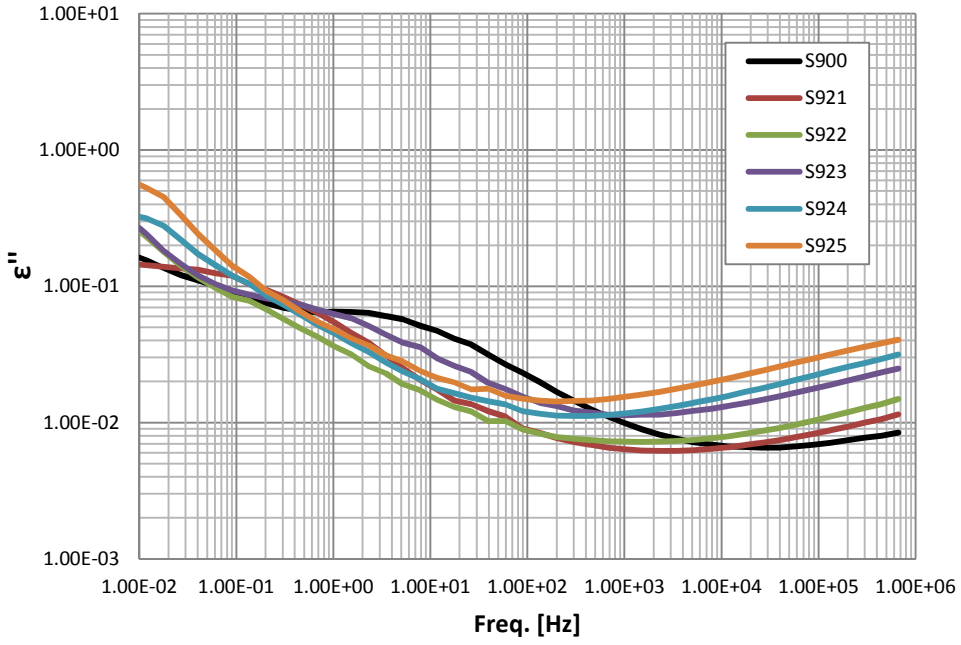

Figure 6.4 Imaginary part of the permittivity for specimens S92x. DR2=0.39 kGy/h - T=85°C - Measurement temperature 50°C

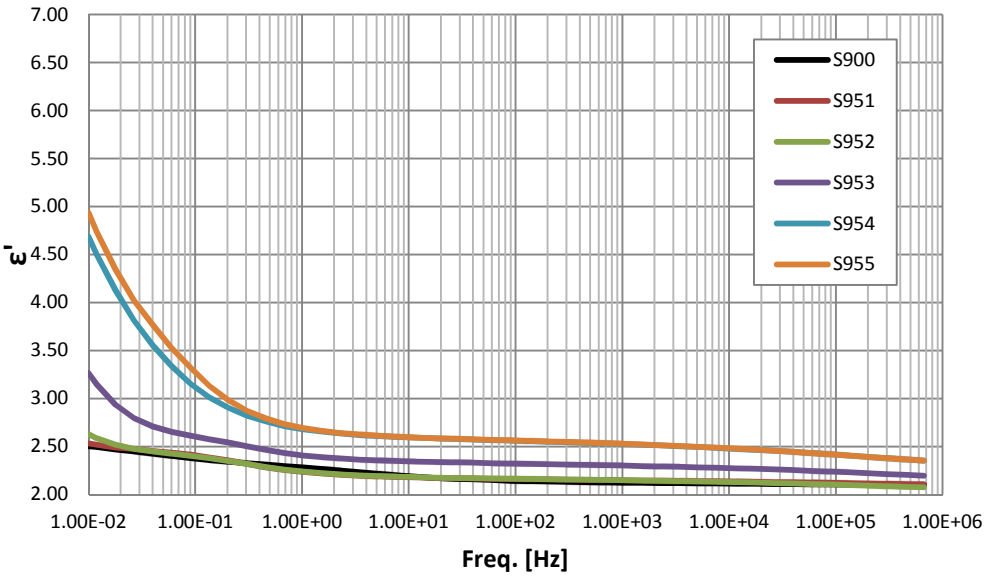

Figure 6.5 Real part of the permittivity for specimens S95x. DR5=1.58 kGy/h - T=85°C - Measurement temperature 50°C

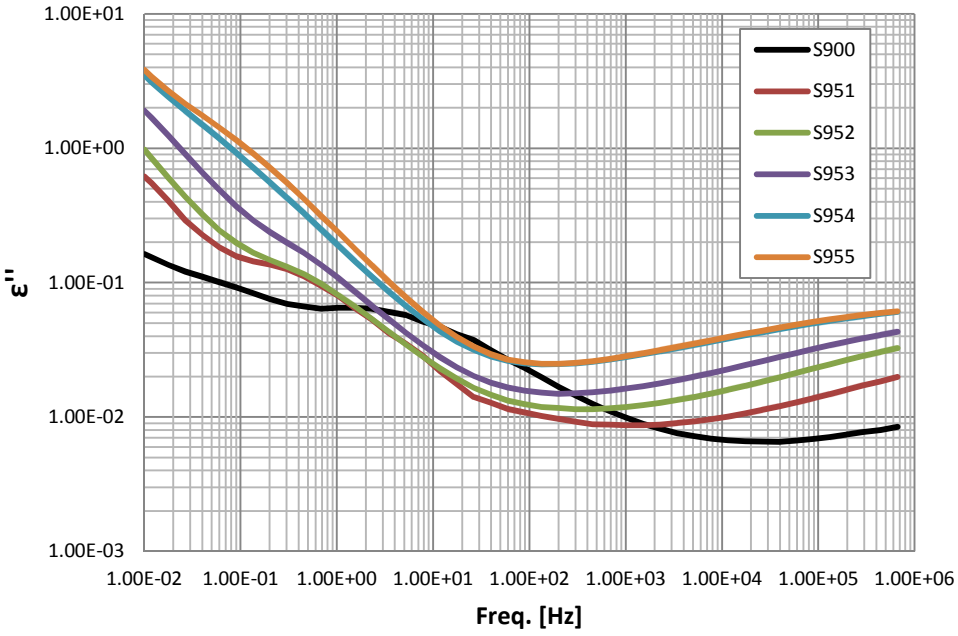

Figure 6.6 Imaginary part of the permittivity for specimens S95x. DR5=1.58 kGy/h - T=85°C - Measurement temperature 50°C

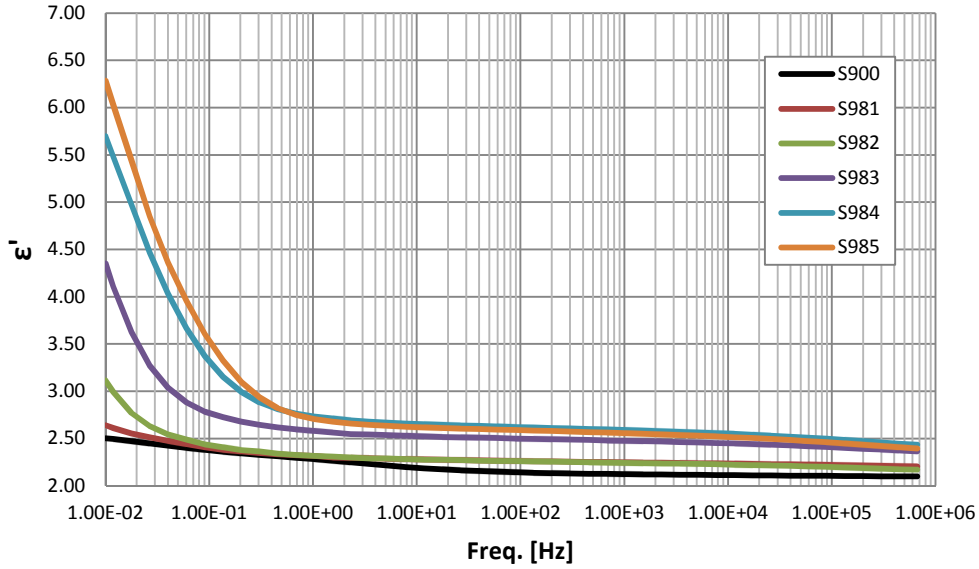

Figure 6.7 Real part of the permittivity for specimens S98x. DR8=1.58 kGy/h - T=55°C - Measurement temperature 50°C

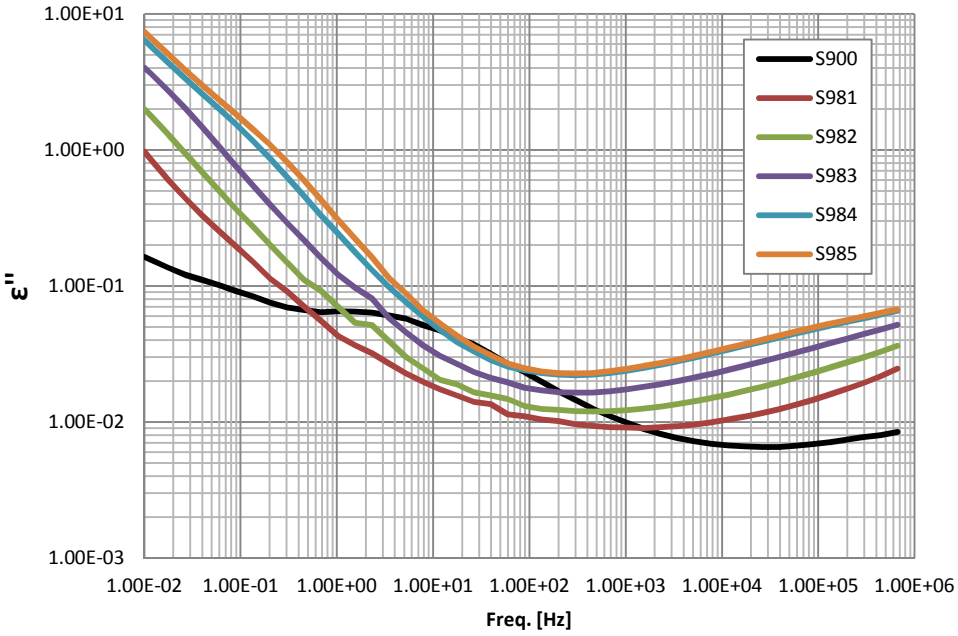

Figure 6.8 Imaginary part of the permittivity for specimens S98x. DR8=1.58 kGy/h - T=55°C - Measurement temperature 50°C

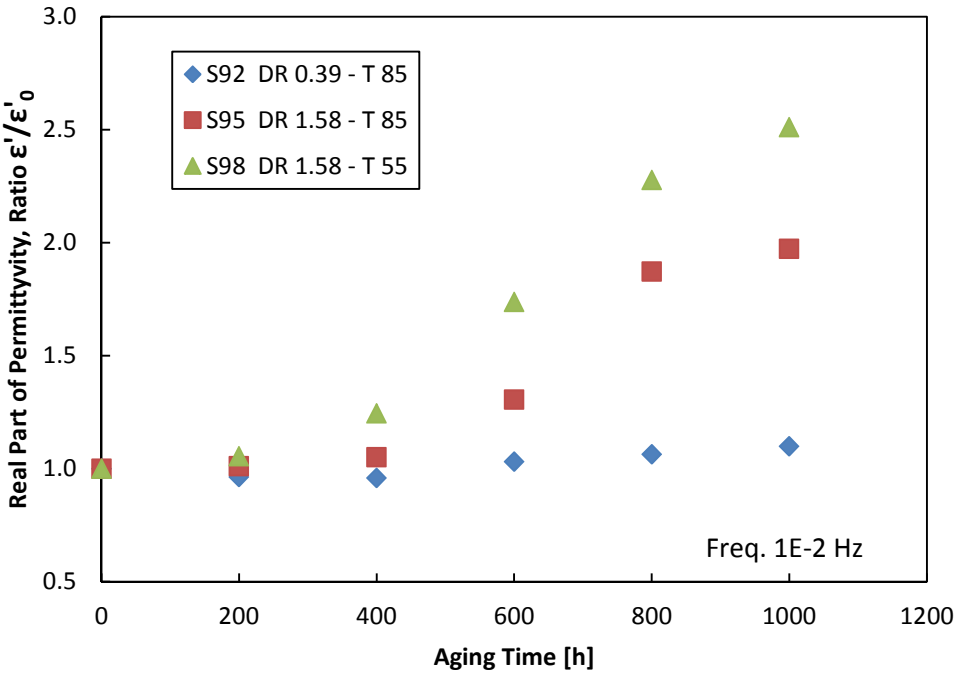

Figure 6.9 Real part of permittivity measured with dielectric analyzer, at a reference frequency of 10^{-2}Hz, vs. aging time for the three DR-T combinations. Permittivity is reported in relative value to that measured on unaged specimens.

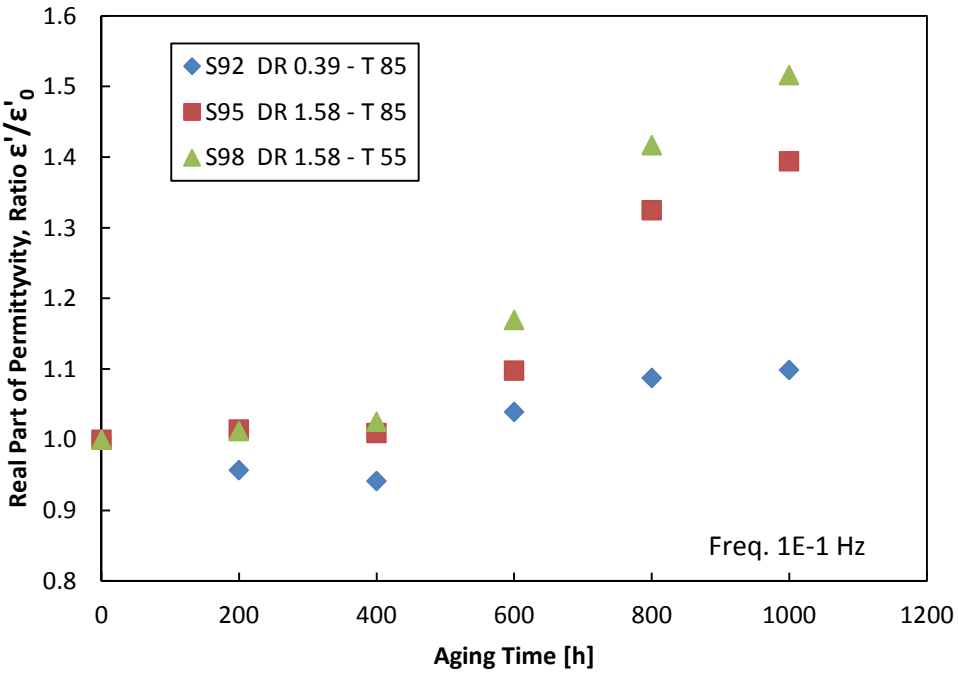

Figure 6.10 Real part of permittivity measured with dielectric analyzer, at a reference frequency of 10^{-1} Hz, vs. aging time for the three DR-T combinations. Permittivity is reported in relative value to that measured on unaged specimens.

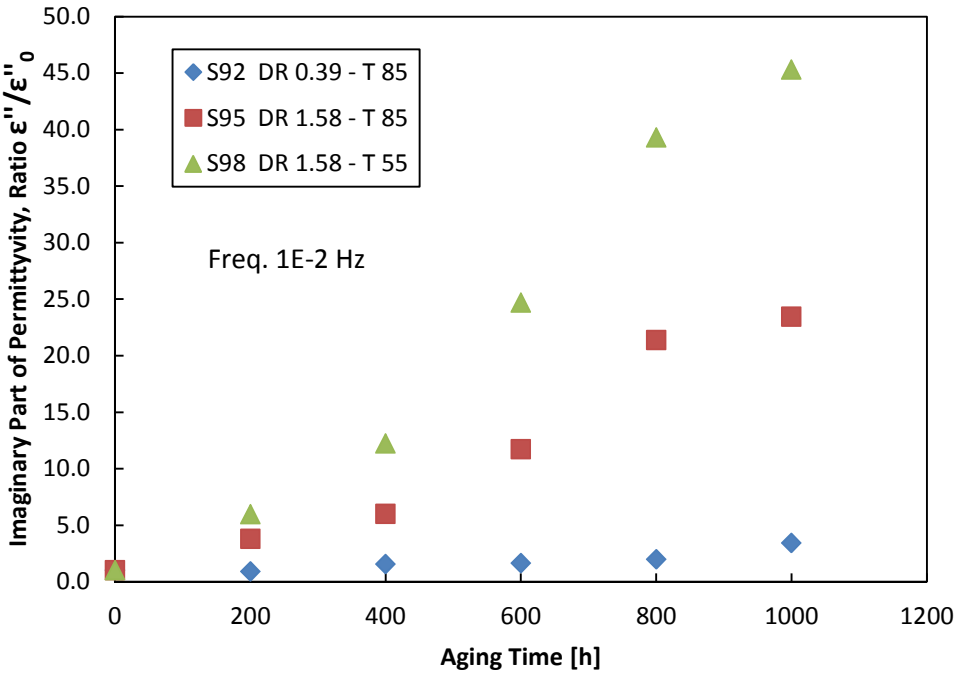

Figure 6.11 Imaginary part of permittivity measured with dielectric analyzer, at a reference frequency of 10^{-2}Hz, vs. aging time for the three DR-T combinations. Permittivity is reported in relative value to that measured on unaged specimens.

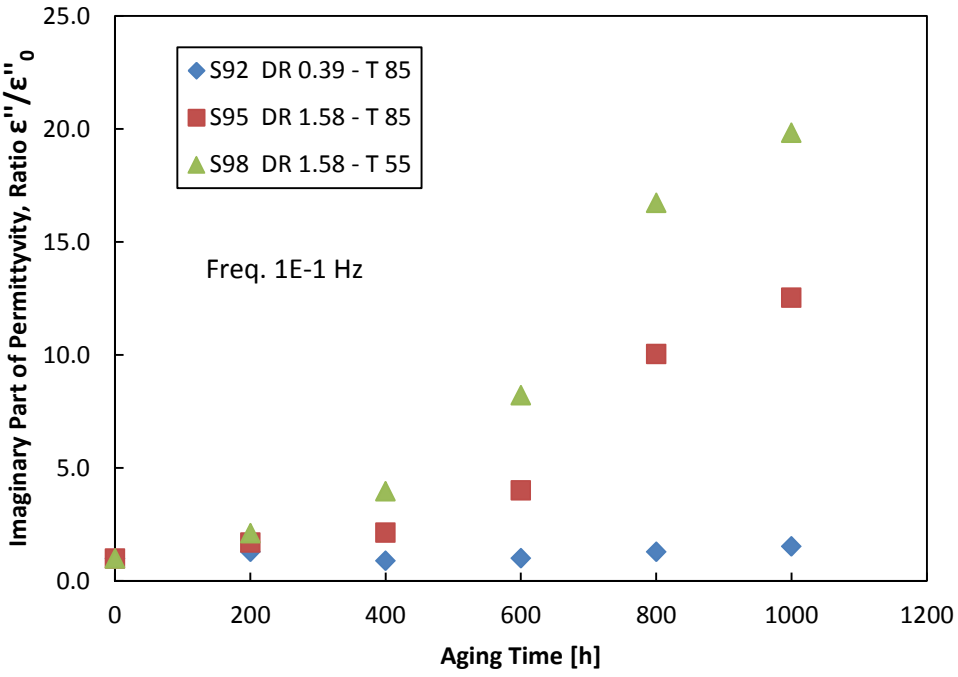

Figure 6.12 Imaginary part of permittivity measured with dielectric analyzer, at a reference frequency of 10^{-1} Hz, vs. aging time for the three DR-T combinations. Permittivity is reported in relative value to that measured on unaged specimens.

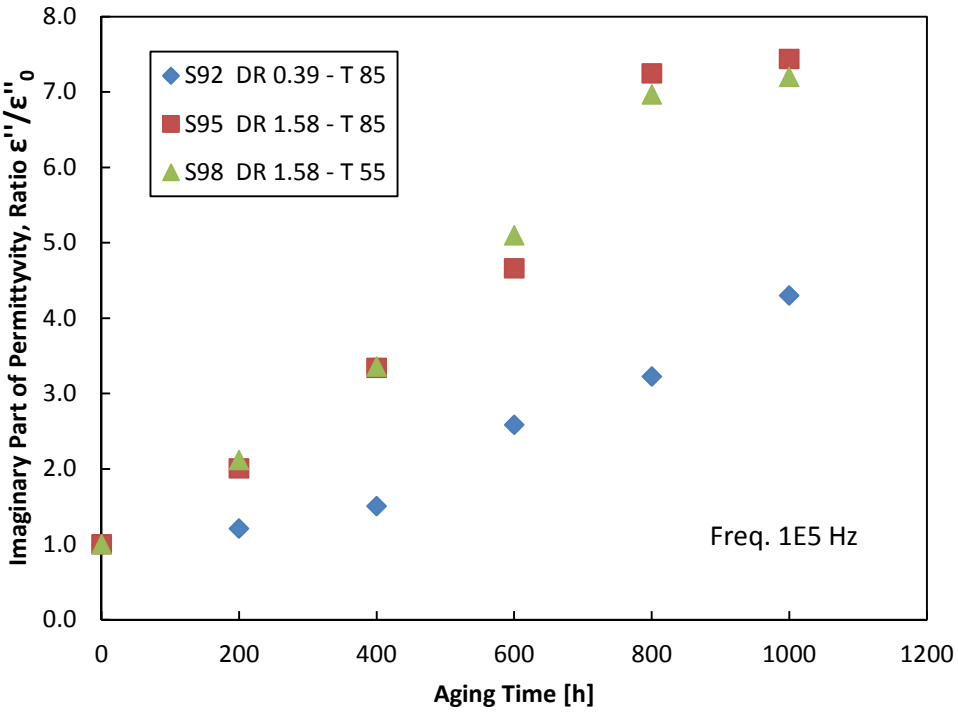

Figure 6.13 Imaginary part of permittivity measured with dielectric analyzer, at a reference frequency of 10^5 Hz, vs. aging time for the three DR-T combinations. Permittivity is reported in relative value to that measured on unaged specimens.

Dielectric spectroscopy results show noticeable increase of the real part of the permittivity with aging time, particularly evident at low frequency, i.e. 1E-2 Hz. The trend is always monotone, with a change of slope which usually occurs at 1 Hz. At the lowest frequency analyzed, the range of values varies from the value of 2.5 of S921 cable, the less aged, to a value of 6.3 of S985 cable, the more radiation aged as S955, but at lower temperature. Effects of aging are progressive with aging time and clearly appreciable.

The increment of the imaginary part, if we consider relative values to those measured on unaged specimens, is even greater. Peaks of polarization are present only in cables aged for 200 and 400 hours at DR5 (see Figure 6.6) but they suddenly disappear for more long aged cables, and for the S923 specimen. S98x shows no peaks. The nature of those peaks of the imaginary part is unclear.

As usual, unaged cable displays a different behavior, presenting a polarization peak of the imaginary part of permittivity centered at about 10 Hz. The trend of the real part, however, remains below the curves of aged cables.

For the real part of permittivity, the comparison in relatives terms to that measured on unaged specimens has been done at 1E-1 Hz (see Figure 6.10) and at 1E-2 Hz (Figure 6.9). At higher frequencies, the variation of this property is low. In both cases we got the so-called "inverse temperature" character observed by Celina and co-workers [35][36][37][43]: this means that the variation of the property (comparing specimens aged at the same dose rate, in the present case 1.58 kGy/h) is greater for specimens aged at lower temperature (typically at around 60°C or below) than at more elevated aging temperatures. The inverse temperature behavior at low frequency was confirmed also by polarisation/depolarisation current measurements. Many EPR/EPDM and XLPE/XLPO materials show this effect.

The phenomenon has only been recognized relatively recently. It has been seen in polyolefin materials which have been radiation aged in air at temperatures below their crystalline melting point. Under these conditions, degradation is more rapid at the lower temperatures than at higher temperatures, which is opposite to what would be expected from normal kinetics of chemical reactions. However it is now realized that the reverse temperature effect is a function of the semi-crystalline nature of the polyolefins. Polyethylene based materials are semi-crystalline and their mechanical properties are determined by their microstructure at the supermolecular level. The material contains randomly oriented crystalline regions linked by amorphous tie molecules. During radiation aging, reactive species such as radicals are generated uniformly throughout both crystalline and amorphous regions. In the crystalline regions at temperatures well below the melting point, these species are trapped and are unable to react to form oxidative products because of the low chain mobility and the low oxygen diffusion rate in the crystalline region. Degradation then proceeds primarily through oxidative scission reactions in the amorphous regions, where both chain mobility and oxygen diffusion rates are higher. Since the amorphous regions form the tie molecules between the

crystalline blocks, chain scission in these regions has a marked effect on the mechanical properties. If the radiation ageing occurs at slightly higher temperatures, nearer the melting region for the crystalline portion, then chain mobility is high enough for the trapped species to react to form chemical crosslinks. In addition, the enhanced mobility enables some recrystallization to occur which can reform tie molecules which were broken by oxidative scission in the amorphous regions. The combination of these effects is to effectively restore some of the damage which is created by the radiation aging. The overall macroscopic effect is a reduced rate of degradation at the higher temperature during radiation aging.

For the imaginary part of permittivity, the comparison in relative terms has been done at 1E-2 Hz (Figure 6.11), 1E-1 Hz (Figure 6.12) and 1E+5 Hz (Figure 6.13). At the two lower frequencies, also this property shows the "inverse temperature" behavior. On the other hand, it is interesting to notice that at 1E+5 Hz only the effect of the dose rate is evident, while the effect of the temperature becomes negligible (the "inverse temperature" effect disappears). Furthermore, at 1E+5 Hz the variation of the imaginary part of permittivity for specimens S92x becomes greater and more clear, compared with its variation at low frequency.

For sake of clarity, both experimental points of the real and imaginary part of conductivity has been plotted as a function of the total absorbed dose expressed in kGy at the fixed frequency of 1E-1 Hz (Figure 6.14 and Figure 6.15). As stated above, starting from 400 kGy the reverse temperature effect is clearly evident. This seems to be in contradiction with what has been reported literature[5]. Real part of permittivity shows a worse behavior at lower dose rate. It is well-known that, at lower irradiation rates, the oxygen has more time to diffuse through the material and the oxidized zone is deeper. Note also that for the imaginary part there is a good correspondence in the results: e.g. cables

[5] It has been observed that at high dose rates, generally above 0.5 kGy/h, an increase in temperature has very little effect on the DED value, whereas at low dose rates, temperature has a very large effect. At high dose rates, radiation degradation mechanisms will dominate the overall degradation process. At low dose rates, thermal degradation processes will dominate and the slope of the plot of DED versus dose rate will approach a value of 1, i.e. a constant time [43].

S924, S951 and S981, aged at different DR-T combinations but having the same absorbed dose, show very close electrical properties. This leads to the hypothesis (to be confirmed with other tests) that for the imaginary part the behavior of the samples at low frequencies, besides being influenced by the aging temperature, is more dependent on the dose absorbed rather than by the dose rate.

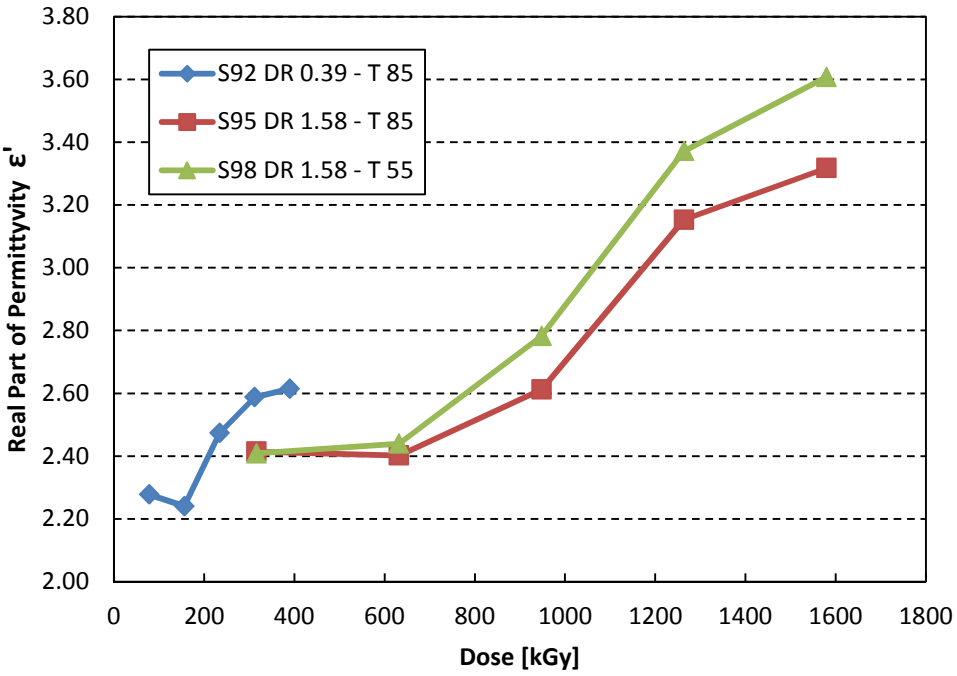

Figure 6.14 Real part of permittivity, at a reference frequency of 10^{-1} Hz, vs. absorbed dose for the three DR-T combinations.

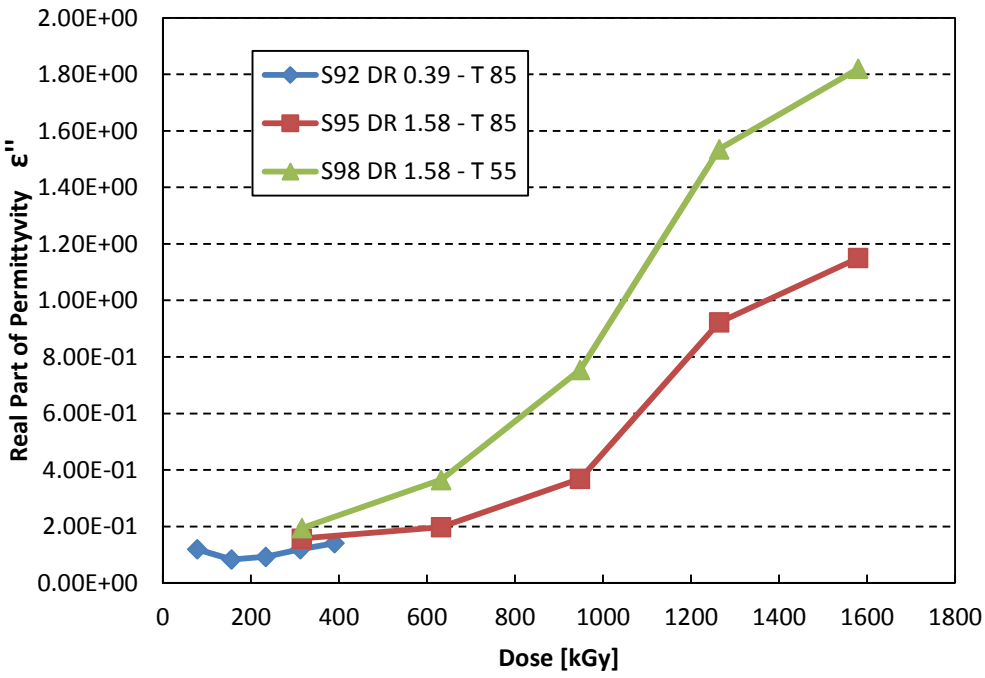

Figure 6.15 Imaginary part of permittivity at a reference frequency of 10^{-1}Hz, vs. absorbed dose for the three DR-T combinations.

6.2 Mechanical analysis description and results

Mechanical properties are investigated through tensile testing, i.e. elongation at break (EaB) and Young's modulus.

When performing tensile test, the specimen is extended along its longitudinal axis at constant speed until it fractures. During the test, the load sustained on the specimen and its elongation are measured. Elongation at break rather than tensile strength is used because for some polymers, particularly thermoplastic, the strength may remain consistently equal to the yield strength after aging even when EaB has decreased to <50% absolute. The method is related to the long chain molecular structure of the polymer. As degradation proceeds, changes usually decrease the elongation at break. Dumb-bell specimens shall have the so-called bone-shape with specified dimensions. Tubular samples are used when the core diameter is too small to enable dumb-bell samples to be cut; they are prepared by removing the conductor from lengths of the insulation material and end tabs or soft inserts are needed to prevent breakage in the grips of the tensile testing machine. A minimum of 5 test specimens is required to obtain reasonable confidence; the arithmetic mean and standard deviation are calculated. Data from any samples which broke in the grips or slipped from the grips are not taken into account. The load exerted on the sample and the correspondence distance between the grips is recorded during the test, using an automated recording system which displays the load-elongation curve during the test, this until specimen breaks. Examples of typical curves are shown in Figure 6.16.

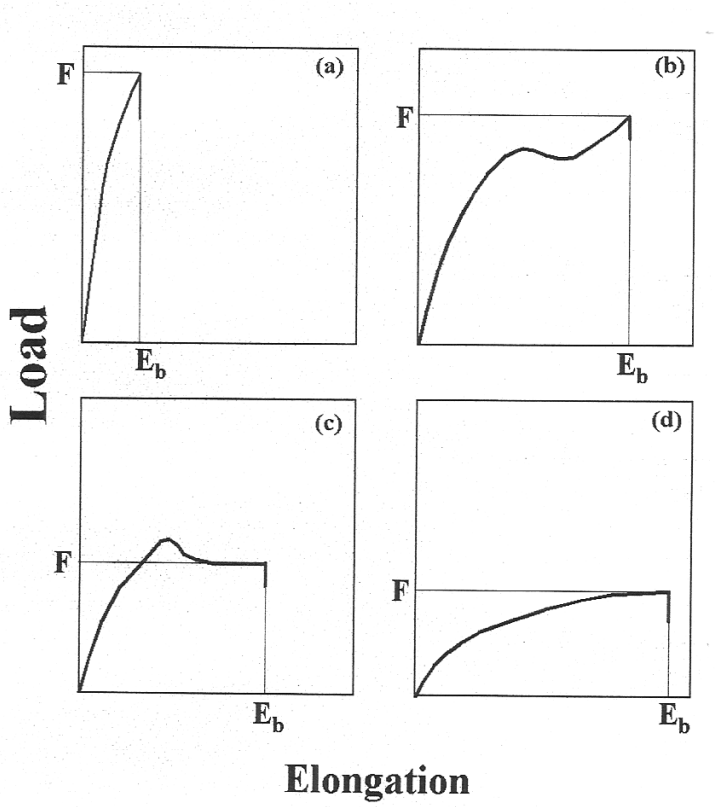

Figure 6.16 Typical load-elongation curves: (a) for a brittle material; (b) and (c) for a material with a yield point; (d) for a material without a yield point. For every types of curve, the values of elongation E_b and load F at break are indicated.

Both for dumb-bell and tubular samples the elongation at break is calculated from:

$$EaB(\%) = 100 \cdot \frac{E_b - E_0}{E_0} \tag{6.2}$$

Where E_b is the distance between the specimen grips at break and E_0 is the initial distance between grips. Tensile strength σ and Young's modulus *E*, both expressed in MPa, can also be extracted from the test, as follow:

$$\sigma = \frac{F}{A} \tag{6.3}$$

where F is the measured load at break, measured in Newton and A is the initial cross-sectional area of the specimen, expressed in mm^2. Young's modulus, *E*, can be calculated by dividing the tensile stress by the tensile strain in the elastic (initial, linear) portion of the stress-strain curve.

For S9 cable insulation the tensile properties were measured using a load frame testing machine with extension rate of 50 mm/min and initial gauge length of 40mm. Samples (dumb-bell type) were conditioned at 25°C and 50% relative humidity for 24 hours prior to testing, in order to avoid possible influences on mechanical properties of some polymeric materials by the moisture content. Values are reported in relative value to that measured on unaged specimens.
For sake of clarity, results for unaged samples are reported in Table 6-2, thus obtaining dimensional values for aged cables.

Table 6-2 Mechanical properties of unaged EPR cable.

CABLE S900	Mean value	Err. Abs
EaB (%)	322	12
Young's Modulus (MPa)	2.83	0.16

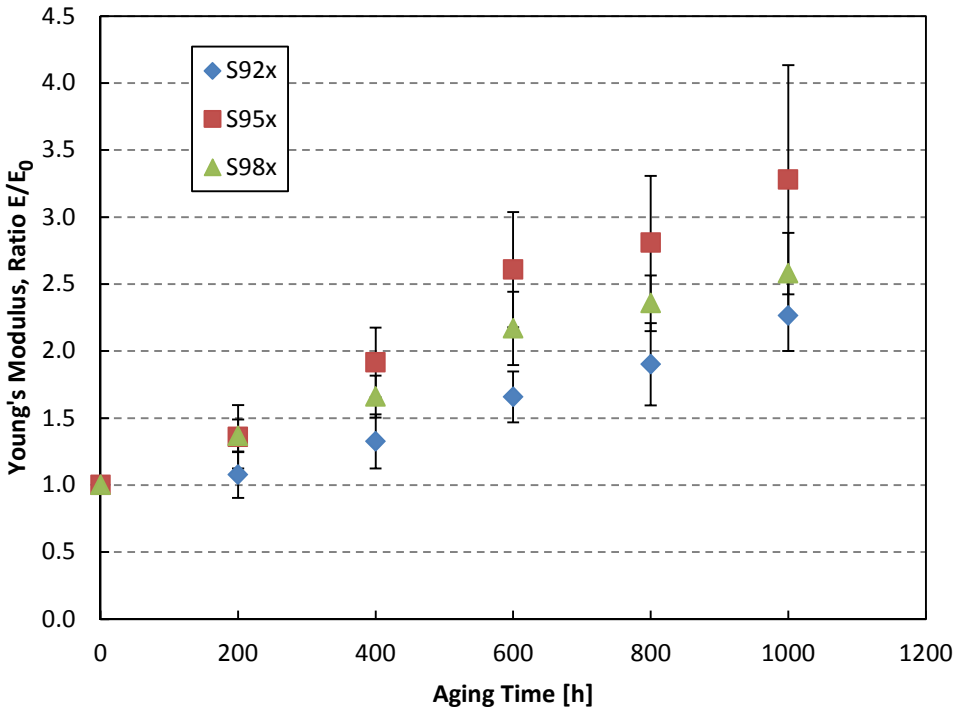

Figure 6.17 Young's Modulus vs. aging time for S9 cable. Young's Modulus is reported in relative value to that measured on unaged specimens.

Figure 6.17 and Figure 6.18 present the results of mechanical tests on specimens S9 at the three DR-T combinations of accelerated aging performed. Figure 6.17 shows the Young's modulus as a function of the aging time; this property appears to vary gradually with aging, as well as electrical properties do. Cables S95x, aged at the highest dose rate and temperature combination, show the worst behavior, while the less aged S92x the best.

Figure 6.18 shows the decrease of the Elongation at Break (EaB) with aging time, as it is usually reported in literature for NPP cables.

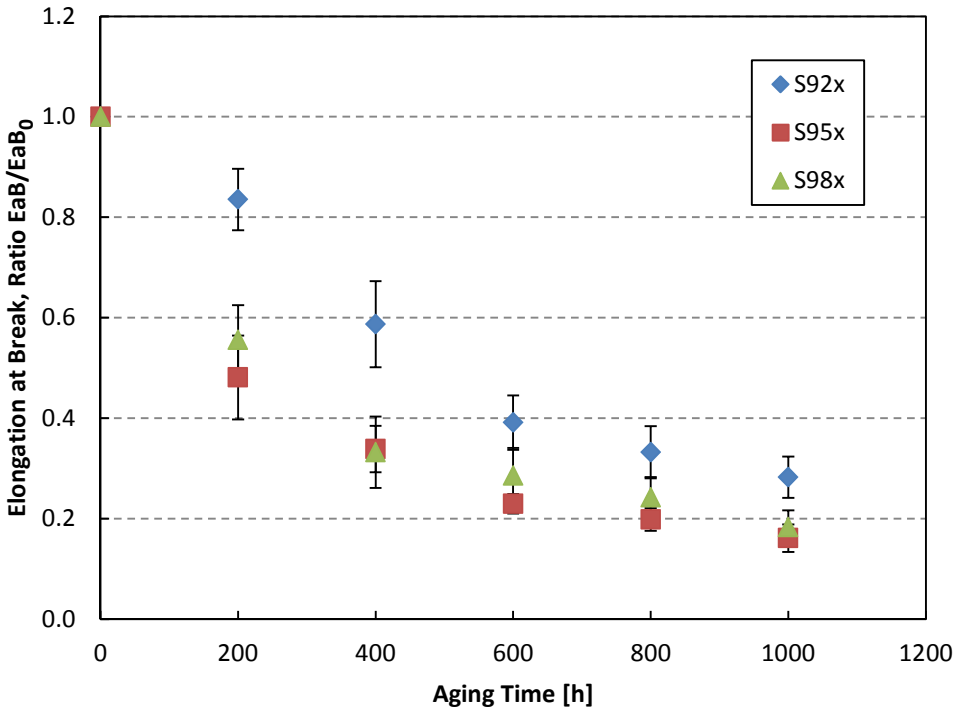

Figure 6.18 Elongation at Break vs. aging time for S9 cable. Elongation at Break is reported in relative value to that measured on unaged specimens.

This behavior is particularly evident in the first 600 aging hours, then variations are smaller. Cables aged at 1.58 kGy/h present an halving of the EaB value even after 200 aging hours and almost no temperature dependency. Cables S92x, aged with the minimum dose rate, display better mechanical properties as expected. A considerable damage is reached only after 1000 aging hours (EaB collapses down to 30 percent of the initial value), while S95x and S98x, aged at the same dose rate (higher than DR2) but at different temperatures, show an even greater decay of properties but no "inverse

temperature" effects. However, considering the size of error bars, specimens S95x and S98x produced very close results.

6.3 Discussion

The large variation of mechanical properties confirms the effectiveness of accelerated aging to which the cables have been subjected. The variation of the measured electrical properties is therefore due to effective aging of the insulating material. The higher the dose rate, the larger the effect on electrical property variation. Aging time is also a determining factor and this is proportional to the electrical as well as mechanical degradation of the polymer.

As already said in the introductive chapter, one of the aim of this thesis is to find reliable electrical diagnostic markers. For the EPR specimen tested a correlation of tensile test with low-frequency dielectric response cannot be made, since for specimens subjected to the higher doses mechanical analysis shows no “inverse–temperature” effects.
However, at high frequencies there is no evidence of inverse-temperature effects both for mechanical and electrical properties. This is the reason why an attempt to correlate electrical permittivity and mechanical properties has been done. In particular, Young’s modulus varies gradually with the aging time, thus a correlation seems to be possible between Young’s modulus and permittivity, obtained at high frequency, 10^5 Hz, of S92 cable aged with the lowest DR-T, 0.39 kGy/h. Figure 6.19 displays the interpolation of experimental points with a linear regression; the quality of correlation is estimated by the correlation coefficient *r*. For both real (a) and imaginary part (b) of permittivity, taking into account also the error bars (omitted in the graph) there is a good correlation with the tensile parameter resulting on large correlation coefficients, 0.93 and 0.98, respectively. Variations of ε' with time at the frequency of 10^5 Hz are very small, so in the follow only the imaginary part ε'' will be taken into account.

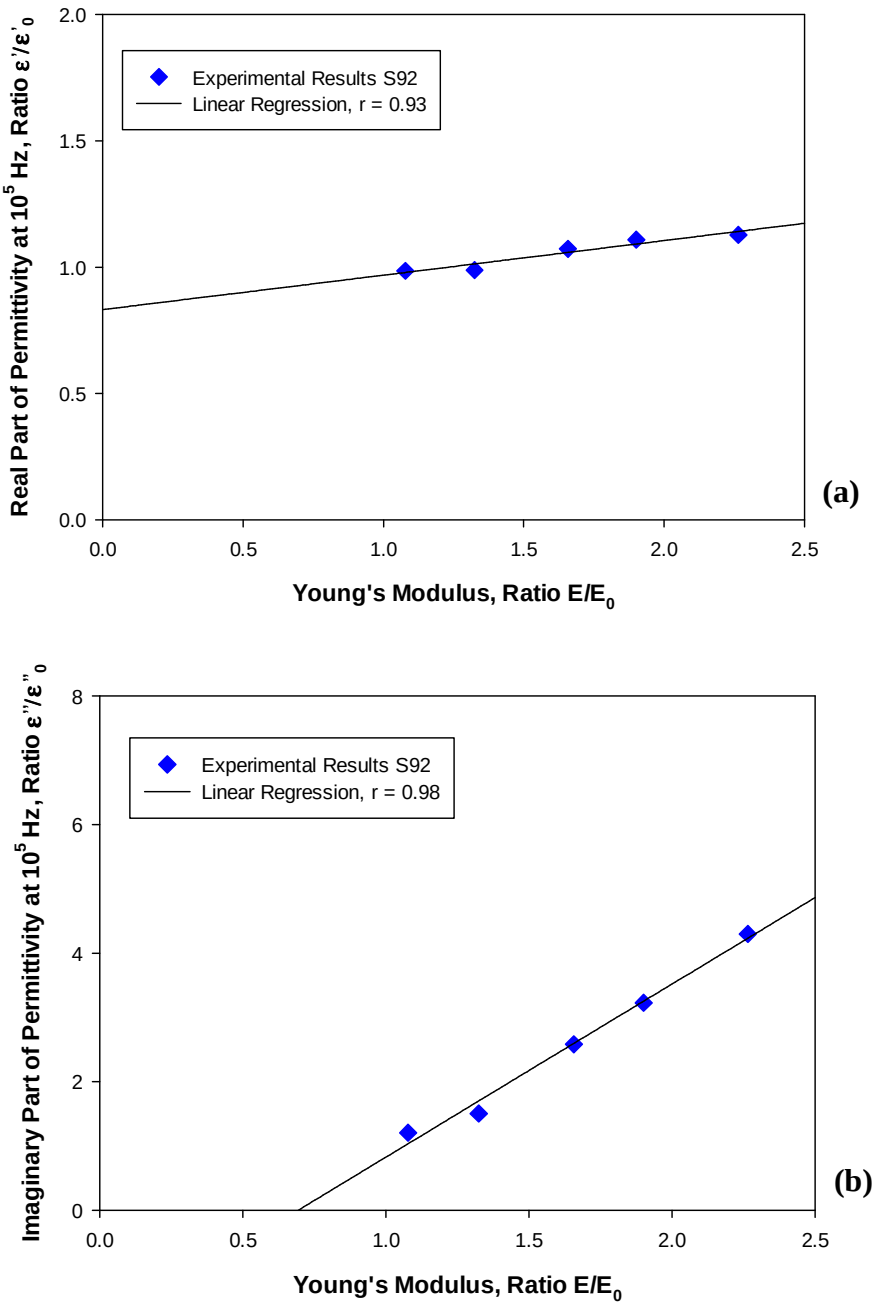

Figure 6.19 Correlation of the real (a) and imaginary part (b) of permittivity at 10^5 Hz with Young's modulus for specimen S92x (aged at 0.39 kGy/h–85°C).

Figure 6.20 shows in a log-log plot the correlation of the imaginary part of permittivity at 10^5 Hz with Young's Modulus, both in relative values to that measured on unaged specimens. A good matching between properties is clearly observable.

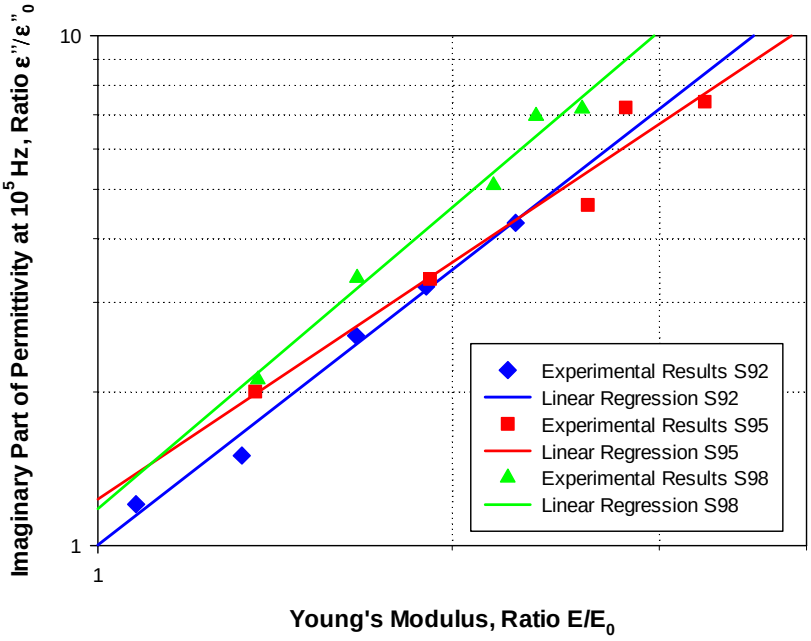

Figure 6.20 Correlation of the imaginary part of permittivity at 10^5 Hz with Young's Modulus for specimen S9.

The imaginary part of permittivity at 10^5 Hz has also been compared with Elongation at Break in relative value. EaB decreases with time while permittivity increases, so the graph should be read from right to left (see Figure 6.21). Even in this case a good correlation is noticeable.

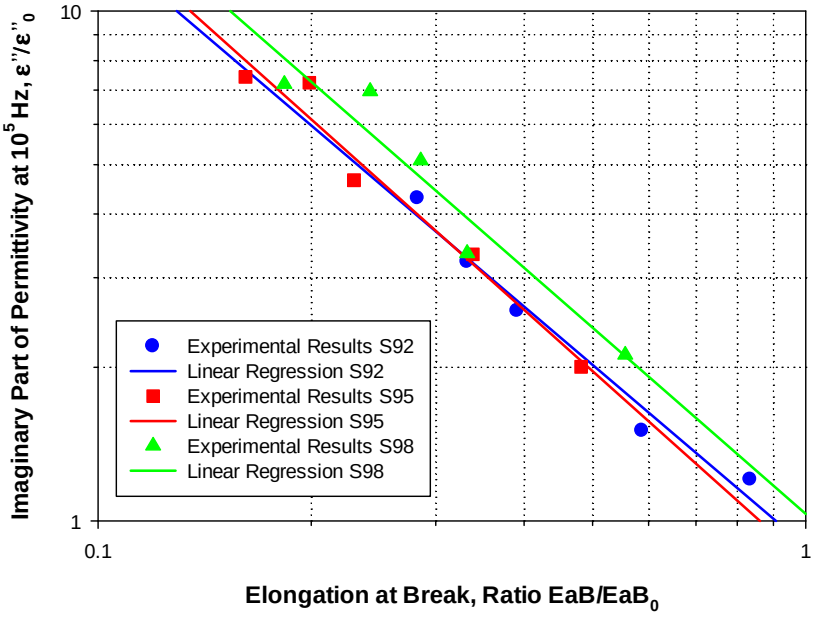

Figure 6.21 Correlation of the imaginary part of permittivity at 10^5 Hz with Elongation at Break ratio for specimen S92, S95 and S98.

Table 6-3 displays coefficients of determination r^2: these are all above the value of 0.92, confirming that the regression lines fit very well the set of experimental data.

Table 6-3 Square correlation coefficients r^2 used for linear regressions, cable insulation (S9).

r^2	ε'' (10^5 Hz)-Young	ε'' (10^5 Hz)-EaB
S92	0.987	0.975
S95	0.955	0.964
S98	0.983	0.925

Chapter 7

7 Dielectric response in EPDM/EVA samples

This chapter deals with dielectric response measurements on EPDM/EVA polymer samples. The label for this cable is S3: this LV cable has five conductors, each one with its colored insulation (see §4.3). In this thesis experimental dielectric response results refers to the "black" cable insulation. Further investigations will concern other different colored insulations. Results of electrical and mechanical test will be discussed and possible correlations between them will be proposed.

7.1 Experimental results

The results from dielectric analyzer are summarized in Figures from 7.1 to 7.24. Frequency behavior of the real and imaginary part of relative permittivity and of the dissipation factor are shown. The results refer to the eight DR-T combinations at which this cable insulation has been aged. Electrical properties are initially reported in absolute values as a function of frequency and then in relative values to those measured on unaged specimens as a function of aging time expressed in hours, for two fixed frequencies, i.e. 10^{-2} Hz, (Fig. 7.25 and 7.26) – and 10^{5} Hz, (Fig. 7.27 and 7.28). Some cables were tested only for aging corresponding to 200 h, 600 h and 1000 h of aging respectively.

Measurement were made at 50°C. Frequency ranged between 10^{-2}-10^{6} Hz with an input voltage of 3 V_{rms}. Characteristic parameters of cable S3 insulation for dielectric spectroscopy measurements are listed in Table 7-1 (equivalent diameter, thickness, area, reference capacitance).

Table 7-1 Cable S3 characteristic parameters for dielectric spectroscopy measurements.

CABLE	Set	d [mm]	s [mm]	S [mm^2]	C_0 [F]
S3	S3XX	52	1	2124	1.88E-11

Regarding the real part of the permittivity, reported in linear scale, a noticeable increase with aging time is particularly evident at low frequency, i.e. 10^{-2} Hz, but only for specimens S34 and S37 which have been aged at the highest dose rate of 2.74 kGy/h. The trend is always monotone, with a change of slope which usually occurs between 1 Hz and 100 Hz. At the lowest frequency analyzed, the range of values varies from a minimum of 6.3 to 19.8 for S345 cable, the one with the harshest DR-T combination. The effects of aging on electrical properties are progressive with time and clearly appreciable only for DR4 and DR7, while others DR display slight changes with aging time or non-monotone behaviors that impede any correlation with aging time. That is more evident looking at the plots reporting the real and imaginary parts of the permittivity at the frequency of 10^{-2} Hz in relative value of the unaged specimens (Figure 7.25 for real part and Figure 7.26 for imaginary part). For all DR-T conditions there is no evidence of "inverse-temperature" effects: the higher the aging temperature, the worse the properties.

Regarding the imaginary part of the permittivity, reported in logarithmic scale, the low frequency increase due aging is evident only for S34x and for S375 cables. For all cables we can appreciate a trend with a minimum at about 10^{4} Hz for lower dose rates. This minimum shifts slightly toward the low frequencies if the dose rate is increased. This "leftward shifting" behavior occurs, taking into account the same dose rate, even if the aging time is increased (see Figure 7.8 and Figure 7.17), and this comes with a shift upwards

of the curves. No peaks of relaxation have been found, neither for the new cable nor for those aged.

A peculiar behavior should be noted: after 200 h of aging, every cable shows better electrical properties when compared with the new cable, occurring regardless from the dose rate. This could be explained considering that the initial DR-T combination condition may act as pretreatment on the polymer, conditioning polymer molecular structure, without any impact on insulation aging.

As we stated above, at low frequencies changes of electrical properties with aging are detectable only for S34x and S37x, aged with the highest dose rate of 2.74 kGy/h. An attempt to highlight differences even for lower dose rates has been done by looking at high frequency permittivity, 10^5 Hz (Figure 7.27 and Figure 7.28). Even in this case, disregarding DR4 and DR7, dielectric properties deterioration appears minimal. However, behavior of S35x aged at 1.38 kGy/h displays higher values of permittivity than S36x aged at 0.85 kGy/h, as reasonably expected.

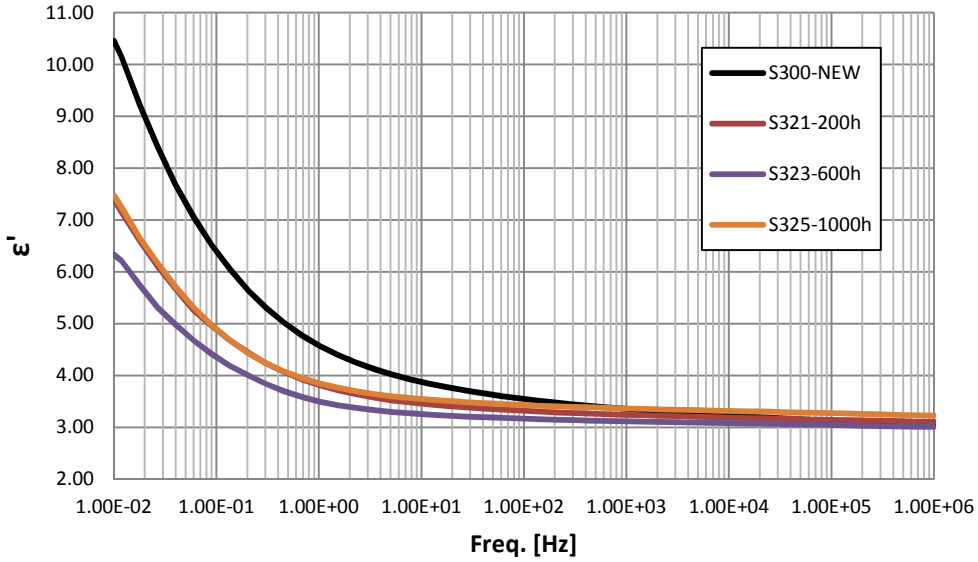

Figure 7.1 Real part of the permittivity for specimens S32x. DR2=0.42 kGy/h - T=85°C - Measurement temperature 50°C.

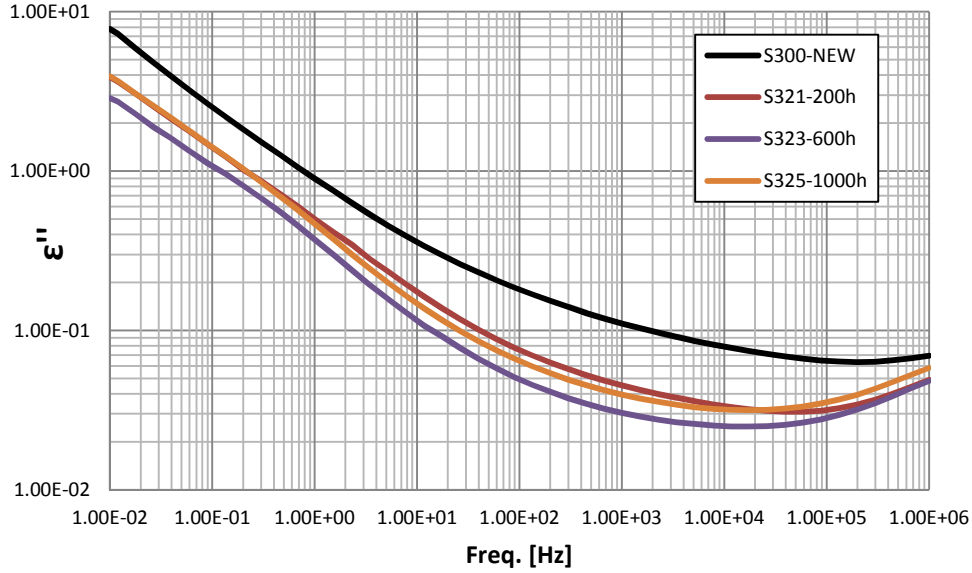

Figure 7.2 Imaginary part of the permittivity for specimens S32x. DR2=0.42 kGy/h - T=85°C - Measurement temperature 50°C.

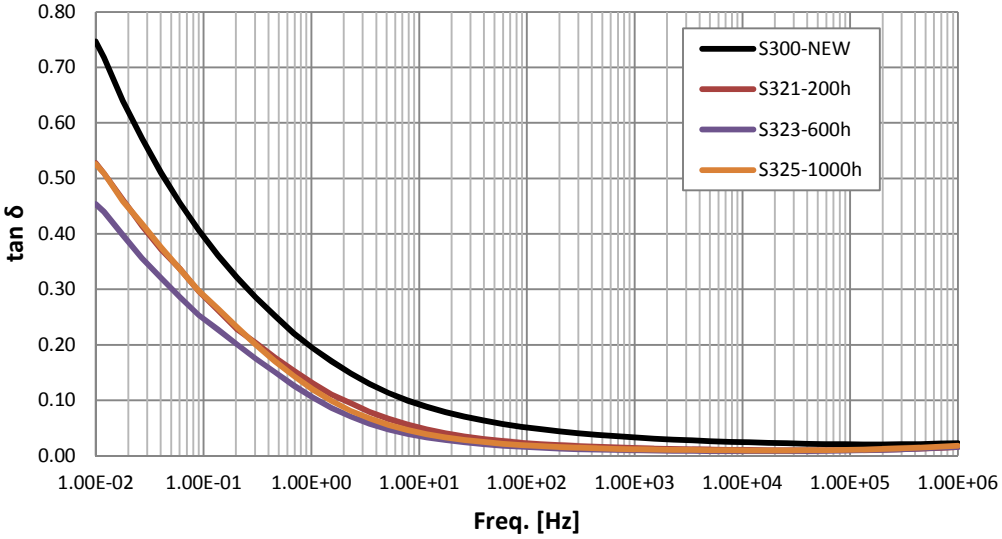

Figure 7.3 Dissipation factor for specimens S32x.
DR2=0.42 kGy/h - T=85°C - Measurement temperature 50°C.

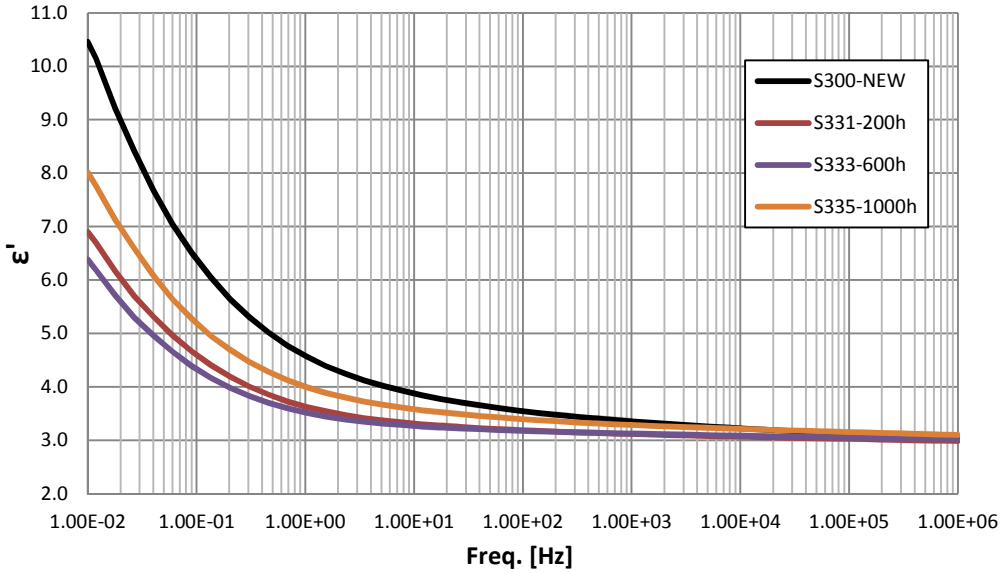

Figure 7.4 Real part of the permittivity for specimens S33x.
DR3=0.29 kGy/h - T=85°C - Measurement temperature 50°C.

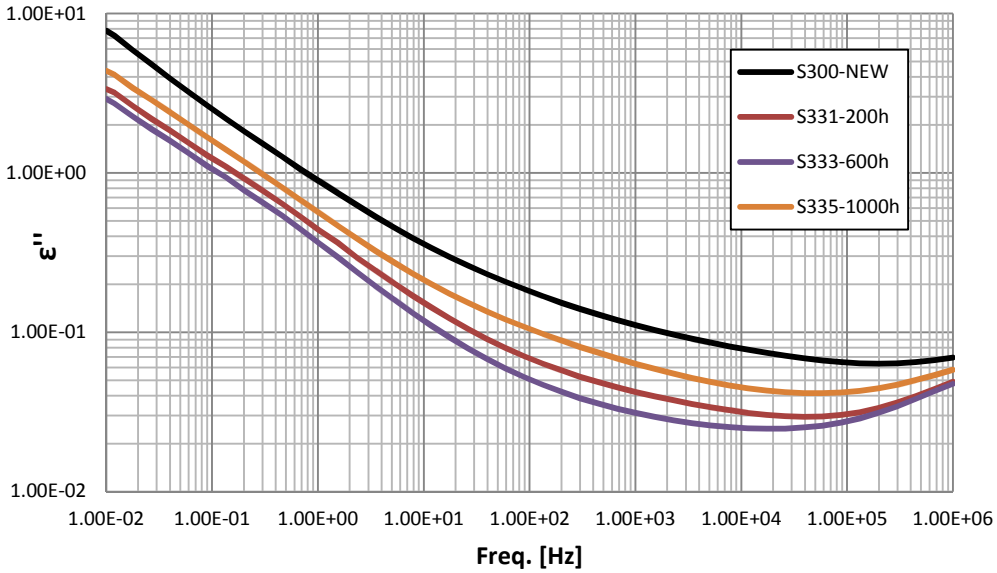

Figure 7.5 Imaginary part of the permittivity for specimens S33x. DR3=0.29 kGy/h - T=85°C - Measurement temperature 50°C.

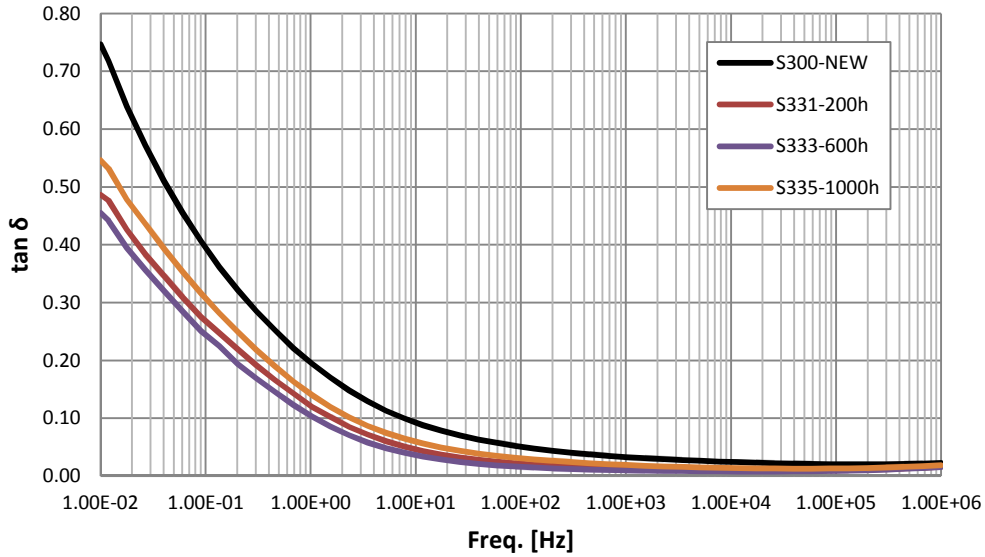

Figure 7.6 Dissipation factor for specimens S33x. DR3=0.29 kGy/h - T=85°C - Measurement temperature 50°C.

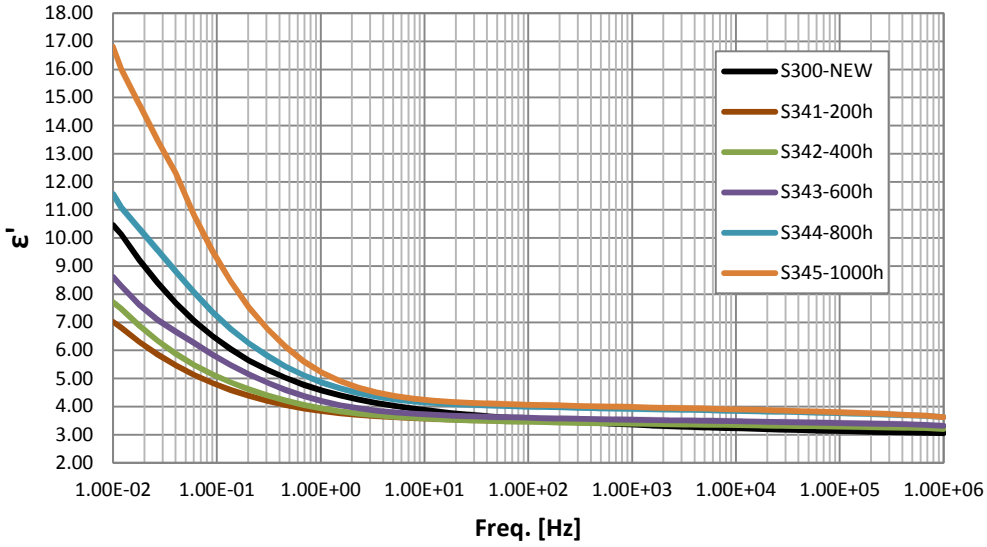

Figure 7.7 Real part of the permittivity for specimens S34x. DR4=2.74 kGy/h - T=85°C - Measurement temperature 50°C.

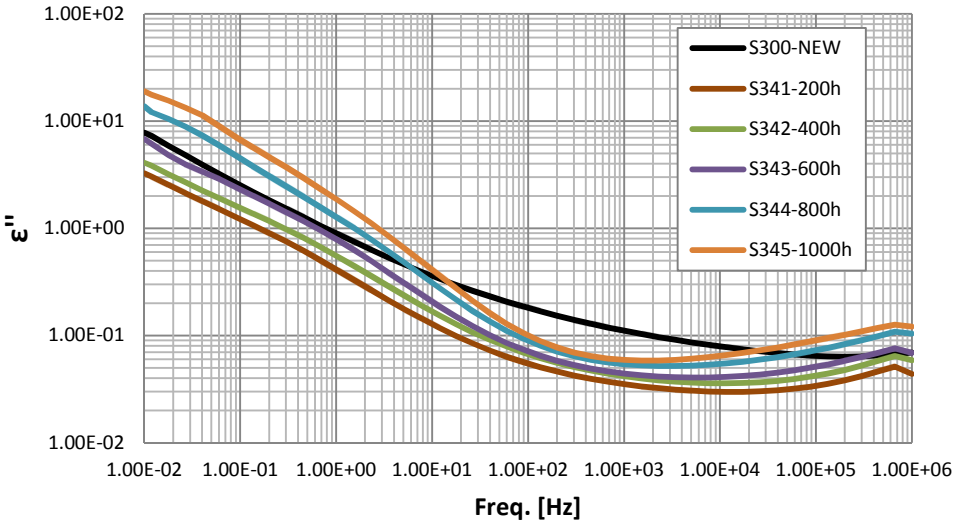

Figure 7.8 Imaginary part of the permittivity for specimens S34x. DR4=2.74 kGy/h - T=85°C - Measurement temperature 50°C.

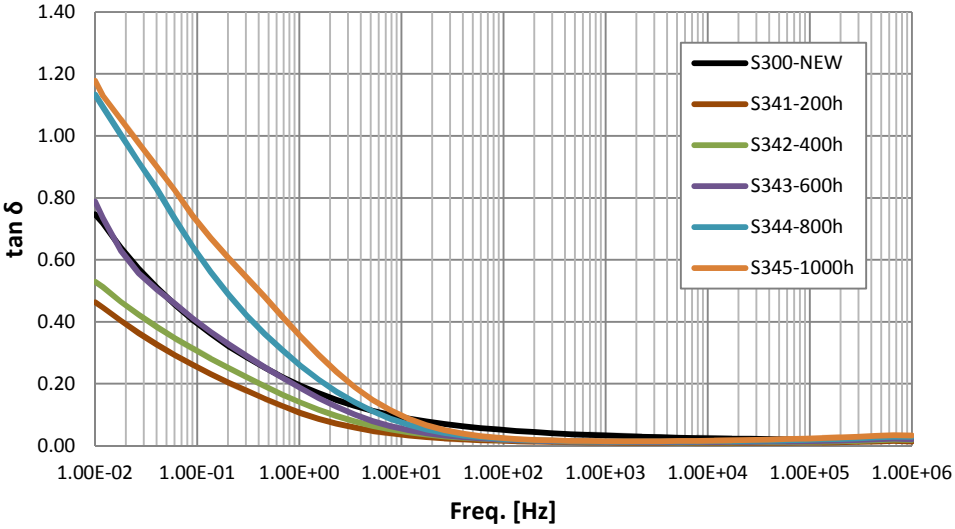

Figure 7.9 Dissipation factor for specimens S34x.
DR4=2.74 kGy/h - T=85°C - Measurement temperature 50°C.

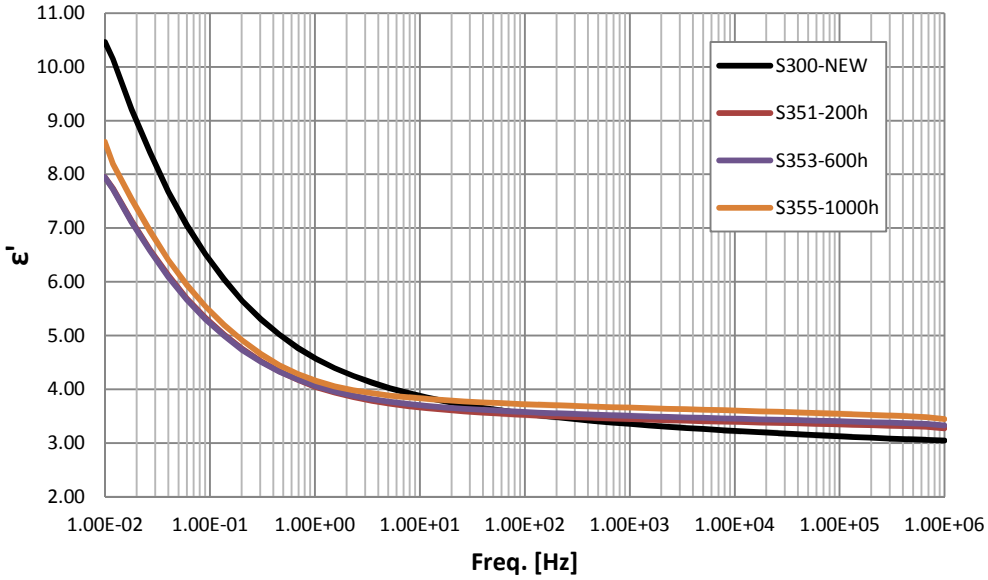

Figure 7.10 Real part of the permittivity for specimens S35x.
DR5=1.38 kGy/h - T=85°C - Measurement temperature 50°C.

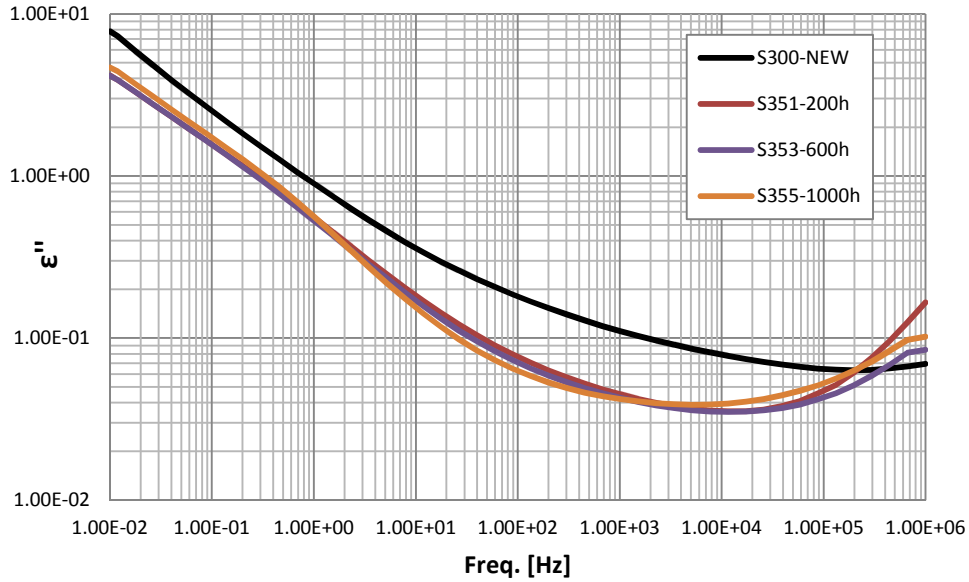

Figure 7.11 Imaginary part of the permittivity for specimens S35x. DR5=1.38 kGy/h - T=85°C - Measurement temperature 50°C.

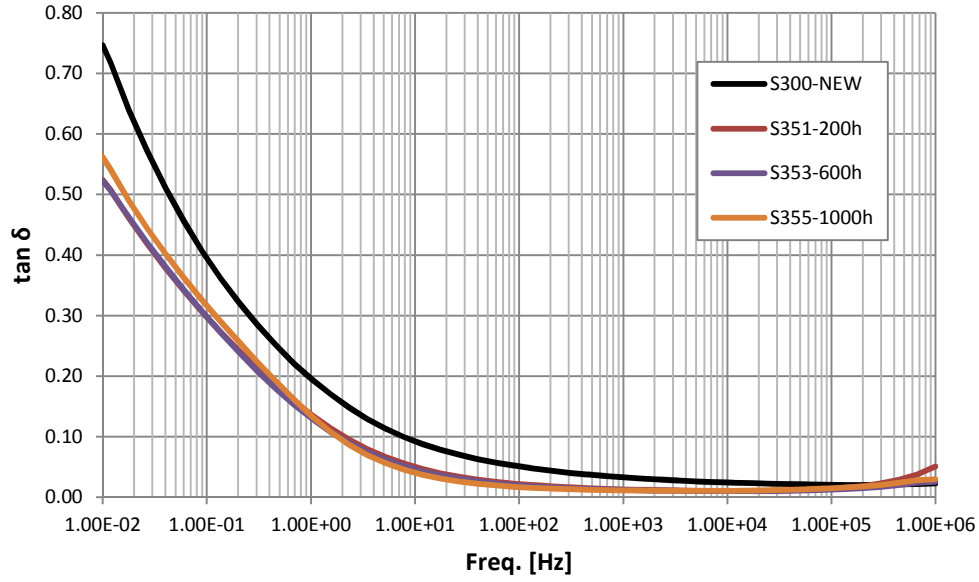

Figure 7.12 Dissipation factor for specimens S35x. DR5=1.38 kGy/h - T=85°C - Measurement temperature 50°C.

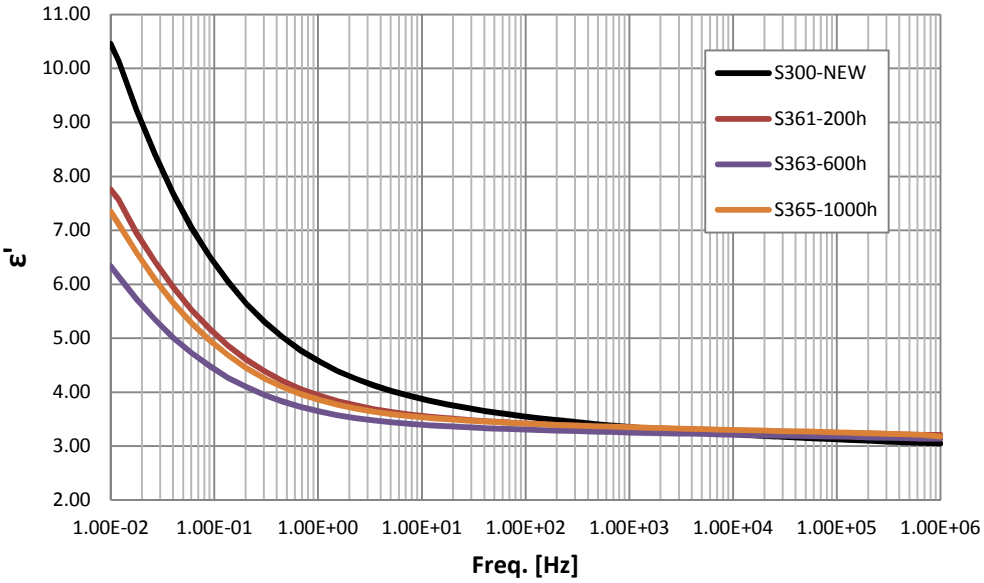

Figure 7.13 Real part of the permittivity for specimens S36x. DR6=0.85 kGy/h - T=85°C - Measurement temperature 50°C.

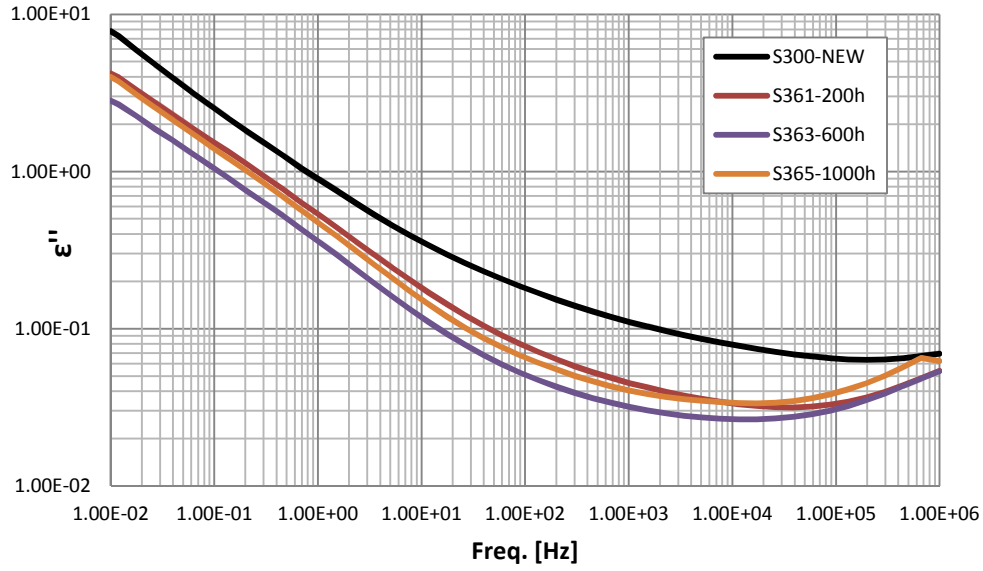

Figure 7.14 Imaginary part of the permittivity for specimens S36x. DR6=0.85 kGy/h - T=85°C - Measurement temperature 50°C.

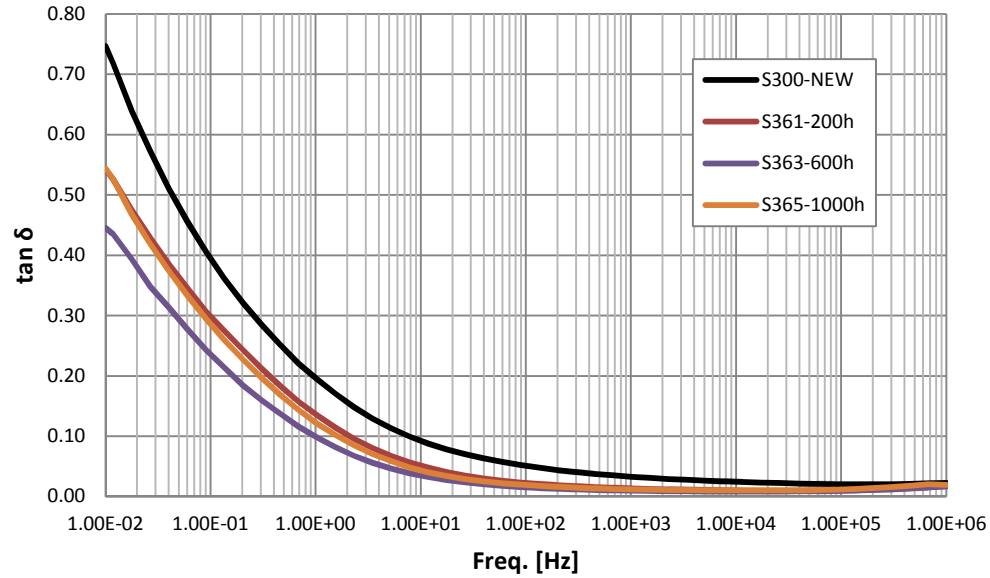

Figure 7.15 Dissipation factor for specimens S36x.
DR6=0.85 kGy/h - T=85°C - Measurement temperature 50°C.

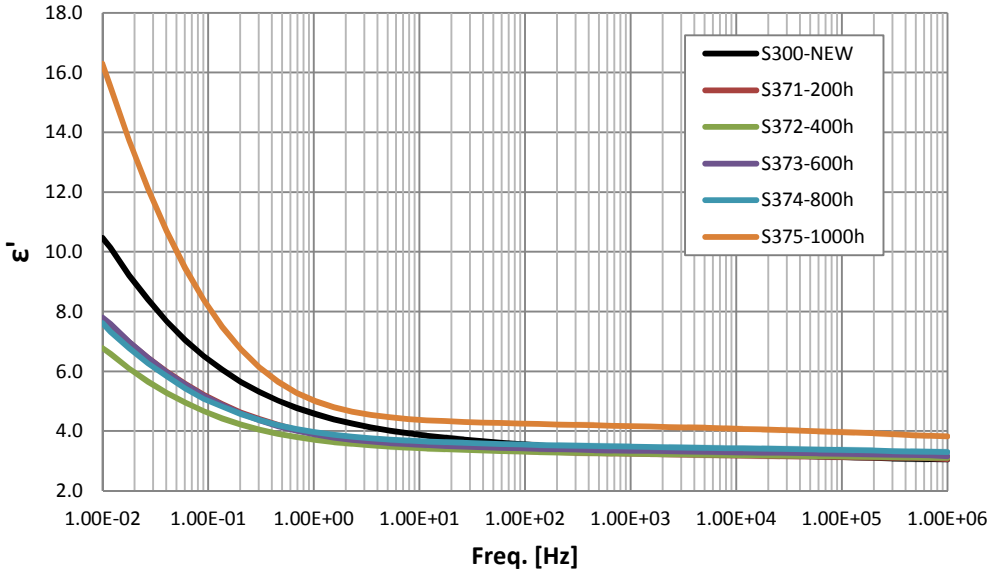

Figure 7.16 Real part of the permittivity for specimens S37x.
DR7=2.74 kGy/h - T=55°C - Measurement temperature 50°C.

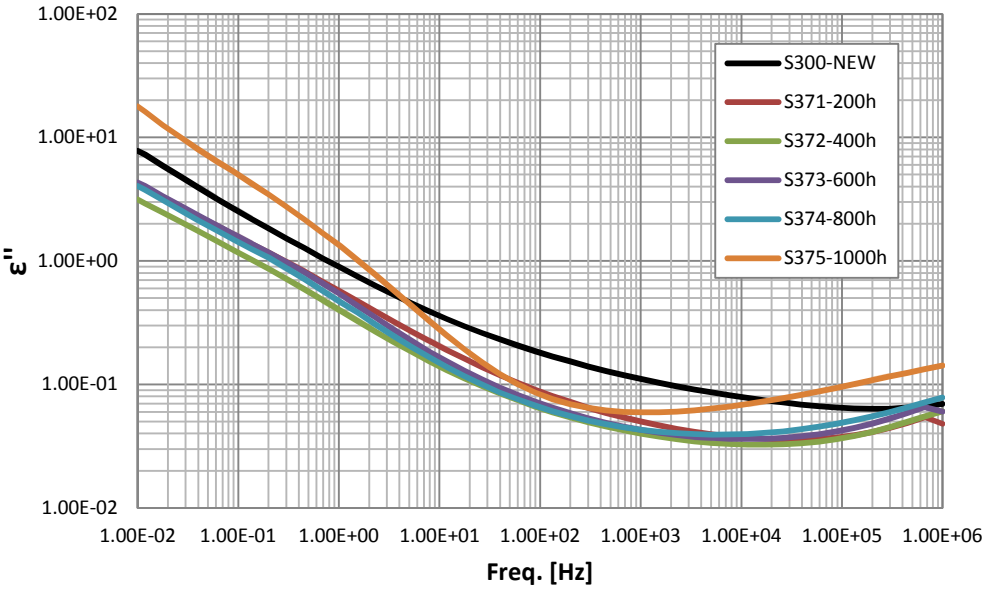

Figure 7.17 Imaginary part of the permittivity for specimens S37x. DR7=2.74 kGy/h - T=55°C - Measurement temperature 50°C.

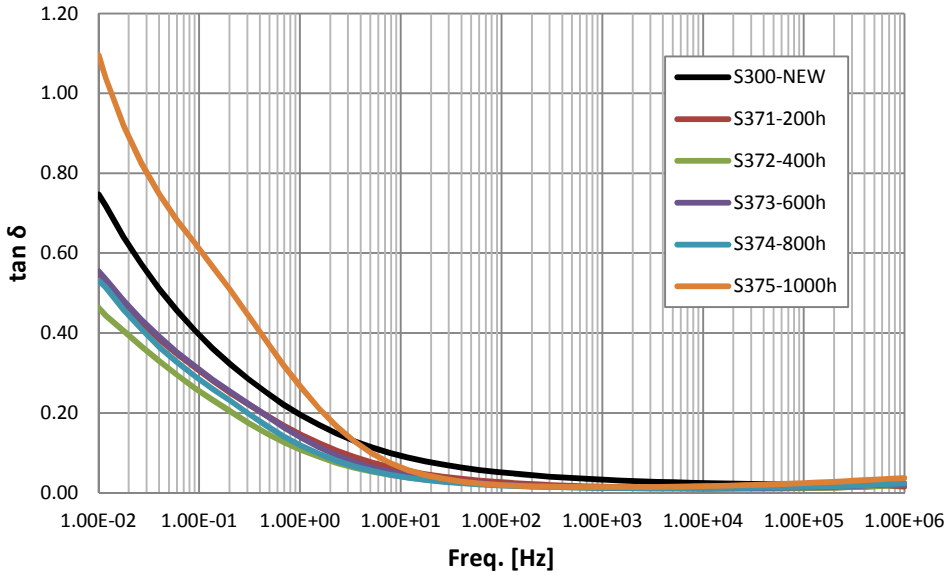

Figure 7.18 Dissipation factor for specimens S37x. DR7=2.74 kGy/h - T=55°C - Measurement temperature 50°C.

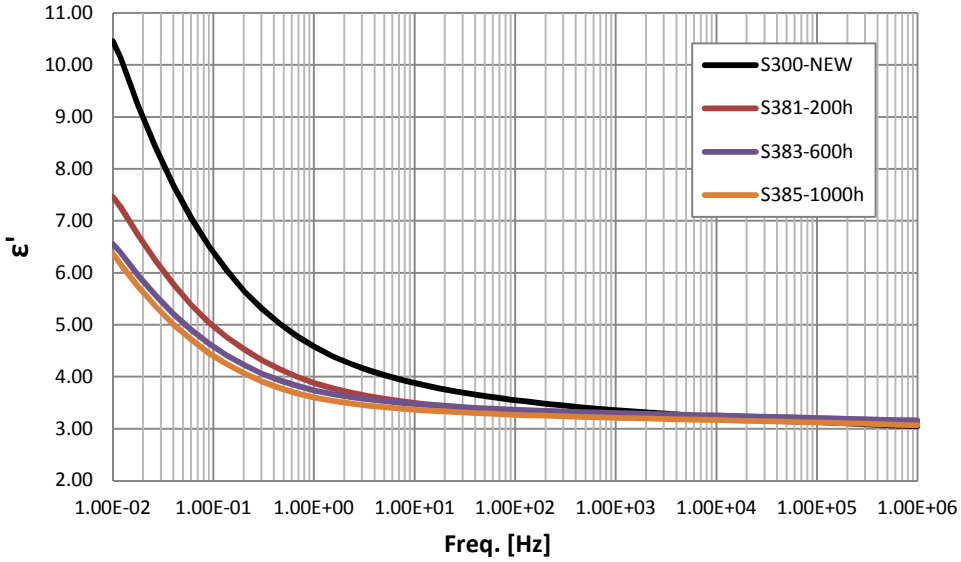

Figure 7.19 Real part of the permittivity for specimens S38x. DR8=1.38 kGy/h - T=55°C - Measurement temperature 50°C.

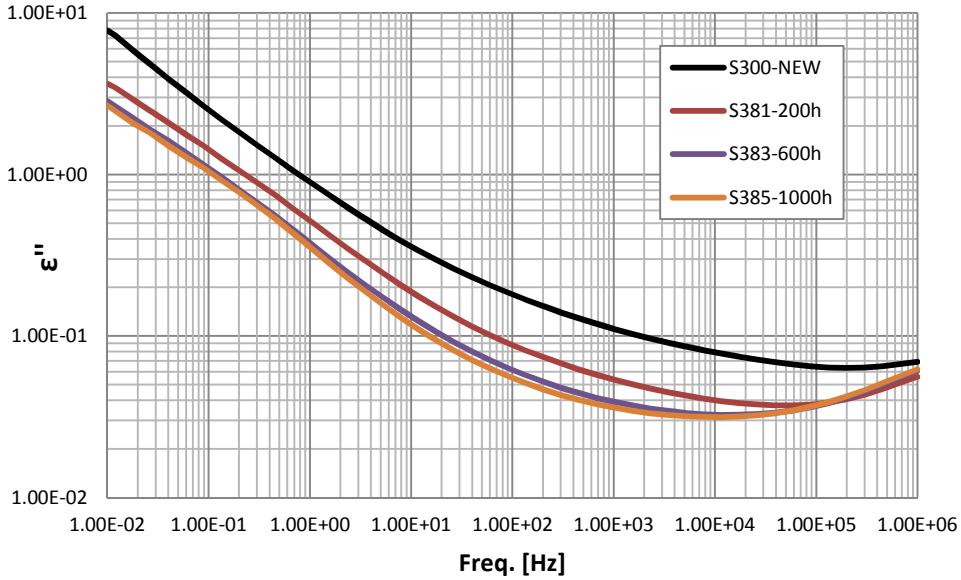

Figure 7.20 Imaginary part of the permittivity for specimens S38x. DR8=1.38 kGy/h - T=55°C - Measurement temperature 50°C.

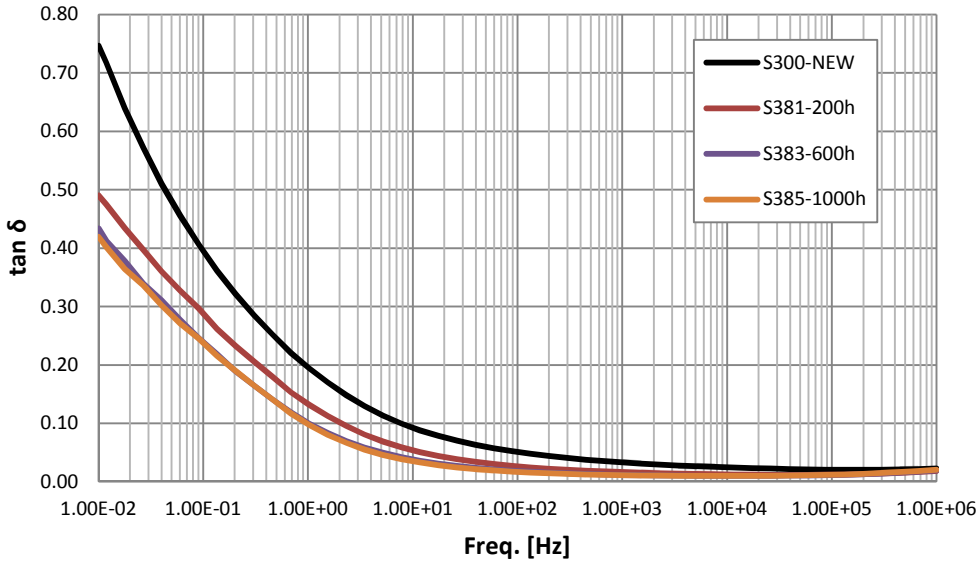

Figure 7.21 Dissipation factor for specimens S38x.
DR8=1.38 kGy/h - T=55°C - Measurement temperature 50°C.

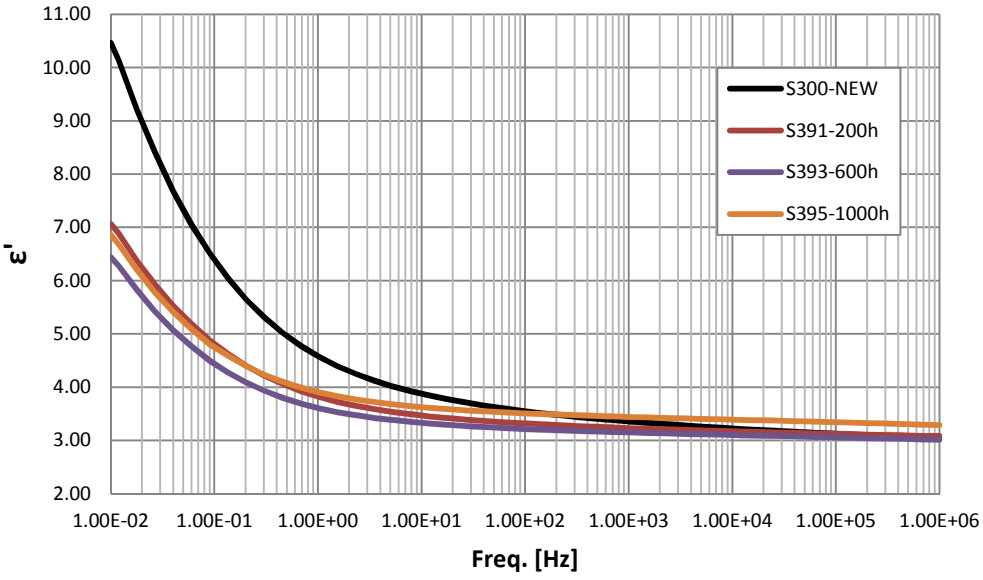

Figure 7.22 Real part of the permittivity for specimens S39x.
DR9=0.85 kGy/h - T=55°C - Measurement temperature 50°C.

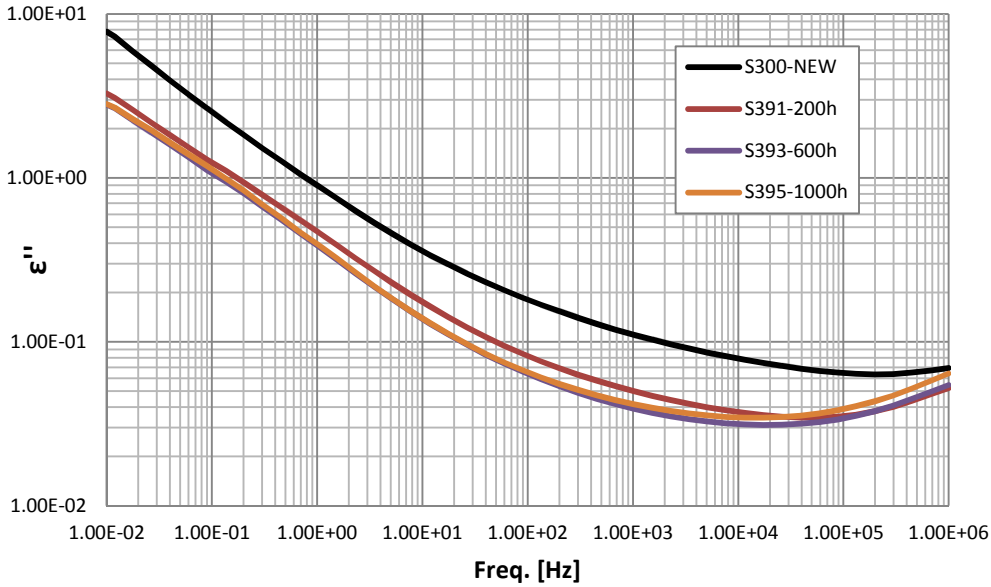

Figure 7.23 Imaginary part of the permittivity for specimens S39x. DR9=0.85 kGy/h - T=55°C - Measurement temperature 50°C.

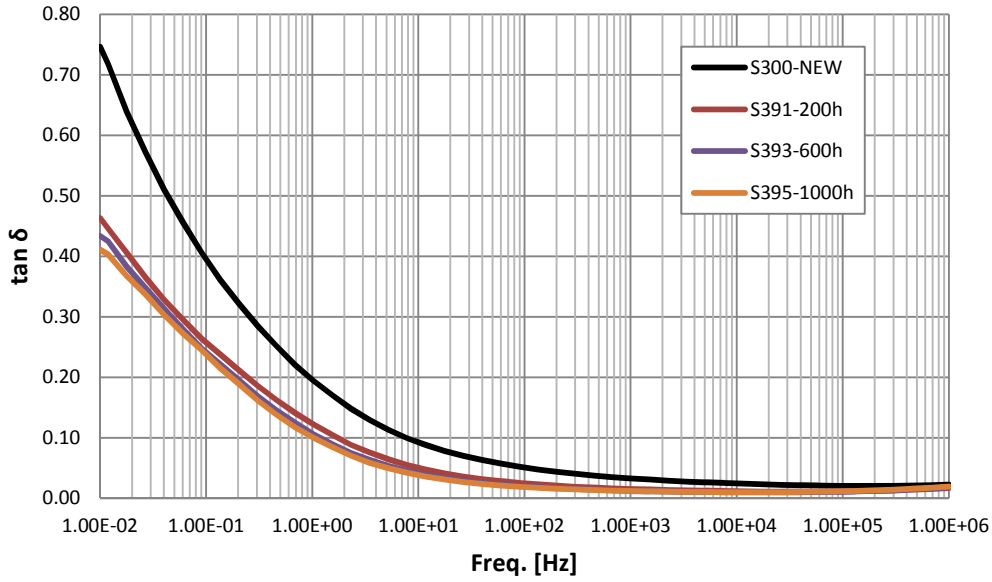

Figure 7.24 Dissipation factor for specimens S39x. DR9=0.85 kGy/h - T=55°C - Measurement temperature 50°C.

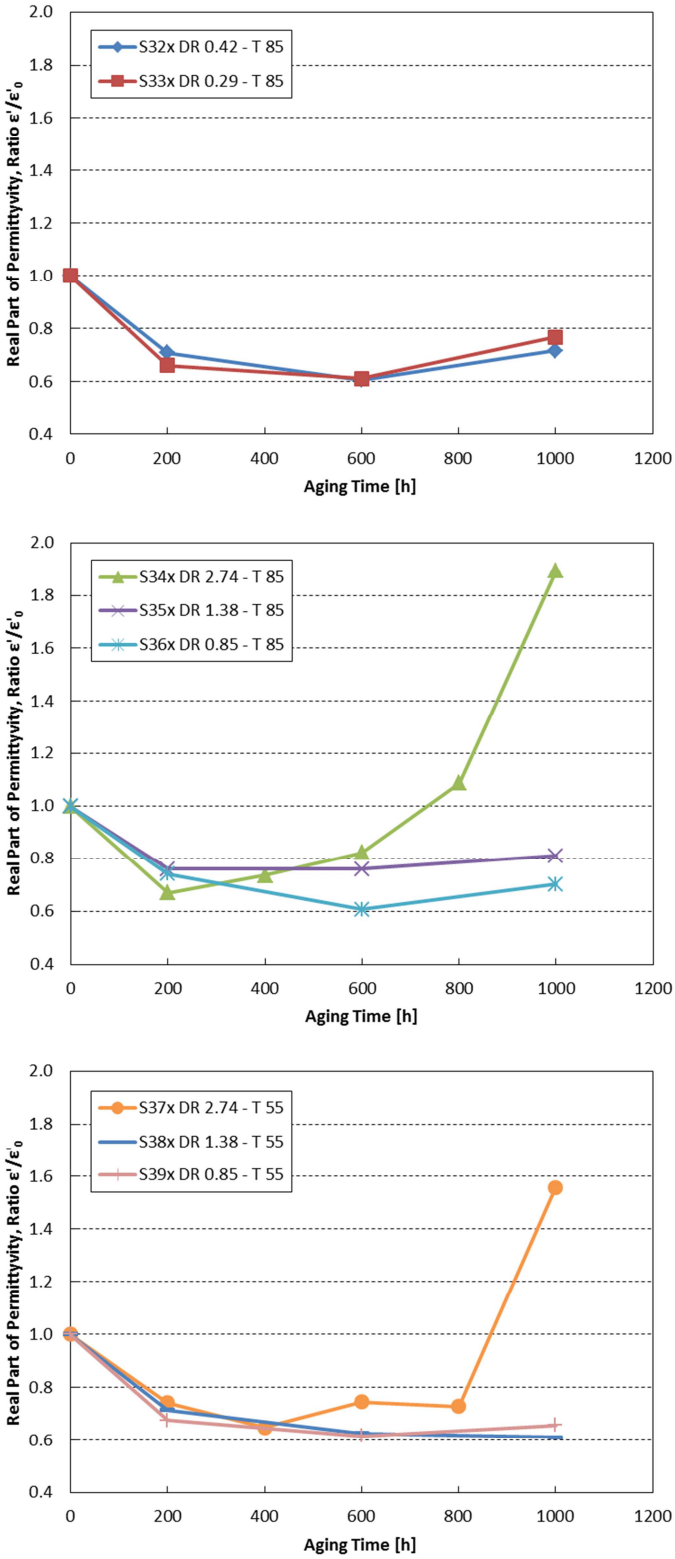

Figure 7.25 Real part of permittivity measured with dielectric analyzer, at a reference frequency of 10^{-2} Hz, vs. aging time for the eight DR-T combinations. Permittivity is reported in relative value to that measured on unaged specimens.

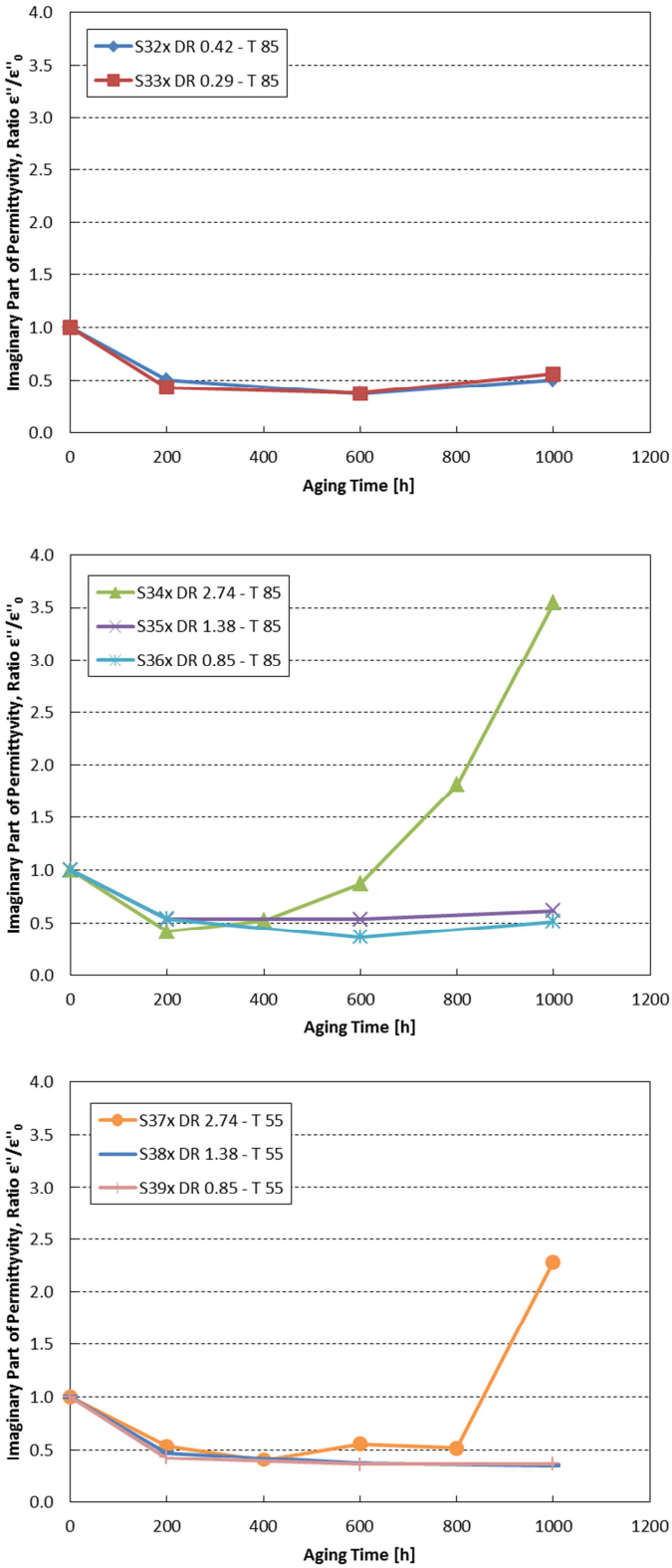

Figure 7.26 Imaginary part of permittivity measured with dielectric analyzer, at a reference frequency of 10^{-2} Hz, vs. aging time for the eight DR-T combinations. Permittivity is reported in relative value to that measured on unaged specimens.

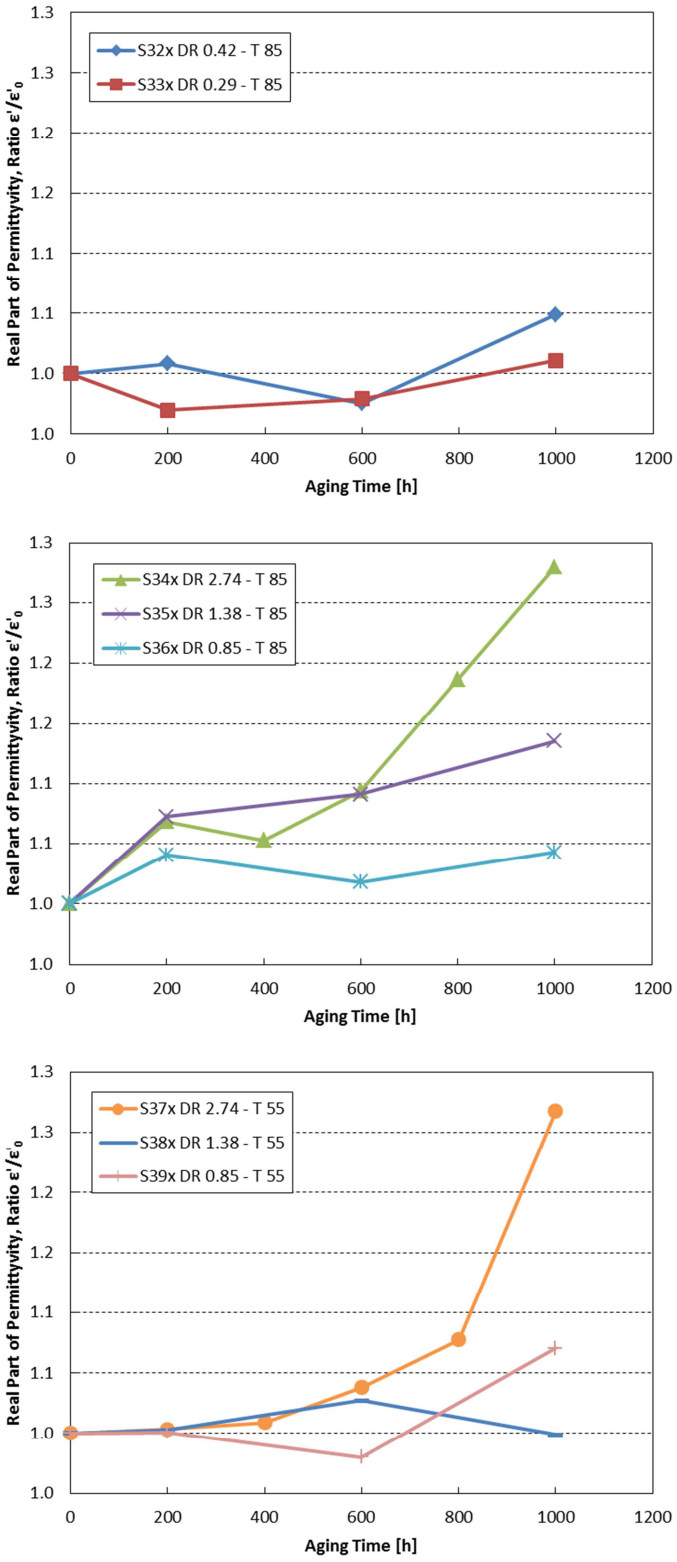

Figure 7.27 Real part of permittivity measured with dielectric analyzer, at a reference frequency of 10^5Hz, vs. aging time for the eight DR-T combinations. Permittivity is reported in relative value to that measured on unaged specimens.

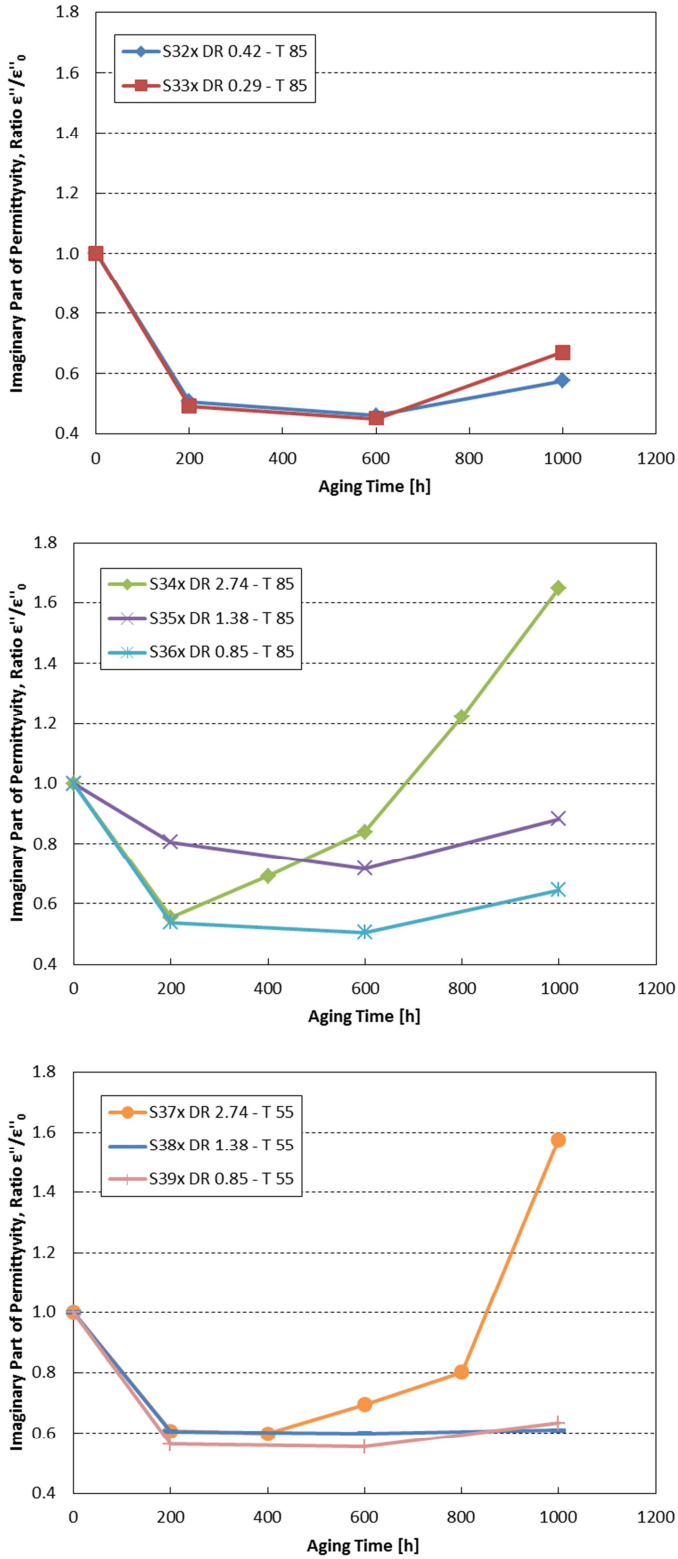

Figure 7.28 Imaginary part of permittivity measured with dielectric analyzer, at a reference frequency of 10^5Hz, vs. aging time for the eight DR-T combinations. Permittivity is reported in relative value to that measured on unaged specimens.

7.2 Mechanical analysis results

For S3 cable insulation the tensile properties were measured using a load frame testing machine with extension rate of 50 mm/min and initial gauge length of 40mm. Samples (tubular type) were conditioned at 25°C and 50% relative humidity for 24 hours prior to testing.

Results for unaged sample S3 "black" are reported in Table 7-2:

Table 7-2 Mechanical properties of unaged S3 EPDM/EVA cable.

CABLE S300	Mean value	Err. Abs
EaB (%)	418	32
Young's Modulus (MPa)	17.7	2.0

Figure 7.30 displays the results of mechanical tests on specimens S3: tests have been splitted, as well as for testing of dielectric spectroscopy, into three experiments depending on aging conditions. Figure 7.29 shows the Young's modulus in relative value as a function of the aging time. It can be observed that considering error bars this property does not show considerable changes with aging time. In particular, S34x aged under the worst conditions, displays no variations, even after 1000 aging hours. Thus, while for EPR cable insulation Young's Modulus appeared a marker correlated with aging, on the contrary for EPDM/EVA cable insulation does not show any variation with aging.

Figure 7.30 displays the decrease of the Elongation at Break with aging time, confirming EaB as a good aging marker as it is usually reported in literature for NPP cables. Aged cables with lower dose rate (corresponding to the first experiment, S32 and S33), considering error bars, show no change in tensile properties. With regard to the other experiments, instead, there is a clear decrease of EaB. The higher the dose rate, the greater the decrease. Temperature affects slightly the aging phenomenon, i.e. cables aged at an higher temperature displays worse behavior: differences related to temperature are, however, within the range of the error bars.

All aged cables present a deterioration of the mechanical properties if compared to the new cable.

A conservative value of ≥50 percent is usually used as an acceptance criterion to define the end of useful service for a cable. Note that cable S36 and S39 aged at 0.85 kGy/h all fall below this threshold after 800 aging hours. Cables S35 and S38 aged at 1.38 kGy/h do that after 600 aging hours and lastly cables aged at the maximum dose rate of 2.74 kGy/h do the same after 200 aging hours. Therefore there is a clear correlation between dose rate and mechanical damage. At such high doses the effect of aging temperature is secondary, as it is widely reported in literature. If we accept the criterion set above, those cables have to be considered out of service.

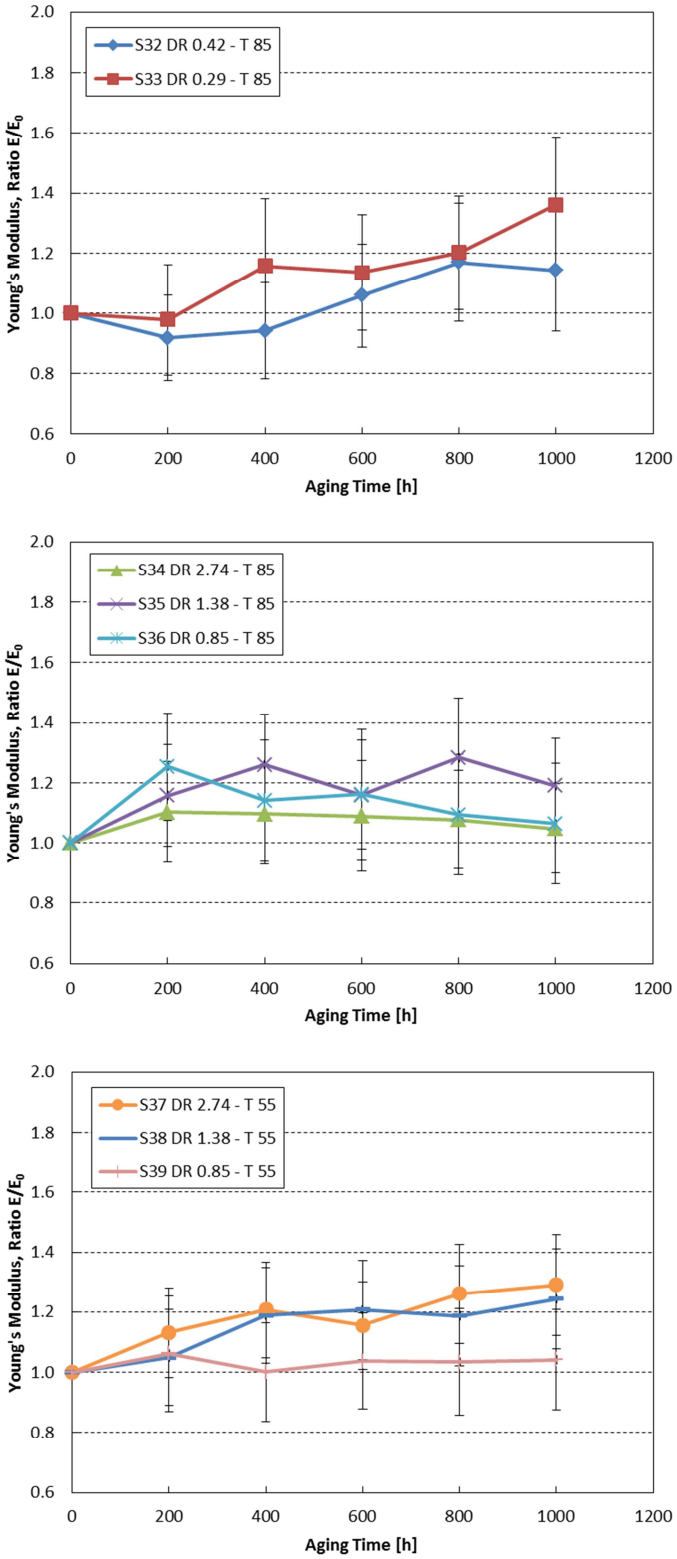

Figure 7.29 Young's Modulus vs. aging time for S3 cable for the eight DR-T combinations. Elongation at Break is reported in relative value to that measured on unaged specimens. Error bars are reported.

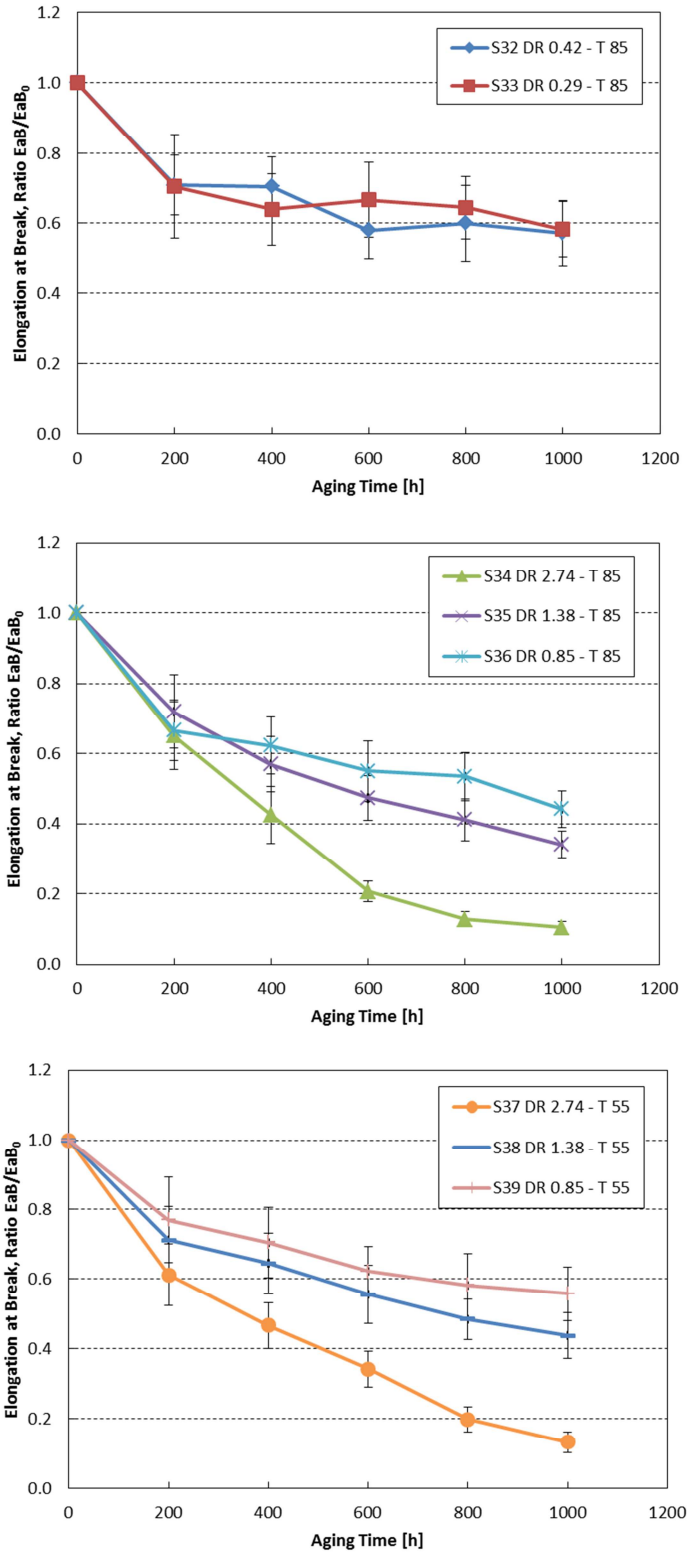

Figure 7.30 Elongation at Break vs. aging time for S3 cable for the eight DR-T combinations. Elongation at Break is reported in relative value to that measured on unaged specimens. Error bars are reported.

In order to highlight the dependence of EaB in relative value on the total absorbed dose (logarithmic scale) Figure 7.31 is presented. Cables of the first and second experiment, aged at isothermal conditions but at different dose rates, have been plotted.

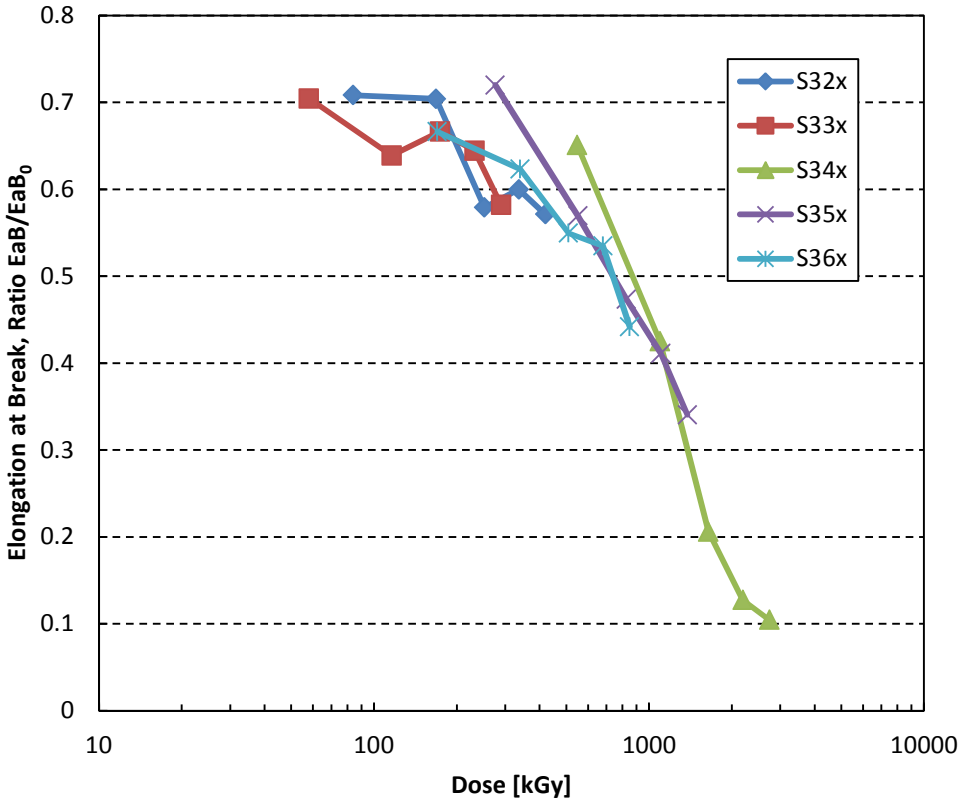

Figure 7.31 Elongation at Break (Ratio EaB/EaB$_0$) vs Total Absorbed Dose for S3 specimens aged at 85°C for different dose rates.

7.3 Discussion

The results presented here have confirmed that Elongation at Break is probably the mechanical property most affected by aging. Degradation of tensile behavior is directly related with dose rate and aging time. This cannot be said for Young's Modulus whose behavior with aging for this cable material does not seem reliable to assess morphological deteriorations. Both dielectric permittivity and dissipation factor showed an increasing trend with aging time, even if variations are small. That seems to be in agreement with tensile analysis results which confirmed that the material suffered structural damage, except for first experiment cables. Figure 7.32 shows experimental points obtained from the second and the third experiment of Elongation at Break reported in relative value to that measured on unaged specimens as function of the total absorbed dose in logarithmic scale: black points refer to cables of the second experiment, aged at 85°C while grey points refers to cables of the third experiment, aged at the lower temperature of 55°C. Experimental points were fitted using a polynomial regression: it is thus seen that the red line, corresponding to the higher aging temperature, is clearly below the blue line of about 10%. Therefore the higher the temperature the worse the mechanical behavior of the cable.

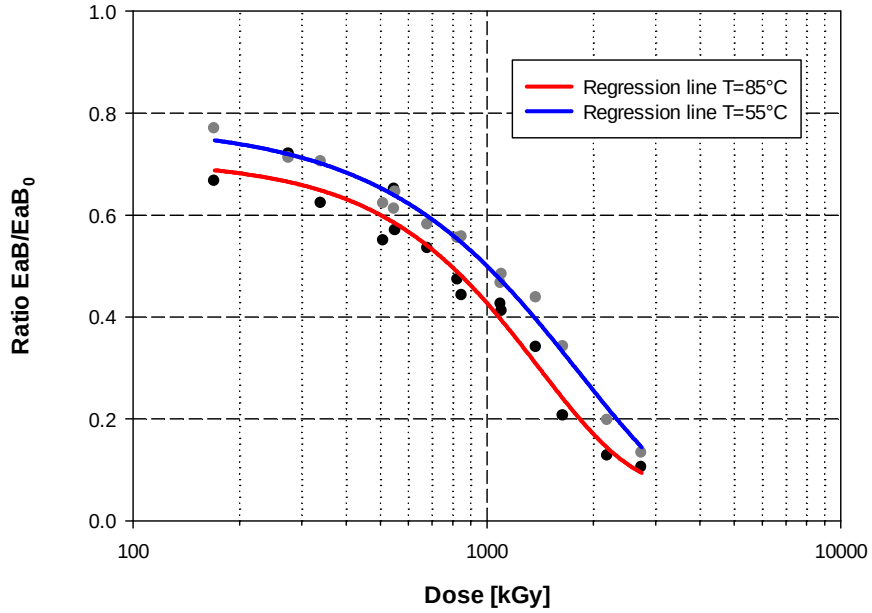

Figure 7.32 Elongation at Break reported in relative value to that measured on unaged specimen as function of the total absorbed dose in logarithmic scale. Black points refer to cables of the second experiment, aged at 85°C while grey points refers to cables of the third experiment, aged at the lower temperature of 55°C. Regression lines are plotted.

In agreement with what was said above, a correlation of the two DR-T combinations that had the largest effects on dielectric properties, i.e. S34 and S37, with the mechanical property that showed modification with aging, i.e. EaB, can be performed. Those two cables were aged at the same dose rate of 2.74 kGy/h but at different aging temperatures. The correlation has been done at the fixed frequency of 10^5 Hz (see Figure 7.33).

As well as reported for EPR cable insulation S9, also this cable material presents a noticeable matching (both real (a) and imaginary (b) part, even if real part has smaller variations) between electrical and mechanical data.

Table 7-3 displays coefficients of determination r^2. These values are lower than those observed for the EPR cable insulation.

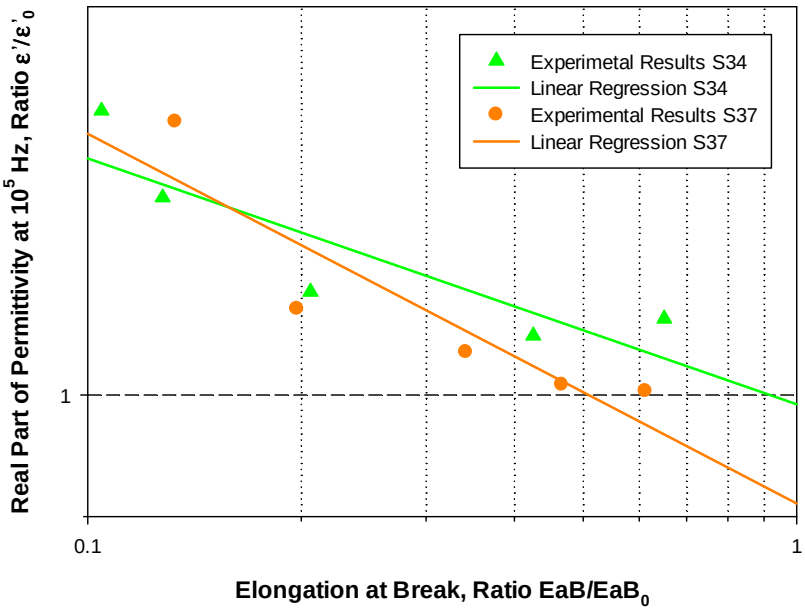

(a)

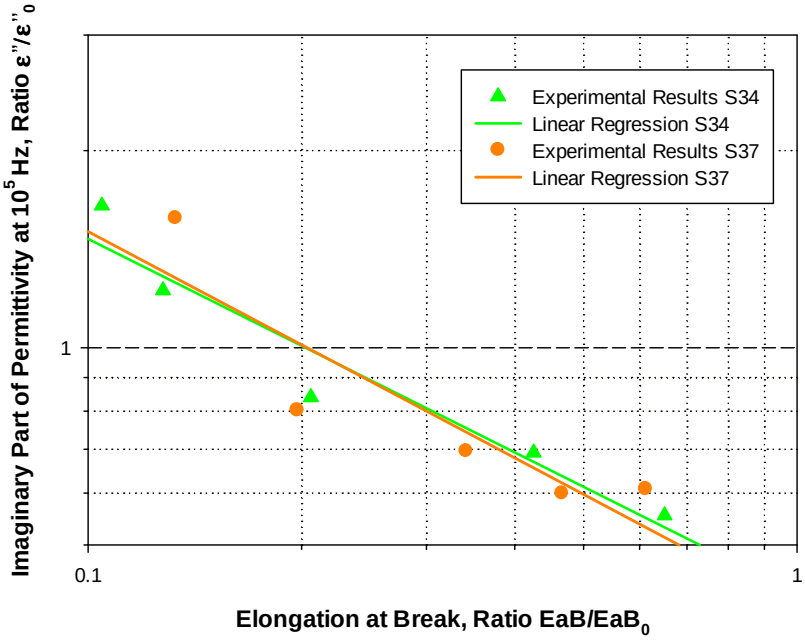

(b)

Figure 7.33 Correlation of the real (a) and imaginary part (b) of permittivity at 10^5 Hz vs. Elongation at Break ratio for specimens S34x and S37x.

Table 7-3 Square correlation coefficients r^2 used for linear regressions cable insulation (S3).

r^2	ε' (10^5 Hz)-EaB	ε'' (10^5 Hz)-EaB
S34	0.773	0.931
S37	0.812	0.804

Chapter 8

8 Space charge formation in CSPE/EPR samples

This chapter reports space charge measurements on CSPE/EPR based samples. Results of electrical and mechanical tests are discussed at the end of the chapter and possible correlations between them are proposed.

Space charge measurement can be performed on every kind of solid insulating materials. This techniques is generally used for HV and MV cable insulations which are usually subjected to high field, where space charge accumulation is an important factor and can create electric field distortion in the insulation bulk. On the contrary, space charge accumulation does not constitute a problem for the insulation of low voltage cables. Anyway, this technique is an useful tool to detect morphology modification of the material due to aging (by radiation and temperature).

Polymeric materials subjected to HVDC stress tend to become charged. These charges may be supplied from the electrodes or be generated within the bulk of the polymer. The supply of charge from the electrodes involves transfer of either electrons or holes across the electrode-polymer interface. These processes are strongly dependent on the conditions at the interfaces, which include electrode material, surface defects, impurities, oxidation and so on. The injected charge must become trapped in the material and is thus dependent on the availability and the nature of the traps. The residence time of a charge

carrier in a trap will be dependent on the depth of the trap, i.e. the energy required to activate the carrier free of the trap, the temperature and the applied electrical field. Several factors affect the trapping of charge in polymers such as crystallinity ratio, oxidation, impurities, by-products from the crosslinking reaction. The generation of space charge within the bulk of the polymer is usually associated with ionization of chemical species introduced during the manufacture of the material, such as residues of crosslinking reaction, antioxidant and other elements like flame retardants and others, found in abundance especially in NPPs cables manufacture. Radiation and temperature may greatly affect the phenomenon, e.g. degradation of the polymer chains can greatly affect space charge formation. That's the reason why quantities such as the total stored charge density in the insulation or trap-controlled charge mobility could be significantly sensitive to aging and could be interesting diagnostic indicators to follow.

The accumulated space charge can be distinguished in homocharge and heterocharge, where the first one implies space charge of the same polarity as the adjacent electrode and heterocharge implies charge of opposite polarity.

Homocharge (Figure 8.1) may be generated by trapping of injected charge near the injecting electrodes. The resulting space charge distribution will reduce the electrode electrical fields and enhance the field in the bulk of the insulation.

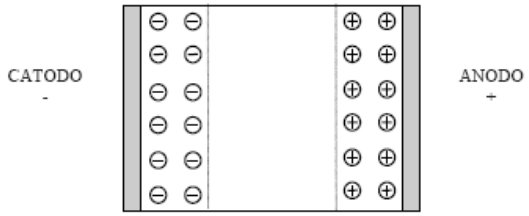

Figure 8.1 Example of homocharge formation.

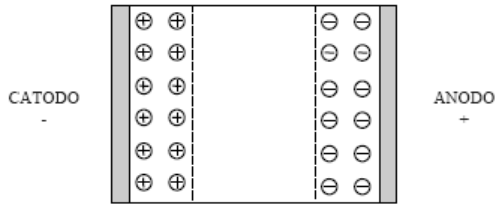

Figure 8.2 Example on heterocharge formation.

Heterocharge (Figure 8.2) can be generated by field assisted ionization of dissociable species in the bulk. In presence of an applied electric field, the charged molecules or ions may migrate to the electrode of opposite polarity where they may become trapped. Heterocharges may also be formed when one of the electrodes partly blocks the extraction of mobile charges injected by the other. Heterocharge formation results in enhancement of one or both electrode fields and reduced field stress in the bulk.

8.1 Experimental results

This section summarizes experimental results obtained from tests performed by PEA method on S9 cable insulation and FSe9 outer sheath flat specimen . In order to ensure reproducibility and comparability, experimental test procedures have been standardized. The PEA test is divided into two phases: a first polarization phase (so-called VOLT-ON phase) for a duration of 5000 seconds: in this step, DC voltage is applied to the sample resulting in space charge accumulation. Afterward a depolarization phase (so-called VOLT-OFF phase) that lasts at least 1000 seconds: in this step electrodes are grounded, allowing space charge depletion. Tests were performed at room temperature (25°C), applying an electric field of 20 kV/mm.

8.1.1 EPR cable insulation

Cable S9 has three conductors: each one with Ø-7 mm and an EPR insulation thickness of 1.2 mm. The overall cable diameter is 31 mm. Figure 8.3Figure 8.4Figure 8.5 display charge patterns (scale ± 2 C/m^3) for specimens with different DR-T combinations (respectively S92x, S95x and S98x cables). Sound velocities through the polymer were around 1800-2000 m/s. Values of relative permittivity may be extracted from dielectric spectroscopy measurements at the fixed operative frequency of 50 Hz.

S921-200h

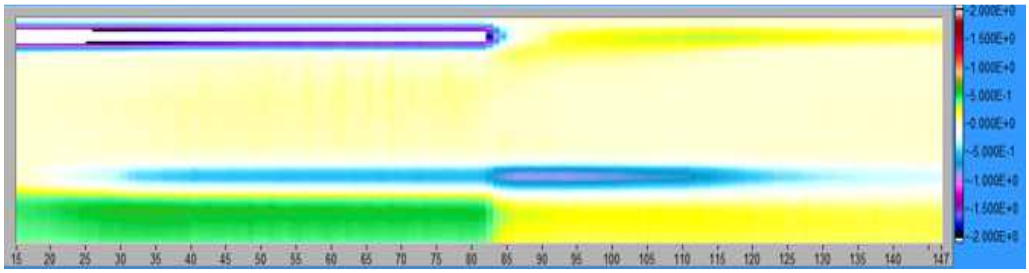

S922-400h

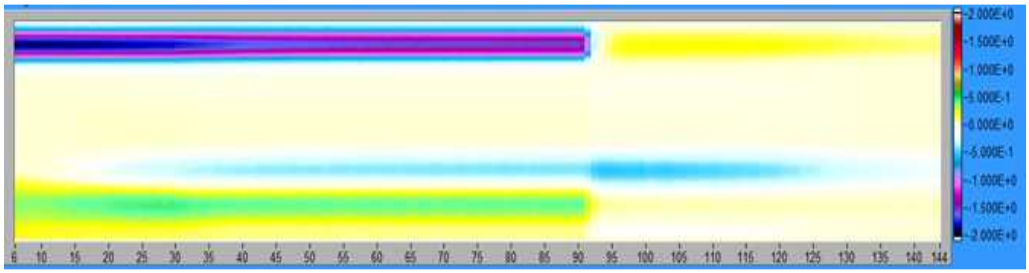

S923-600h

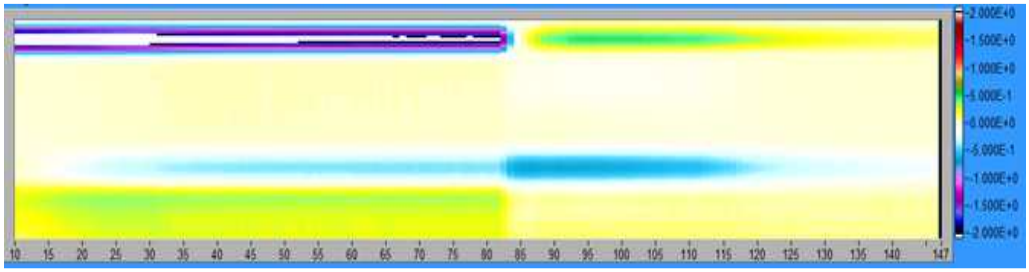

S924-800h

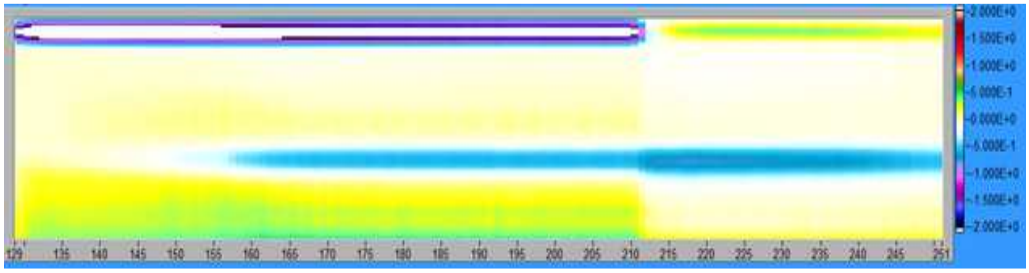

S925-1000h

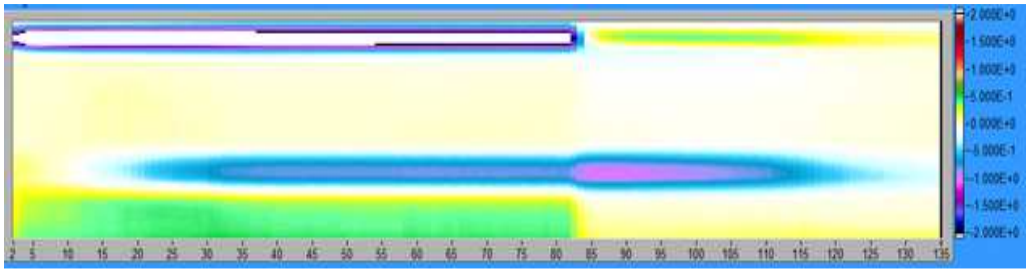

Figure 8.3 Charge patterns - scale 2 C/m^3 – S92x
Aging Levels T=85°C, DR=0.39 kGy/h

S951-200h

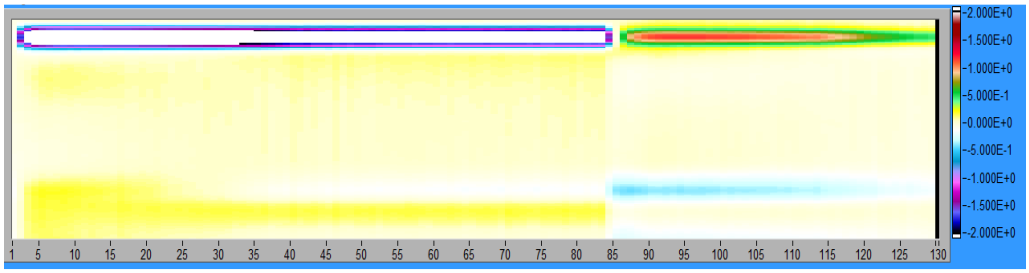

S952-400h

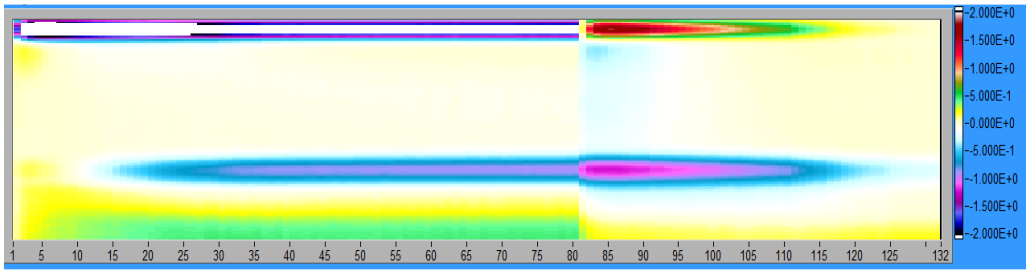

S953-600h

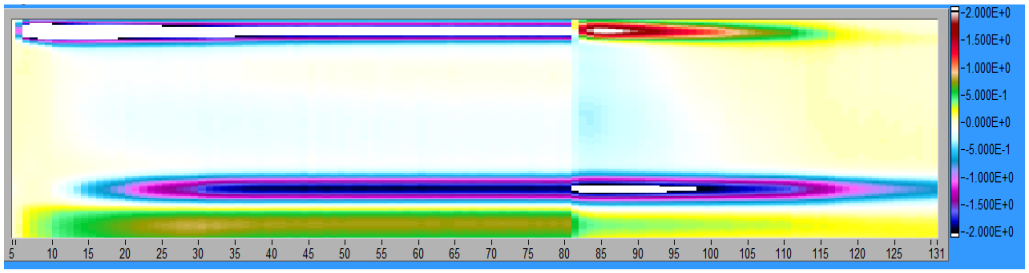

S954-800h

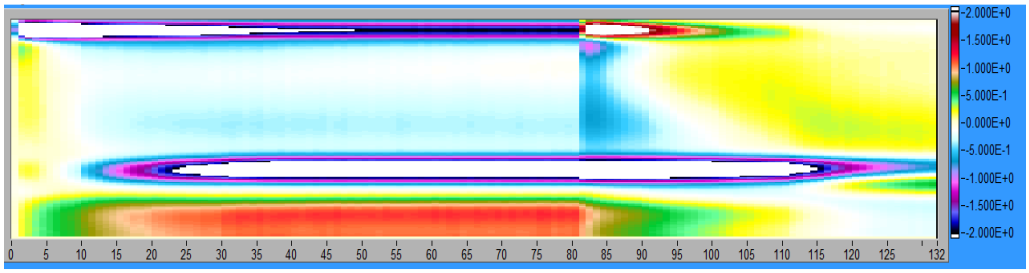

S955-1000h

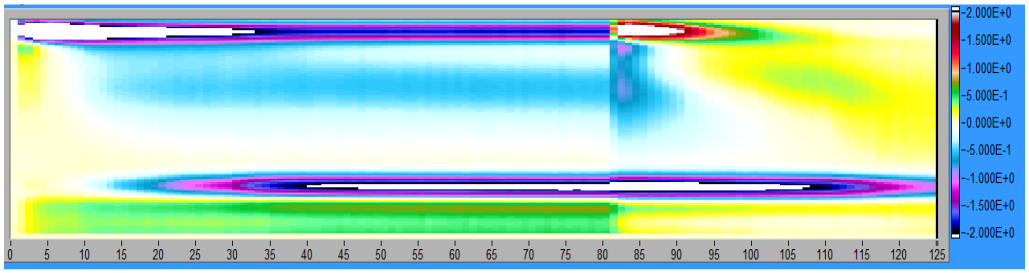

Figure 8.4 Charge patterns - scale 2 C/m^3 – S95x

Aging Levels T=85°C, DR=1.58 kGy/h

The main characteristic of every pattern is heterocharge formation at the anode. Almost certainly this charge accumulates at the interface between the EPR insulation and the PET film placed between conductor and insulation to improve the extrusion process. This layer, however, can create a barrier to charge transport in the insulation. This behavior clearly increases with aging. Heterocharges may be formed when one of the electrodes (in this case the anode, where PET foil is located) partly blocks the extraction of charges injected by the other. Heterocharge formation results in enhancement of both electrode fields and reduced field stress in the bulk as it is clearly appreciable in S95x and S98x cables aged at 1.58 kGy/h.

Specimens S92x display a very small space charge formation. In addition to the heterocharge accumulating at PET foil, for all samples some positive charge appears in the bulk of the insulation.

The increase of space charge formation with aging time is more evident in specimens S95x. S951 resulted of difficult calibration: the anode appears only after 1000 seconds; test was repeated several times with similar outcomes.

In particular, specimens 954 and 955, aged for 800 and 1000 hours respectively, show also a small amount of homo-charge at the cathode.

The density of the negative charge at the cathode is three or four times larger than the previous case. This is probably due to the higher dose rate even if physical interpretation of this behavior, especially after electrodes grounding (where there’s an anomalous increase in charge, likely due to a change in the offset), is difficult. Even in this case tests was repeated several times with similar outcomes.

For specimens S98x, density of the negative charge at the cathode is similar to the one measured on specimens S95x. As for S92x, an amount of positive charge is stored in the bulk. The effect of the temperature is evidenced only by the formation of homo charge in specimens S954 and S955, not present for specimens aged at 55°C.

S981-200h

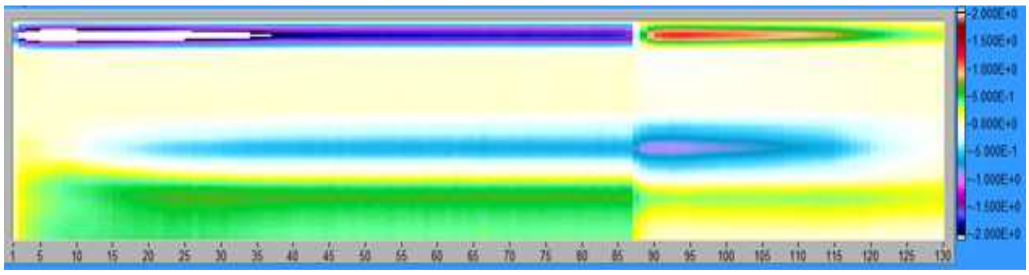

S982-400h

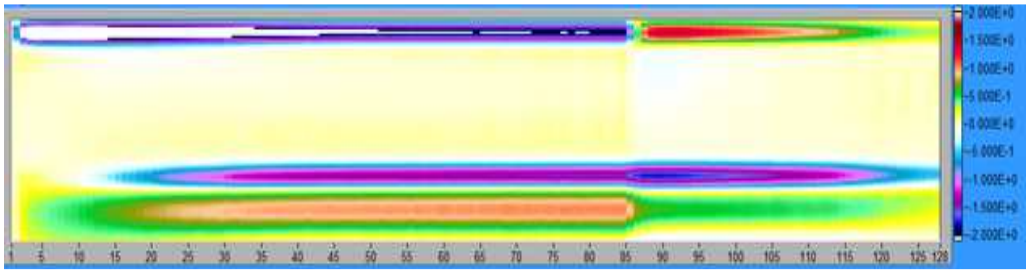

S983-600h

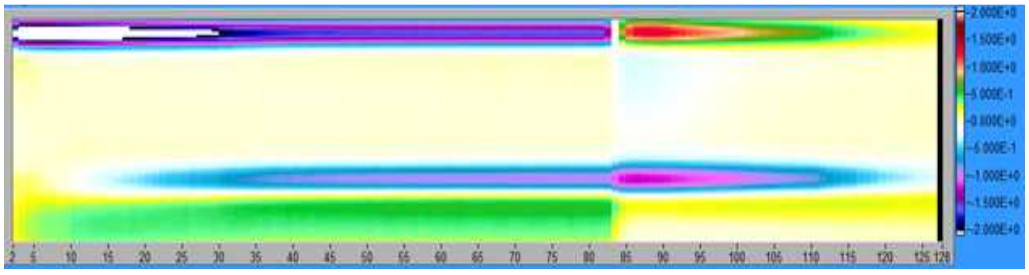

S984-800h

The signal during the test shows a disturbance (similar to an interface) between the first and second peak that makes the calibration impossible, despite the test has been repeated several times changing the position of the cable and the test zone.

S985-1000h

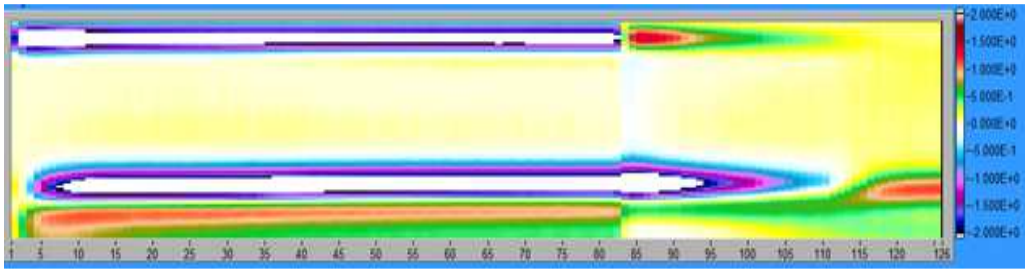

Figure 8.5 Charge patterns - scale 2 C/m^3 – S98x

Aging Levels T=55°C, DR=1.58 kGy/h

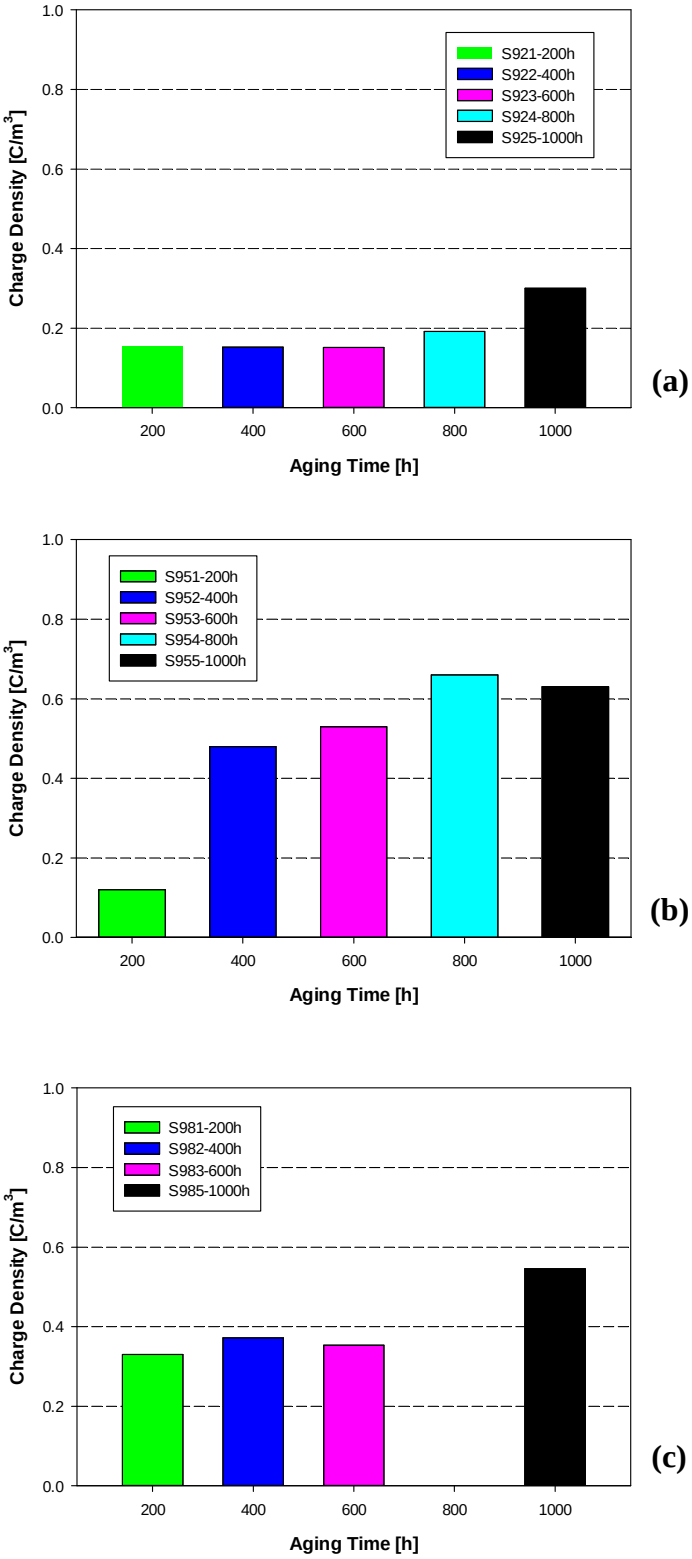

Figure 8.6 Max charge density 10s after the Volt-Off for specimens s92x (a), S95x (b) and S98x (c).

Figure 8.6 displays charge density variations with aging time. A slight increase of accumulated charge can be observed for DR-T combination. A remarkable increment comes out increasing the dose rate (comparing S92x and S95x). Also the higher aging temperature seems to cause an increment of the maximum charge density after the Volt-off (comparing S95x and S98x). Anyway, these variations are close to the sensitivity of the instrument, which is (0.1 C/m^3).

Depolarization curves (Figure 8.7) are obtained 10 seconds after the Volt-off . Transient effect of voltage removal or neutralization from electrodes injection is avoided (occurring when electric field is still high, typically Schottky injection), thus allowing to adopt the de-trapping theory [5].

Once the characteristic of depolarization has been extracted, space charge decay in per unit is converted into an apparent mobility by Eq. 3.4 (Figure 8.8). The equation is the result of many approximations. Apparent mobility μ is governed by the deepest empty traps[6] encountered in transport and it decreases in time because the traps are emptying in charge.

The depolarization curves obtained from specimens s92x show small variations with the aging time. The charge slowly leaves the insulation: after 100 seconds the amount of charge is still the 90% of the initial value. The charge density for these samples is close to the system sensitivity. Specimens 95x and 98x show a different behavior: the amount of charge after 100 seconds is around the 50% of the initial value. A higher dose rate leads to more evident aging effects. Furthermore, the charge decay seems to be faster increasing the aging time. S951 depolarization curve (as well as mobility curve) has not been plotted because of its noisy trend due to the low accumulated charge density, close to sensitivity of the PEA system.

[6] Decay of space charge is governed by the deepest unoccupied traps just as for the de-trapping theory.

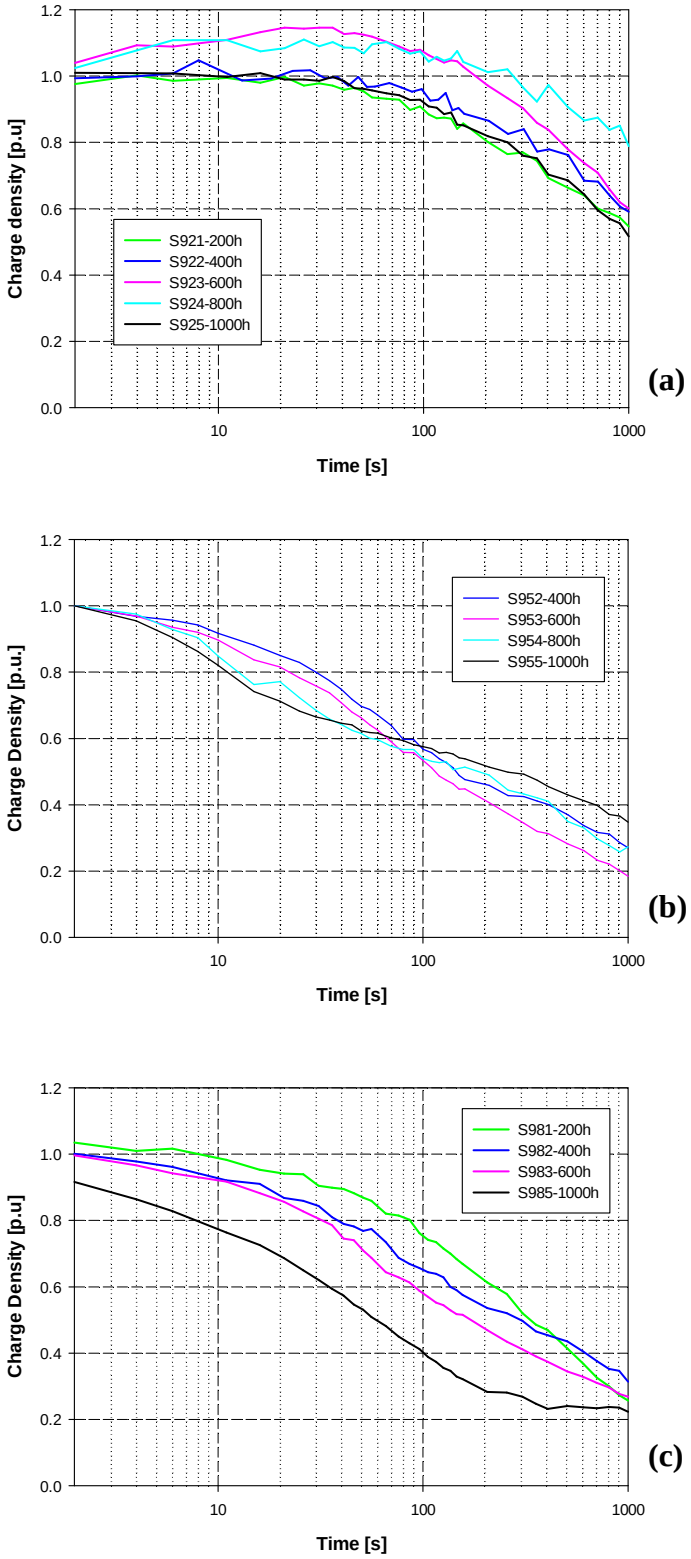

Figure 8.7 Depolarization curves recorded from 10s after the Volt-Off for specimens S92x (a), S95x (b) and S98x (c).

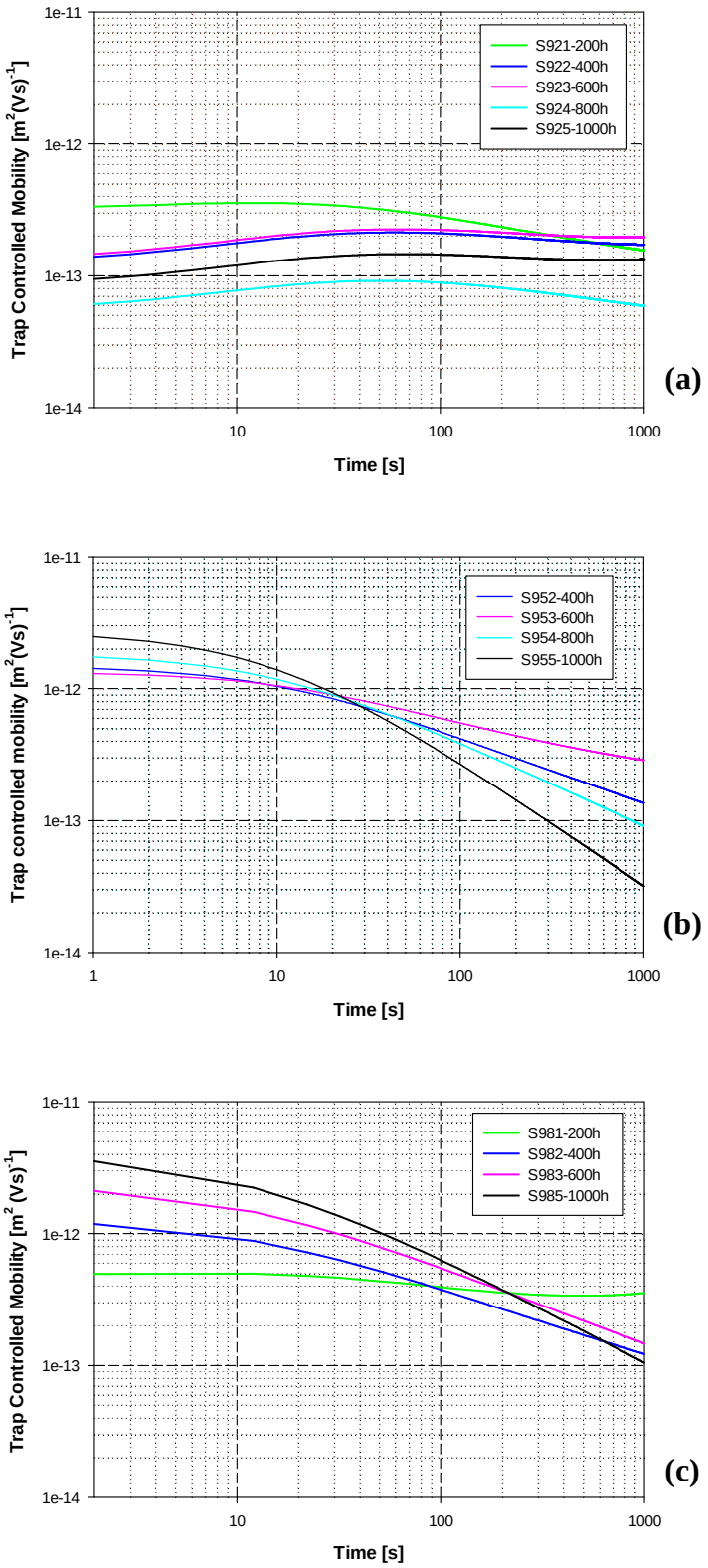

Figure 8.8 Trap Controlled Mobility curves vs. Time for specimens S92x (a), S95x (b) and S98x (c).

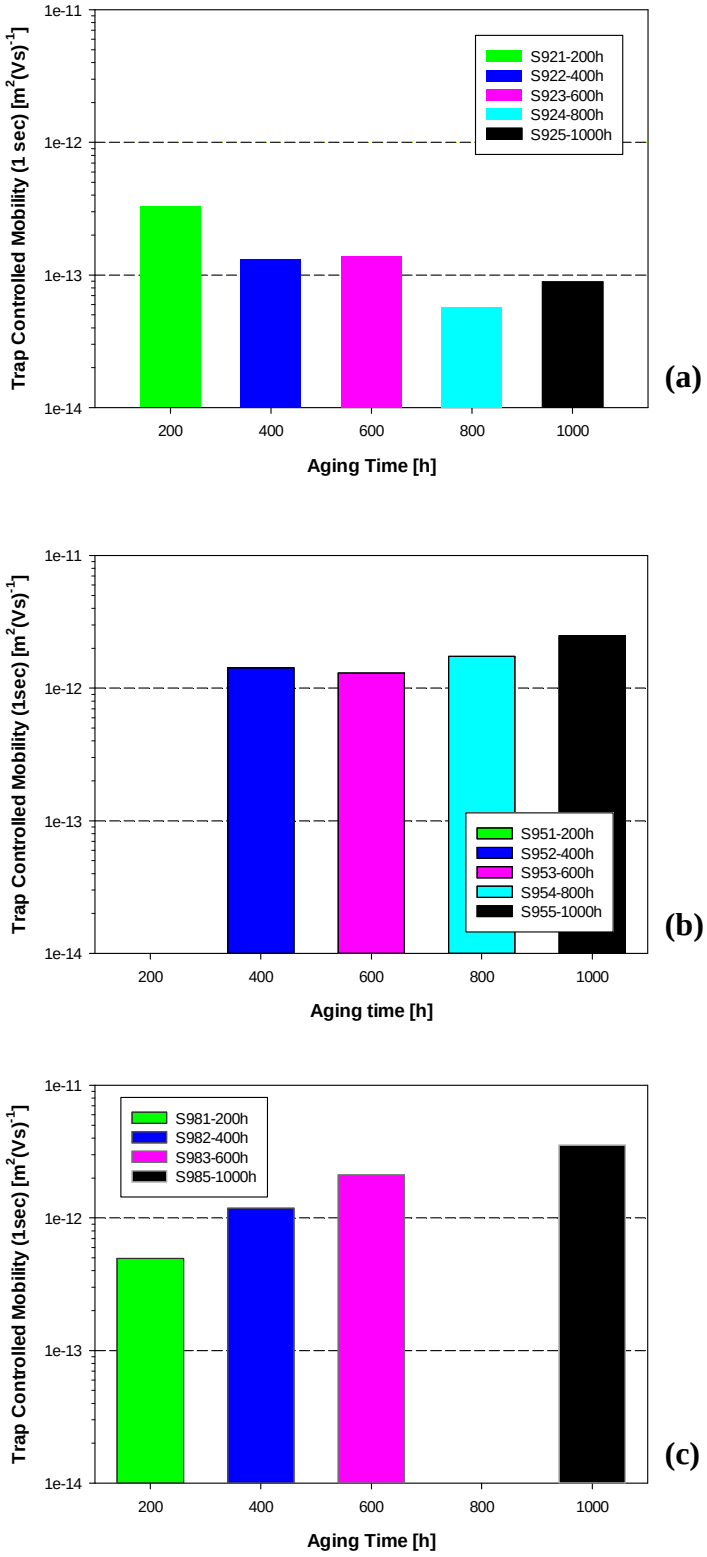

Figure 8.9 Trap Controlled Mobility (measured 1s after the first acquisition of the depolarization curve) vs. Aging Time for specimens S92x (a), S95x (b) and S98x (c).

For specimens S92x the trap controlled mobility oscillates around values of 10^{-13} $m^2/(Vs)$. No significant variations with aging time are noticeable.

The mobility of specimens S95x and S98x, aged with higher dose rate, shows values around 10^{-12} $m^2/(Vs)$ at the beginning, then decreases with time down to 10^{-13} $m^2/(Vs)$. If we take into account the mobility calculated 1s after the first acquisition of the depolarization curve (Figure 8.9), it can be clearly seen a slight increase of mobility with the aging time..

8.1.2 CSPE cable sheath

In this thesis the CSPE outer sheath aged with DR6 (i.e. FSe96x aged at 0.85 kGy/h and 85°C, second experiment) has been tested using the PEA system for flat specimens.

It has to be noted that visual inspection revealed that specimens presented here were very hardened by aging. Applying an electric field of 20 kV/mm, FSe962, FSe964 and FSe965 gave insulation breakdown, demonstrating effectiveness of aging in polymer chemical-physical degradation. Thus results elaboration for those specimens is not available.

Charge densities were 0.31 C/m^3 for FSe961 and 0.17 C/m^3 FSe963.

In both cases the amount of charge 20 seconds after the Volt-off is around the 30% of the initial value, so depletion of charge is a very fast phenomenon for these samples. The trend of the curves doesn't currently allow a good interpolation, that's the reason why mobility has not been derived. Charge patterns of tests completed are shown in Figure 8.10. In both cases it is noted an accumulation of positive charge in the bulk. For FSe961 there is homocharge formation at the anode while for FSe961 there is heterocharge formation at the cathode. After the Volt-off positive charge migrates to the electrode of opposite polarity, as reasonably expected.

FSe961-200h

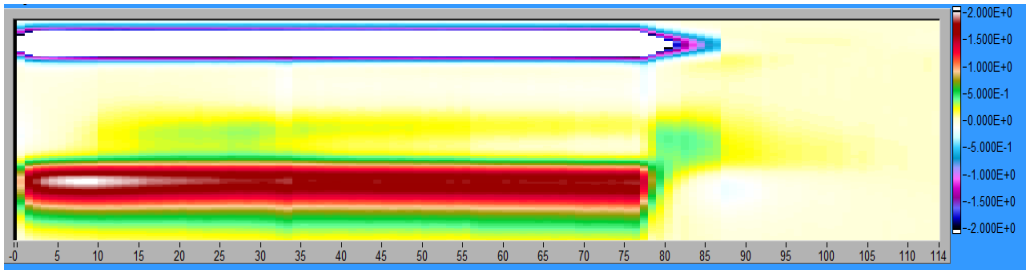

FSe963-600h

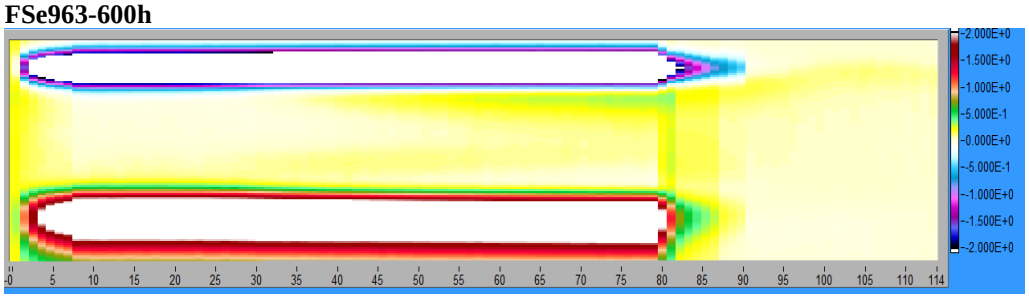

Figure 8.10 Charge patterns - scale 2 C/m^3 – FSe96x Aging Levels T=85°C, DR=0.85 kGy/h

8.2 Mechanical analysis results

Experimental results of mechanical tests for S9 specimens are presented in §6.2.

8.3 Discussion

Space charge measurements can evidence the effect of aging, but only at very high dose rates the evolution of the extracted quantities with the aging time appears evident. The amount of accumulated charge increases with the aging time, even if the phenomenon is more notable in the patterns rather than in extracted quantities such as the net charge density.

Figure 8.11 shows trends of total charge density with the total absorbed dose. A clear effect of radiation and temperature on space charge formation is highlighted. Moreover, the higher the temperature the larger the space charge accumulation, thus confirming that for this cable (as observed in mechanical analysis) no “inverse-temperature” effects occur.

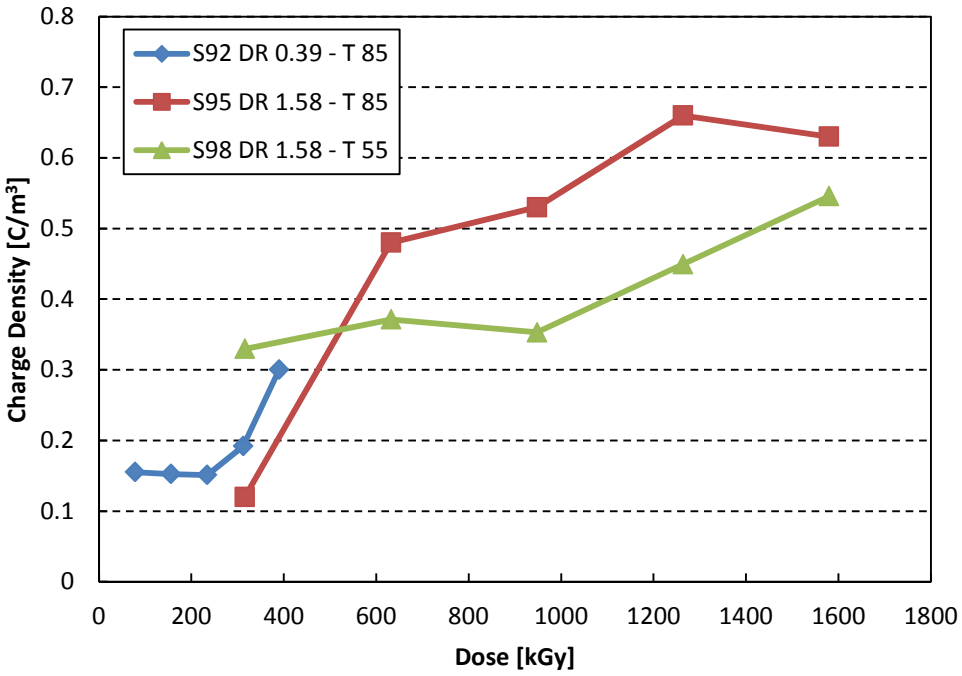

Figure 8.11 Charge Density vs. absorbed dose for the three DR-T combinations.

The increase in mobility for the higher dose rates (S95x and S98x samples) is clearly noticeable. As well as accumulated charge, hence, it is a good aging marker.

Correlations with mechanical data have been investigated but relations between properties didn't show unfortunately a good matching.

Chapter 9

9 Space charge formation in EPDM/EVA samples

This chapter deals with space charge measurements on EPDM/EVA based samples. Results of electrical and mechanical tests will be discussed.

9.1 Experimental results

This section summarizes experimental results obtained from tests performed by PEA method on S3 “black” cable insulation, S4 “blue” cable insulation and FS3 sheath flat specimen.
Standardized experimental test procedure is descripted in §3.1 and §8.1.
All tests were performed at room temperature (25°C), applying an electric field of 20 kV/mm.

9.1.1 EPDM/EVA cable insulations

As described in cable description S3 cable has five conductors, each one with different color: the conductor diameter is 3.7 mm with an EPDM/EVA insulation thickness of 1 mm. The overall cable diameter is 16 mm. Figure 9.1 - Figure 9.6 - Figure 9.11Figure 9.16 show charge patterns (scale ± 2 C/m^3) for specimens with different DR-T combinations (in this thesis DR5, 1.38 kGy/h, and DR6, 0.85 kGy/h, have been investigated, both with an aging temperature of 85°C, i.e. S35x, S36x, S45x and S46x cable insulations). Sound velocities

through the polymer were around 2200-2500 m/s. Values of relative permittivity may be extracted from dielectric spectroscopy measurements performed at RT at the frequency of 50 Hz.

All cables tested except S45x (both black cable and blue cable, as well as for the higher dose rate and for the lower) display the same qualitative behaviour with time. A slight homocharge formation at the anode that decreases with aging time is always present. This charge begins to accumulate immediately after the Volt-on but the phenomenon may become stronger after about 1000 seconds, as it can be seen in cables aged for 200 hours or in S462 and S463.

A negative charge amount remains close to the cathode during the Volt-off for a period that decreases with the aging time. The larger the stored charge the longer the time needed for the charge to be dissipated.

Only specimens S354 and S452 present homocharge formation at the anode.

As stated above, specimens S45x do not present homocharge formation at the cathode. In general, the amount of space charge build-up is very low and charge depletion is faster resulting in higher mobilities (Figure 9.13). S455 present low heterocharge at the cathode.

The net amount of space charge (Figures 9.5, 9.10, 9.15 and 9.20) also decreases with time, even if variations are small. After 800 or 1000 aging hours, quantities involved are close to the sensitivity of the instrument (0.1 C/m^3), making difficult post-processing of data. The maximum space charge registered is 0.73 C/m^3 for S451 specimen.

Anode signal is mostly low, this is due to a bad contact between conductor and insulation. It has to be noted once again that this is a very common feature for LV cables whose standard manufacturing has to fulfill less strict electrical requirements with respect to MV and HV power cable insulation. The absence of a semicon layer results in a bad contact between conductor and insulation.

S351-200h

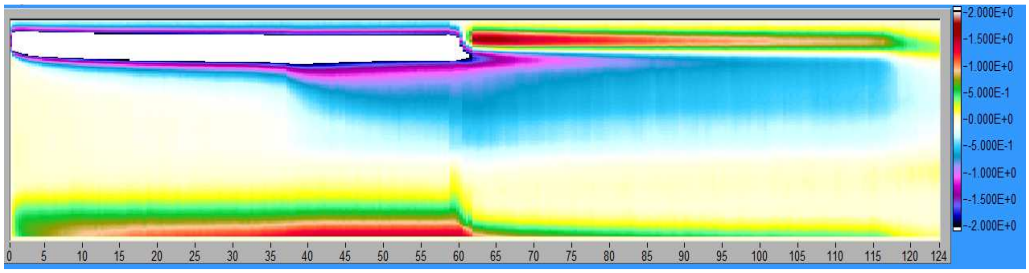

S352-400h

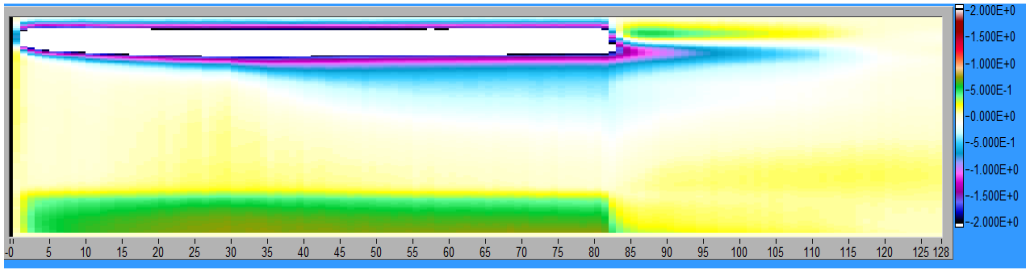

S353-600h

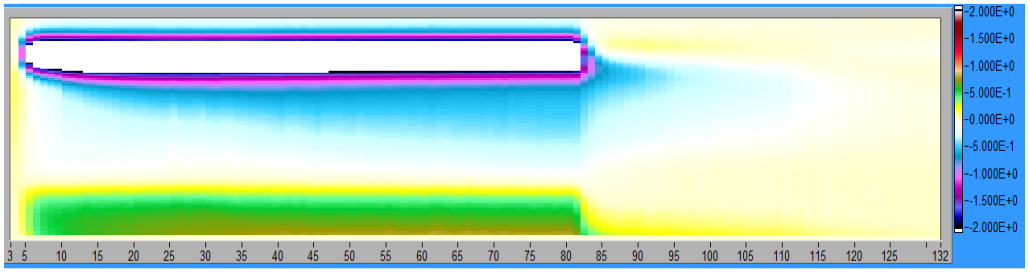

S354-800h

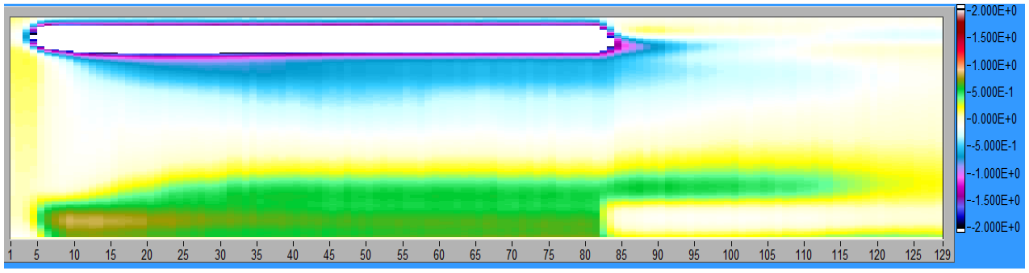

S355-1000h

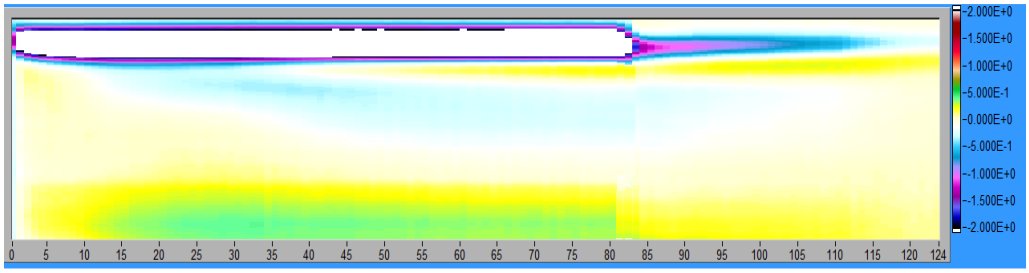

Figure 9.1 Charge patterns - scale 2 C/m^3 – S35x
Aging Levels T=85°C, DR1.38 kGy/h

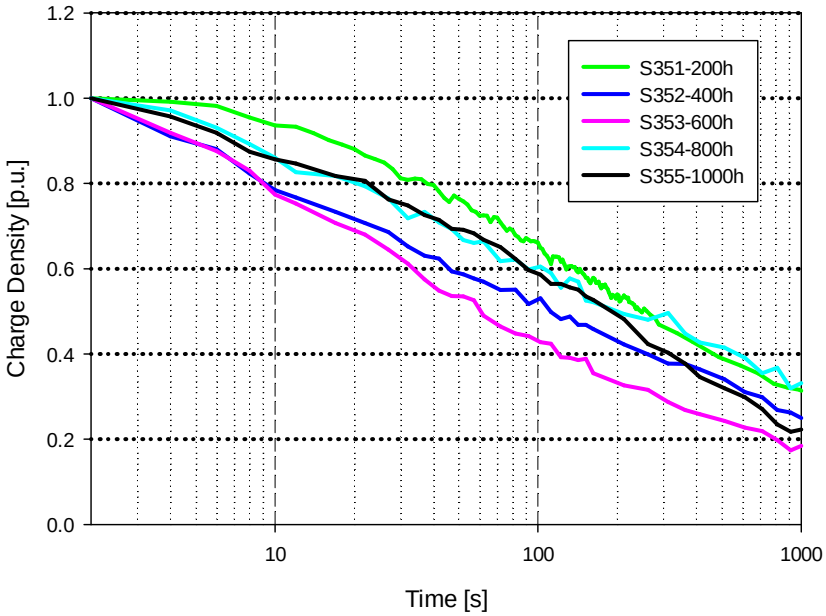

Figure 9.2 Depolarization curve recorded from 10s after the Volt-Off for specimens S35x.

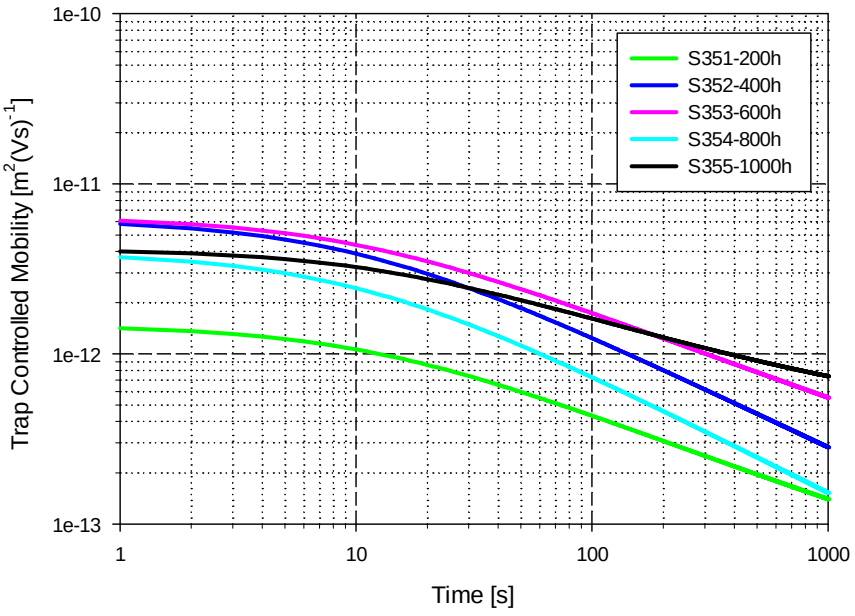

Figure 9.3 Trap controlled mobility vs. time for specimens S35x (logarithmic scale).

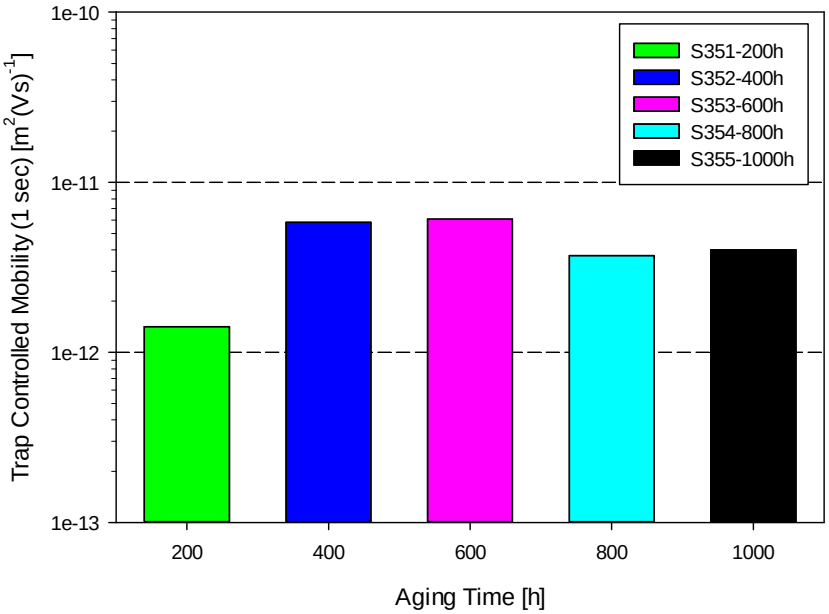

Figure 9.4 Trap Controlled Mobility (1s after the first acquisition of the depolarization curve) vs. Aging Time for specimens S35x (logarithmic scale).

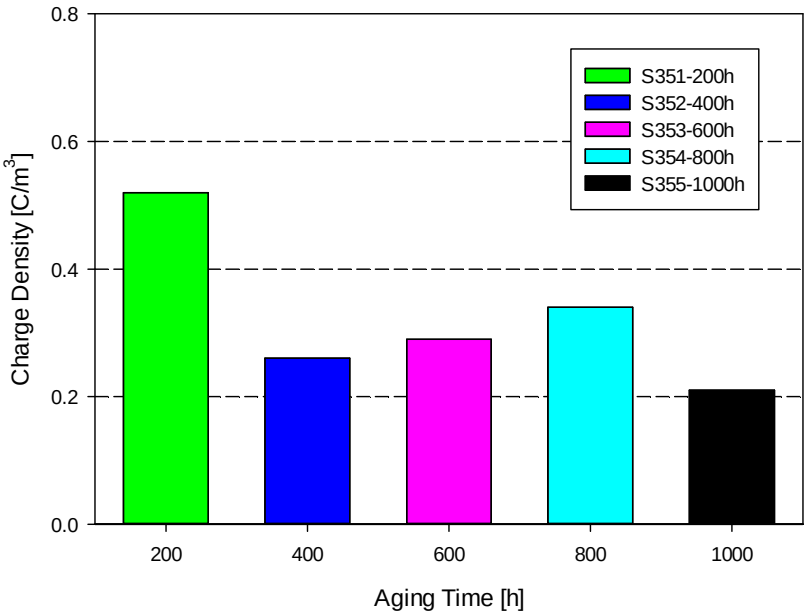

Figure 9.5 Max charge density 10s after the Volt-Off vs. Aging Time for specimens S35x.

S361-200h

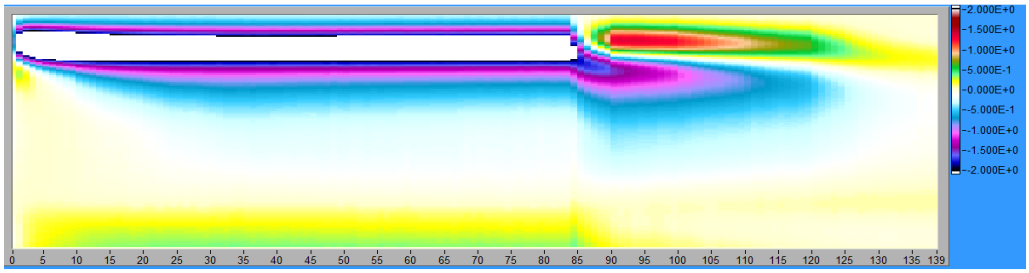

S362-400h

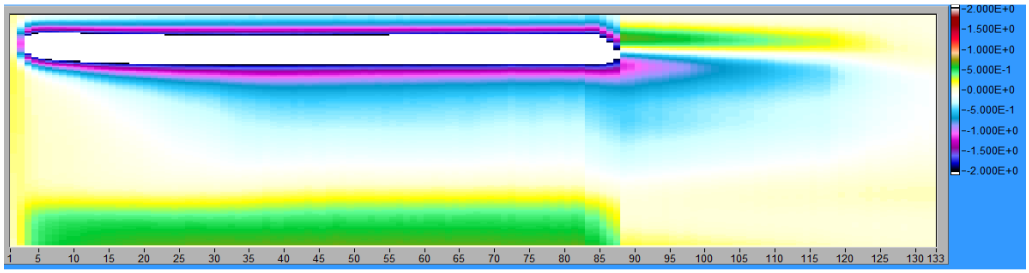

S363-600h

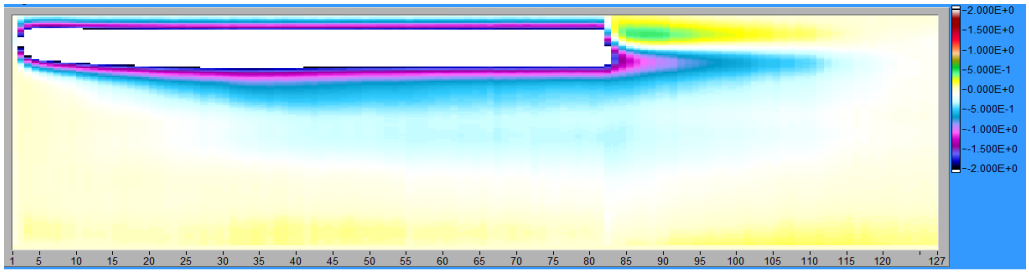

S364-800h

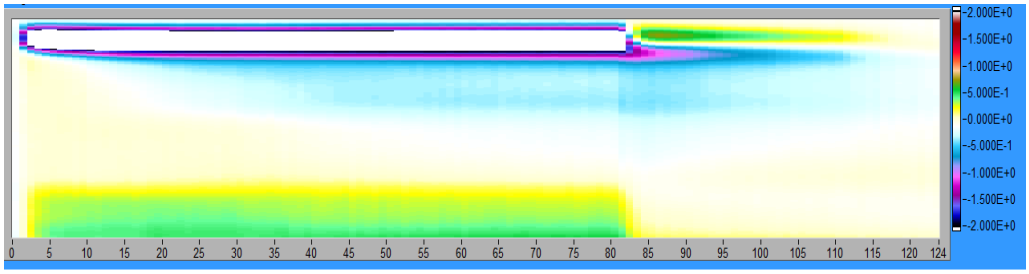

S365-1000h

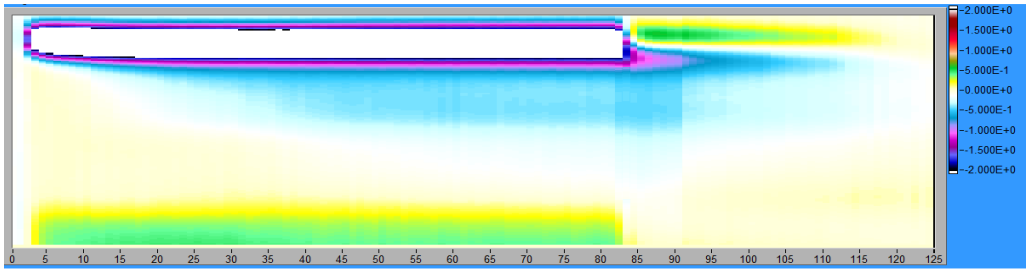

Figure 9.6 Charge patterns - scale 2 C/m^3 – S36x Aging Levels T=85°C, DR=0.85 kGy/h

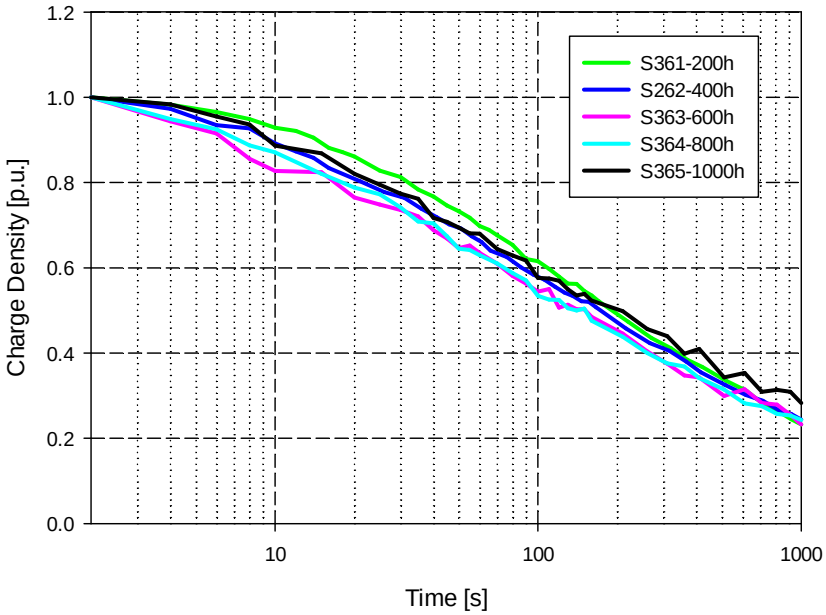

Figure 9.7 Depolarization curve recorded from 10s after the Volt-Off for specimens S36x.

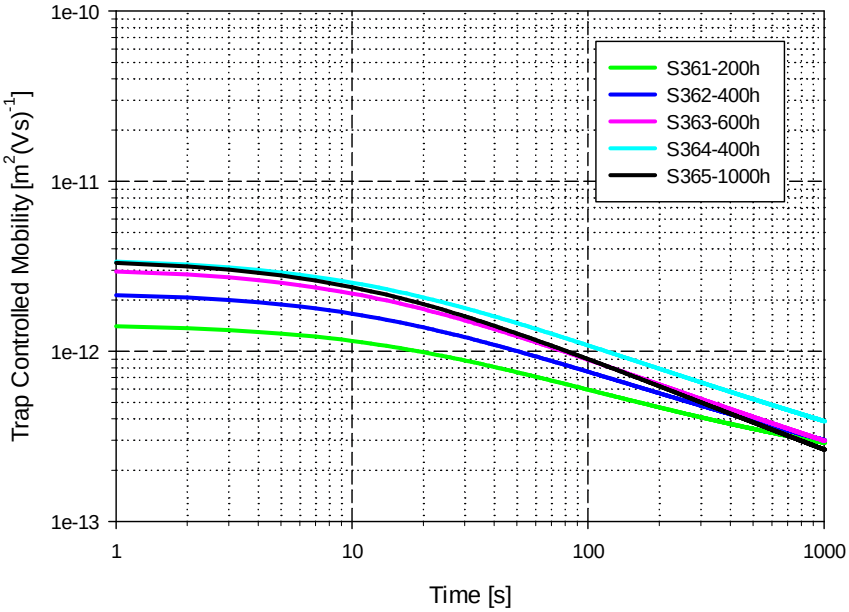

Figure 9.8 Trap controlled mobility vs. Time for specimens S36x (logarithmic scale).

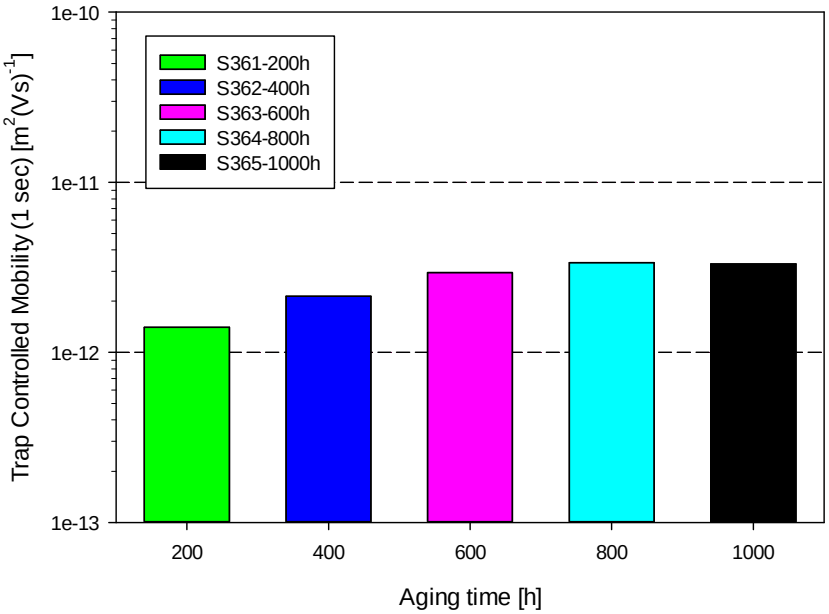

Figure 9.9 Trap Controlled Mobility (1s after the first acquisition of the depolarization curve) vs. Aging Time for specimens S36x (logarithmic scale).

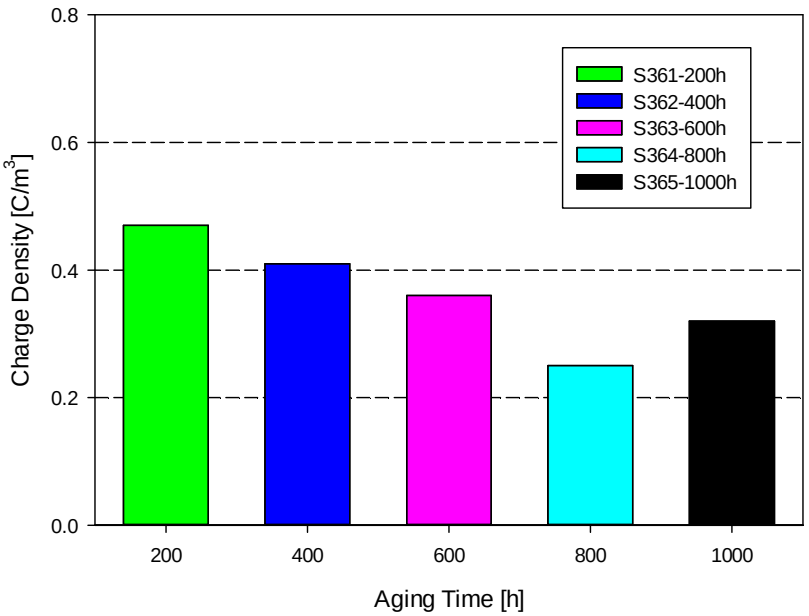

Figure 9.10 Max charge density 10s after the Volt-Off for specimens S36x.

Depolarization curves obtained 10 seconds after the Volt-off are shown in Figures 9.2, 9.7, 9.12 and 9.17: trends are monotones and very similar except for S45x samples which presents differences in slope (the longer the aging time the larger the slope of the curve). Anyway, the amount of charge after 100 seconds is nearly 50% of the initial value and 20% after 1000 seconds. Depolarization curves data have been interpolated, allowing mobility to be extracted. The mobility of specimens S35x, S36x and S46x, takes values around 10^{-12} $m^2/(Vs)$ at the beginning, then decreases with time down to 10^{-13} $m^2/(Vs)$[7]. Anyway, if we take into account the comparison of mobility 1 second after the first acquisition of the depolarization curve (Figures 9.4, 9.9 and 9.19) these values increases with time. But be that as it may, for specimens S45x (Figure 9.13) significant variations with aging time are noticeable: the mobility increases gradually with the aging time, if we compare mobility 1 second after the first acquisition of the depolarization curve, values shift from 10^{-12} $m^2/(Vs)$ of S451 to $3 \cdot 10^{-11}$ $m^2/(Vs)$ of S455.

[7] Note that the charge injected from the electrodes is able to cross cable insulation with a mobility of 10^{-10} $m^2/(Vs)$.

S451-200h

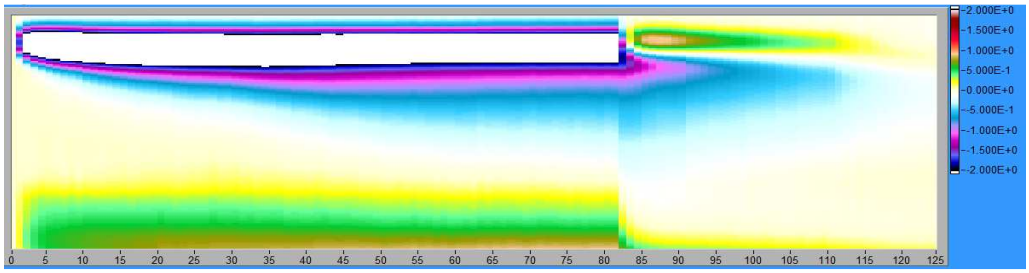

S452-400h

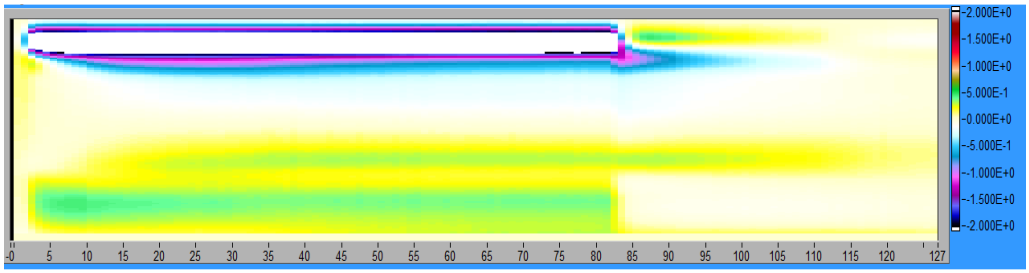

S453-600h

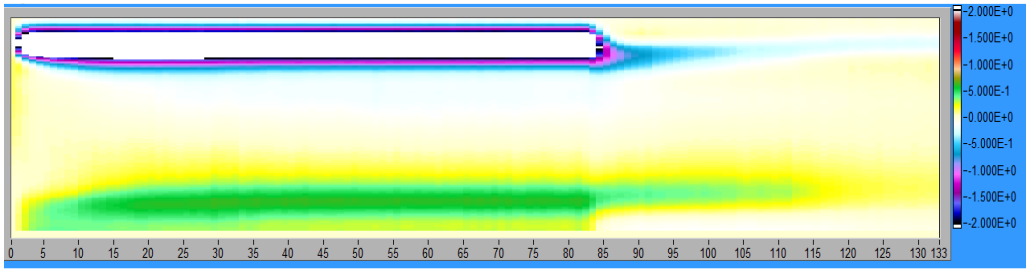

S454-800h

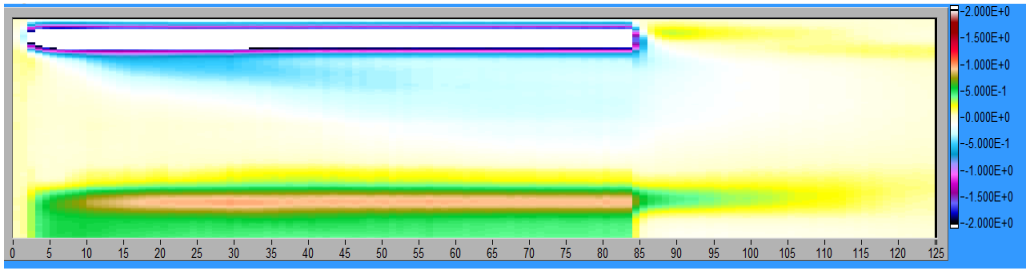

S455-1000h

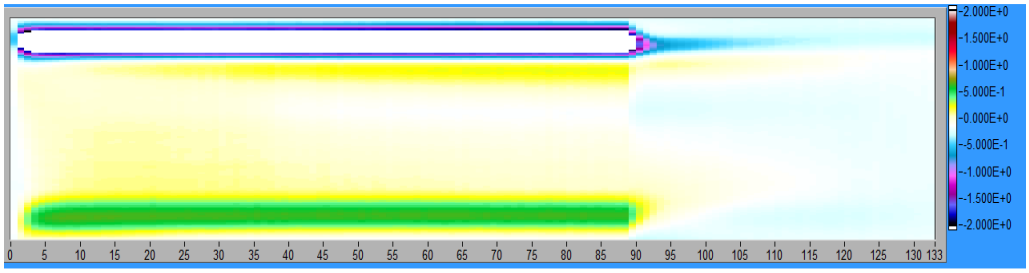

Figure 9.11 Charge patterns - scale 2 C/m^3 – S45x Aging Levels T=85°C, DR1.38 kGy/h.

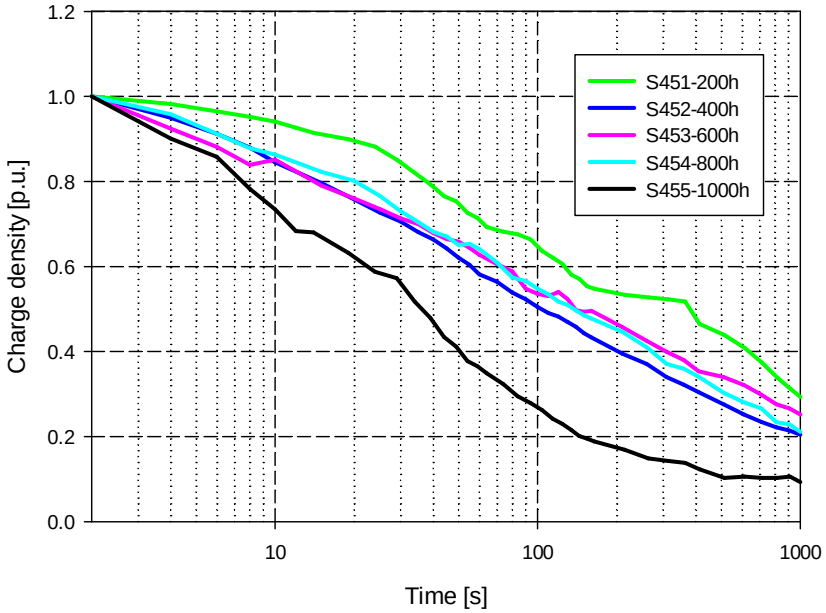

Figure 9.12 Depolarization curve recorded from 10s after the Volt-Off for specimens S45x.

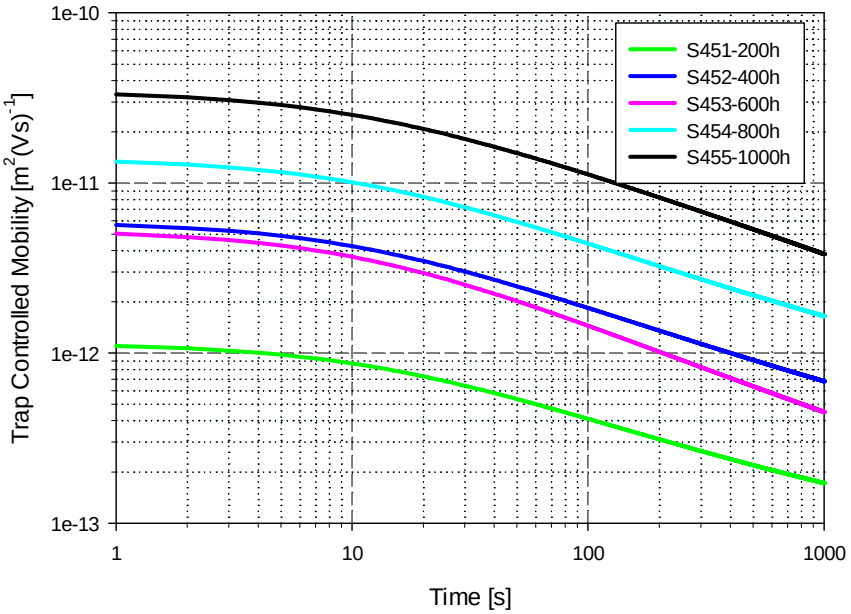

Figure 9.13 Trap controlled mobility vs. Time for specimens S45x (logarithmic scale).

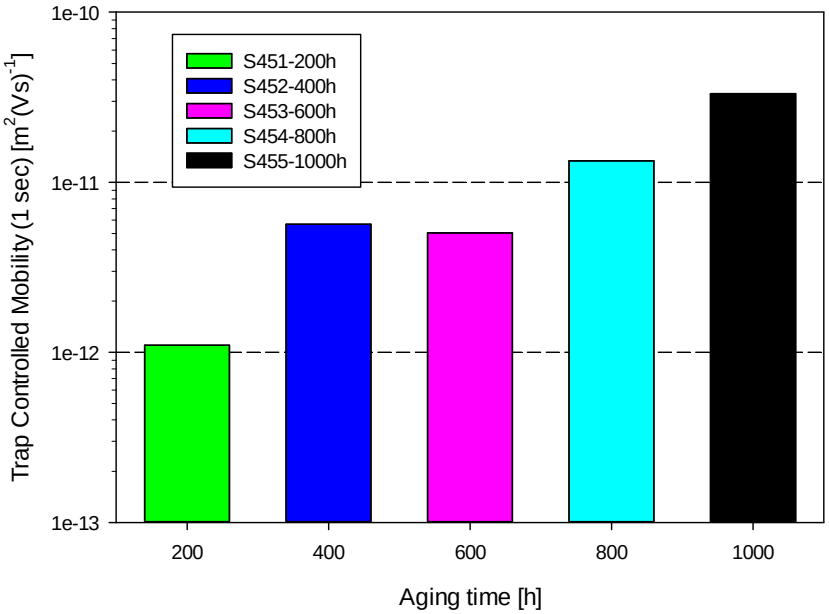

Figure 9.14 Trap Controlled Mobility (1s after the first acquisition of the depolarization curve) vs. Aging Time for specimens S45x (logarithmic scale).

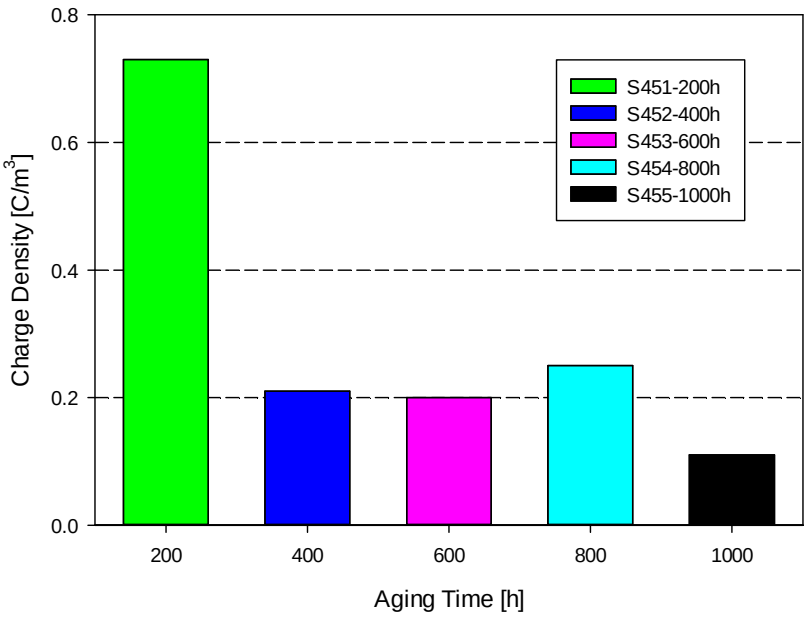

Figure 9.15 Max charge density 10s after the Volt-Off vs. Aging Time for specimens S45x.

S461-200h

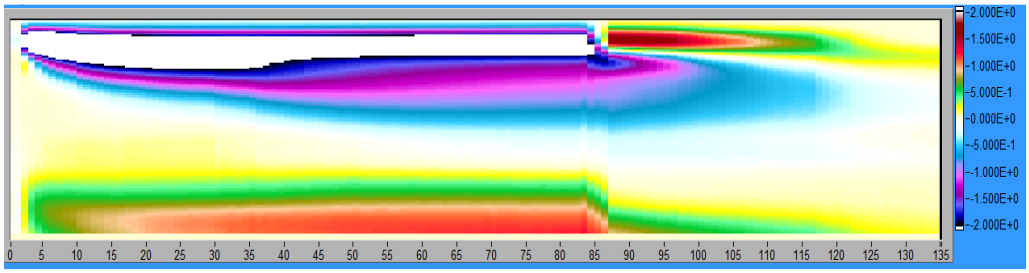

S462-400h

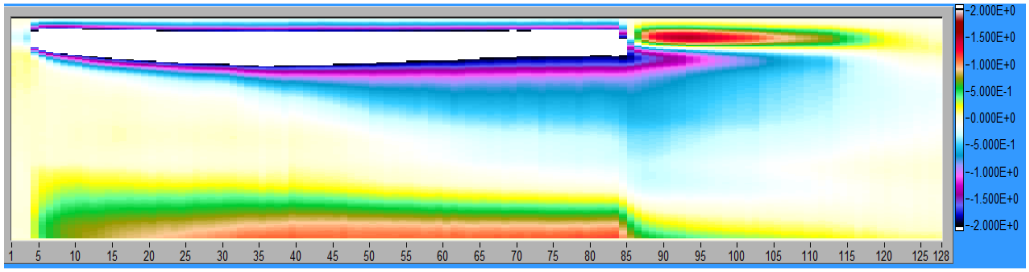

S463-600h

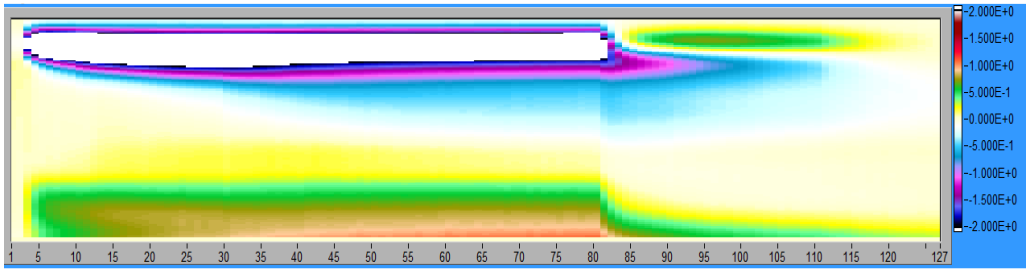

S464-800h

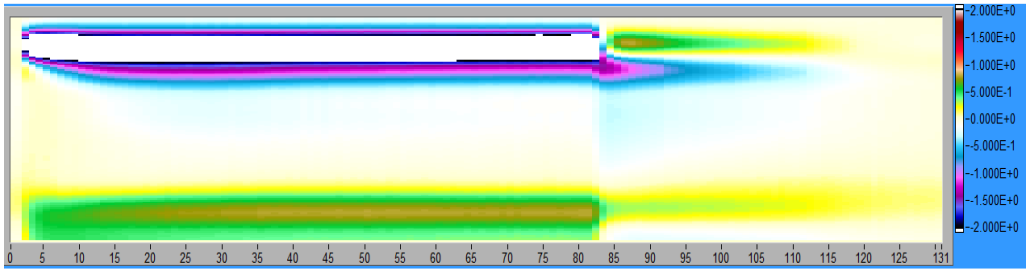

S465-1000h

The signal during the test shows a disturbance between the first and second peak that makes the calibration impossible, despite the test has been repeated several times changing the position of the cable and the test zone.

Figure 9.16 Charge patterns - scale 2 C/m^3 – S46x Aging Levels T=85°C, DR=0.85 kGy/h

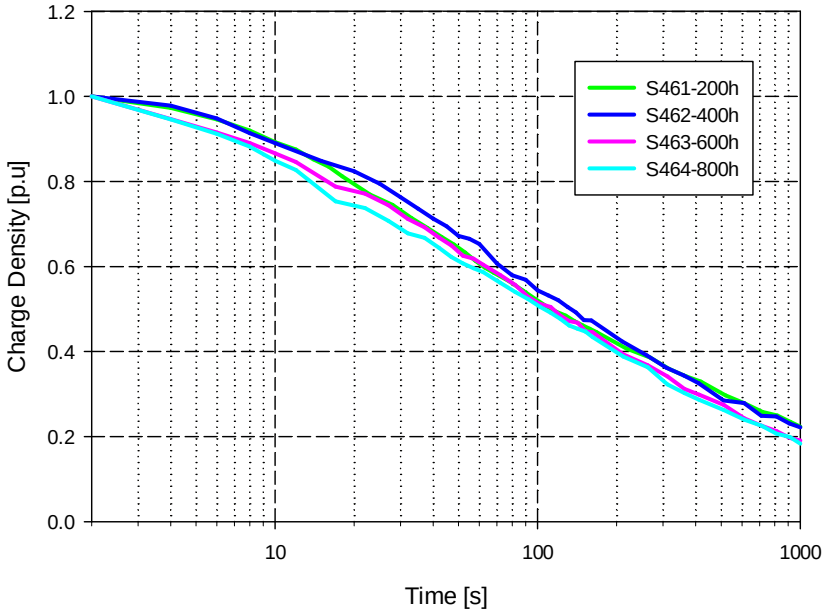

Figure 9.17 Depolarization curve recorded from 10s after the Volt-Off for specimens S46x.

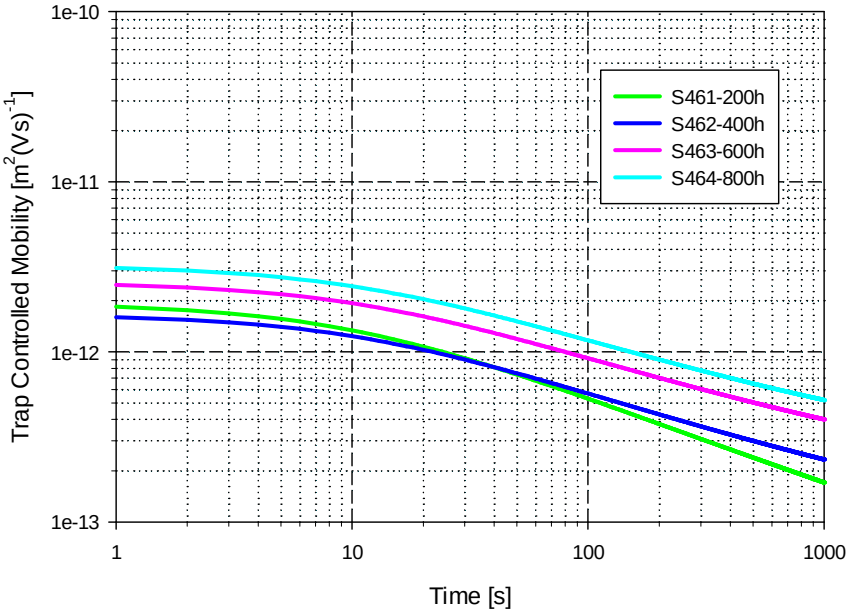

Figure 9.18 Trap controlled mobility vs. time for specimens S46x (logarithmic scale).

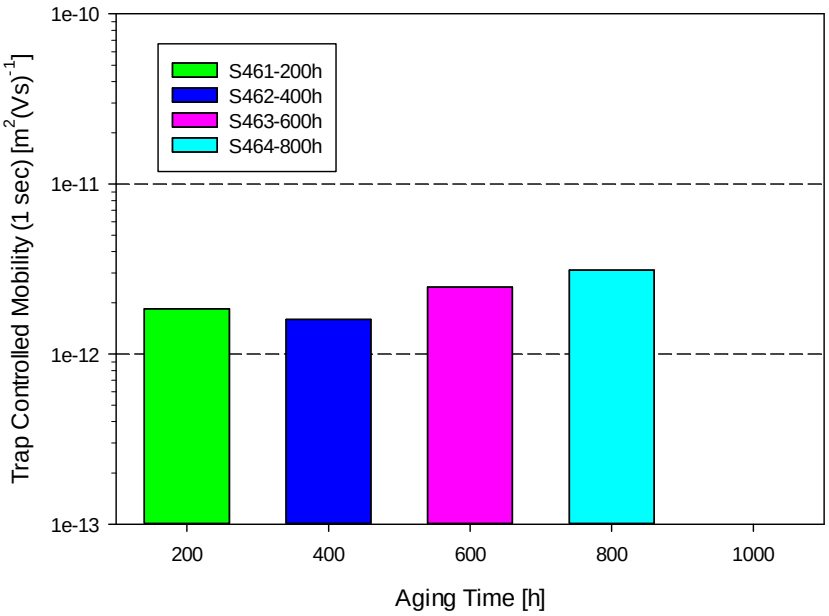

Figure 9.19 Trap Controlled Mobility (1s after the first acquisition of the depolarization curve) vs. Aging Time for specimens S46x (logarithmic scale).

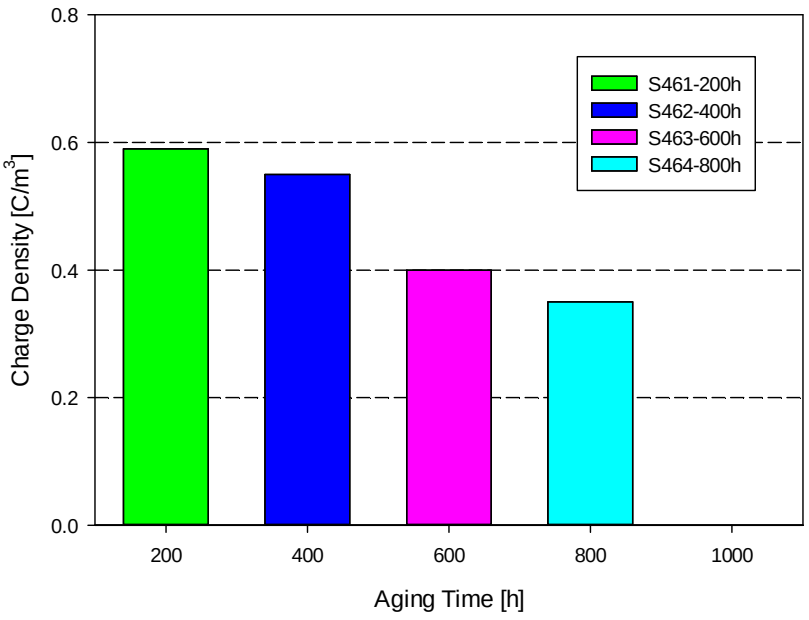

Figure 9.20 Max charge density 10s after the Volt-Off for specimens S46x.

9.1.2 EPDM/EVA cable sheath

In this thesis the EPDM/EVA peeled sheath aged with DR6 (i.e. FS36x aged at 0.85 kGy/h and 85°C, second experiment) has been tested using the PEA system for flat specimens.

Even in this case (as well as reported for EPR flat specimens in §8.1.2), it has to be noted that visual inspection revealed that specimens were very embrittled by aging. Anyway, the electric field of 20 kV/mm was withstood by the specimen for the whole test time.

Charge patterns for different aging times are not presented here for sake of brevity. The amount of space charge accumulated 10 seconds after the Volt-off is shown in Figure 9.21: values decreases with aging time, confirming what we saw with PEA measurements on EPDM/EVA cable insulations. Another confirmation of what we stated in §9.1.1 comes from depolarization curves (Figure 9.22a shows depolarization curves taken 10 seconds after the Volt-off while Fig. 9.22b show curves taken 1 seconds after, thus taking into account also charge injection by electrodes): it is clearly visible how for specimens FS364 and FS365 the charge after 10 seconds (Fig. 9.22b) is nearly 20% of its

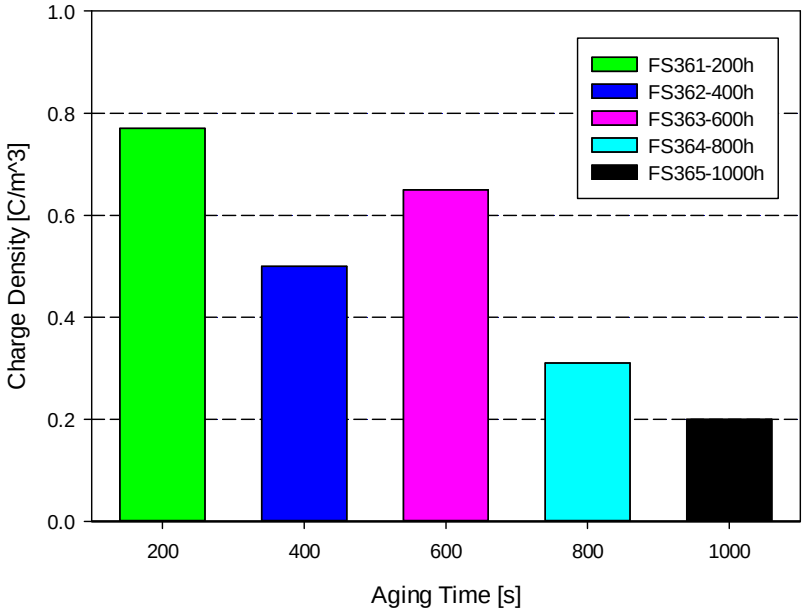

Figure 9.21 Max charge density 10s after the Volt-Off for specimens FS36x.

initial value, so we are unable to plot depolarization curves for these samples 10 seconds after the Volt-off. Then depletion of charge is a very fast phenomenon for these samples. The trend of the curves doesn't allow a good interpolation, mobility has not been derived but it is supposed to increase with aging time.

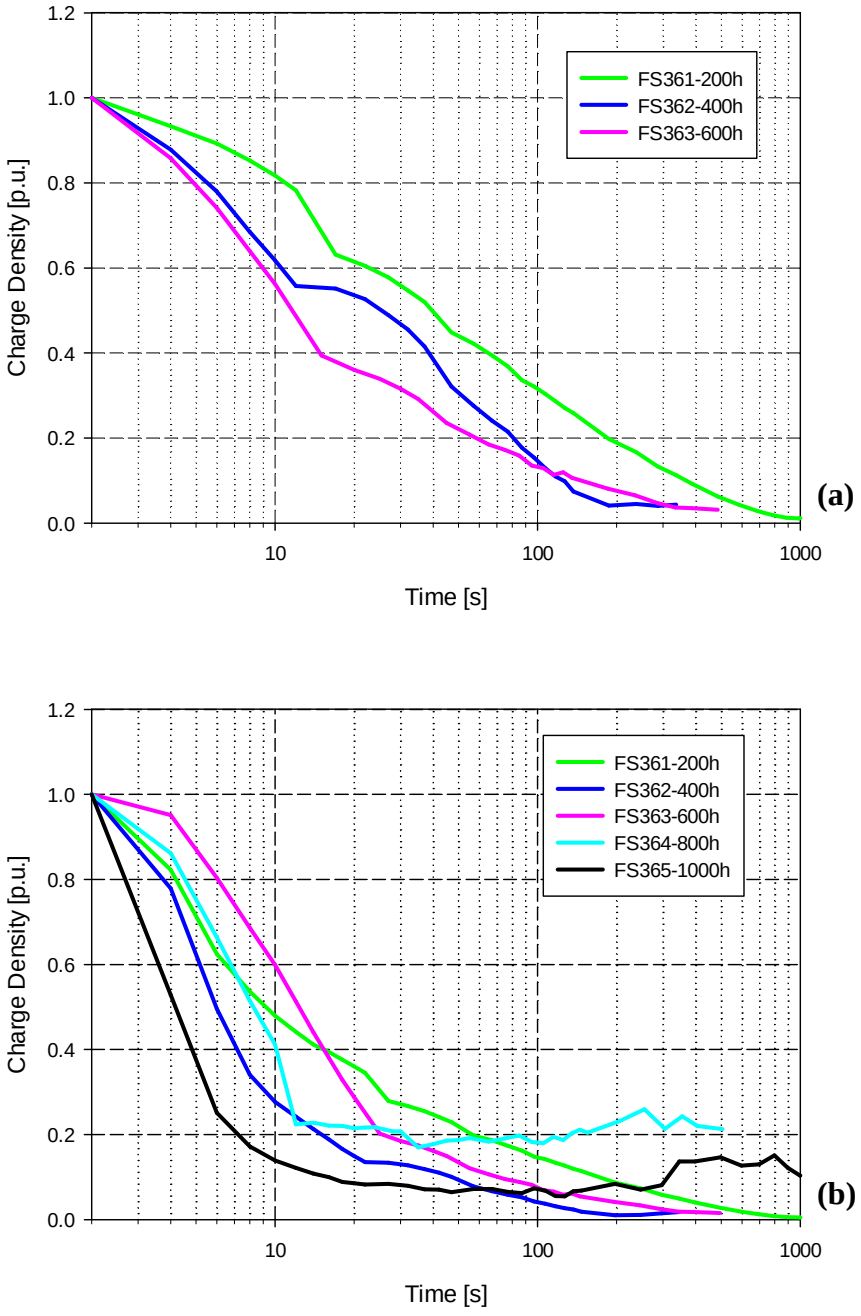

Figure 9.22 Depolarization curve recorded from 10s after the Volt-Off (a) and 1s after the Volt-Off (b) for specimens FS36x.

9.2 Mechanical analysis results

For S3 and S4 cable insulations the tensile properties were measured using a load frame testing machine with extension rate of 50 mm/min and initial gauge length of 40mm. Samples (tubular type) were conditioned at 25°C and 50% relative humidity for 24 hours prior to testing.

In addition to Table 7-2 (regarding S3 "black" new cable) results for unaged sample S4 "blue "are reported in Table 9-1. Young's modulus values have not been reported due to their unreliability as aging marker for EPDM/EVA material, as explained in §7.2.

Table 7-2 Mechanical properties of unaged S3 EPDM/EVA cable.

CABLE S300	Mean value	Err. Abs
EaB (%)	418	32
Young's Modulus (MPa)	17.7	2.0

Table 9-1 Mechanical properties of unaged S4 EPDM/EVA cable.

CABLE S400	Mean value	Err. Abs
EaB (%)	612	32
Young's Modulus (MPa)	16.1	0.4

The behavior of the EaB with aging time is reported in Figure 9.23. As we can see, insulations having different colors show very similar behaviors, both for the higher and for the lower dose rate. However, it has to be noted that the mean value of EaB for S4 unaged specimen is greater than S3, so "blue" cable insulation exhibits better mechanical properties. However, all aged cables present a deterioration of the mechanical properties if compared to the new cable, confirming the effectiveness of aging.

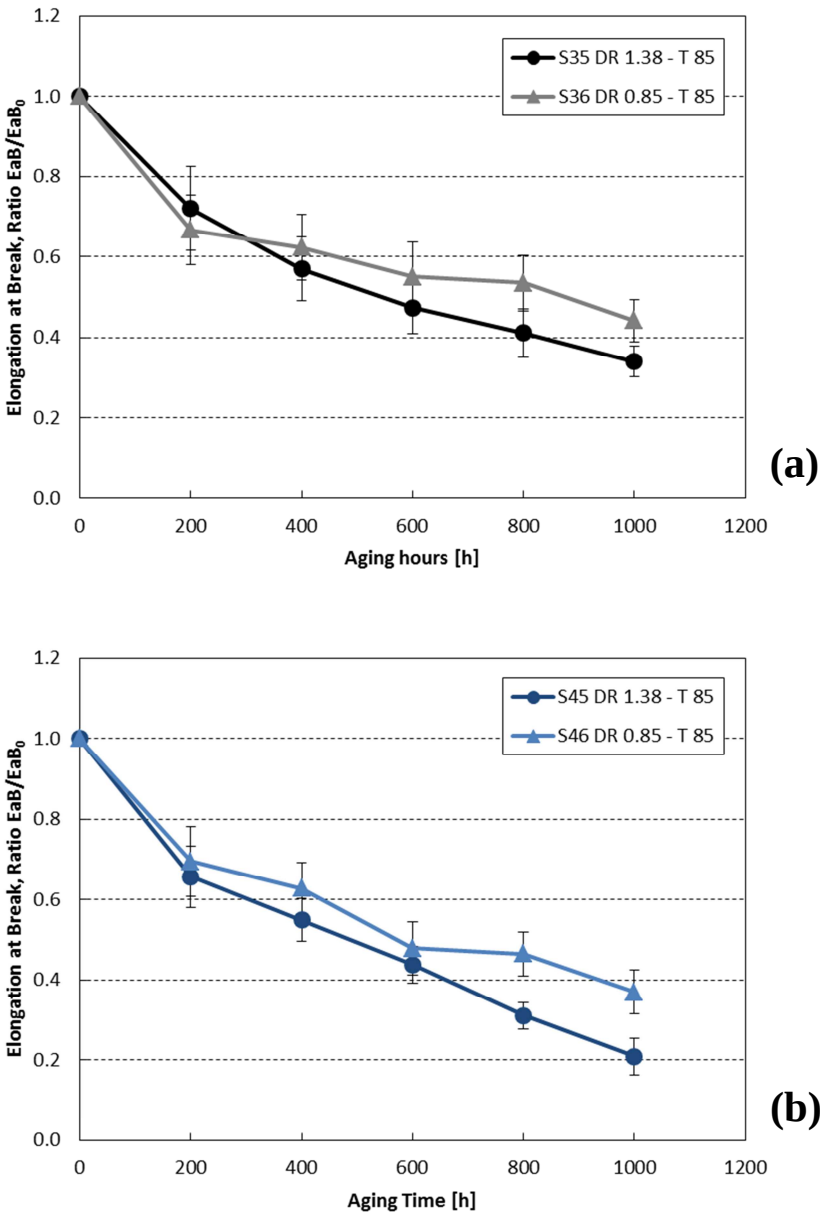

Figure 9.23 Elongation at Break vs. aging time for S3 "black"(a) and S4 "blue"(b) insulations for the two DR-T combinations (DR4 and DR5 at 85°C). Elongation at Break is reported in relative value to that measured on unaged specimens. Error bars are reported.

9.3 Discussion

S3 “black” and S4 “blue” cable insulations as well as FS3 external sheath flat specimen showed a decrease in space charge formation and a consequent increase of mobility with aging time. This phenomenon does not seem affected by the dose rate and has not been observed commonly. Previous studies experimental results often showed that space charge accumulation increases (and charge mobility decreases) with aging time under temperature due to the increased number of deep traps created by insulation degradation [29][30]. In this case, on the contrary, aging seems to create a number of shallow traps which result in trap-controlled mobility increase and smaller charge accumulation. Indeed, the large amount of chemical species, such as flame retardants, inorganic fillers, plasticizers and antioxidant used in nuclear cables manufacture could play a key role in chemical/physical reactions involved during aging. In particular flame retardants may greatly affect space charge formation: chemical analysis performed on these EPDM/EVA cable materials revealed a massive use (even more than 60 percent in weight) of compounds like aluminum hydroxide $Al(OH)_3$, magnesium hydroxide $Mg(OH)_2$, $Al_2O_3x3H_2O$: it is clearly evident their high hygroscopicity. These compounds may breakdown when subjected to high temperatures, removing heat from the substrate, thereby cooling the material. It is possible that radiation could have activated some reaction involved in flame retardants decomposition causing the decrease of trap depth for space charge accumulation with aging time observed. Lastly, mechanical properties, i.e. EaB, confirmed the effectiveness of aging and the structural degradation of the polymeric material.

Conclusions

Condition monitoring techniques are considered an important aspect of managing cable aging. In this thesis both destructive mechanical and not destructive electrical methods have been discussed for two different kinds of cable material (CSPE/EPR and EPDM/EVA insulations).

The large variation of mechanical properties has confirmed the effectiveness of accelerated aging to which the cables have been subjected.

The results presented here have validated EaB as the most affected property by accelerated aging. Degradation of tensile behavior is significant and directly related to dose rate, temperature and aging time, confirming its great reliability as diagnostic aging marker, whatever the type of material. This cannot be said for Young's Modulus whose behavior with aging is material dependent: for EPR cable material it increases gradually with aging while for EPDM/EVA material a clear trend with aging time has not been observed. Moreover, it has to be remembered that such methods are destructive and mainly assessed in laboratory (not in-situ) and this is definitely a disadvantage.

Among electrical measurements, dielectric spectroscopy results have shown a noticeable increase of both real and imaginary part of the permittivity with dose rate, temperature and aging time, as well as of the dissipation factor. Therefore they turn out to be good aging markers. However, we have to distinguish between the two types of material tested.

CSPE/EPR cable insulation has shown a noticeable increase of both real and imaginary part of permittivity with aging time throughout the range of frequencies analyzed. Temperature effect on high dose rates has been investigated: at low frequency, it has been found the so-called "inverse-temperature" effect and this has been confirmed also by polarization/ depolarization current measurements. At high frequencies, on the contrary, there is no evidence of inverse-temperature effects and this is confirmed by mechanical test results. Thus, since a correlation of tensile tests with low-frequencies dielectric response cannot be made, an attempt of correlating

Young's modulus and EaB with permittivity obtained at high frequency has been done leading to a linear correlation with high correlation coefficients.
EPDM/EVA cable material has shown smaller variations of permittivity with aging time compared to EaB. Variations are quite large only for high dose rate. For this material, the higher the temperature the worse the mechanical behavior of the cable. Correlation with mechanical tests has been done between permittivity (both real and imaginary part) obtained at high frequency and elongation at break: even in this case correlation is linear with good correlation coefficients.

Space charge PEA measurements confirmed a good sensitivity spatial resolution across insulation thickness. The interpretation of the results, however, is not easy. The amount of accumulated charge is sometimes low and, although differences depending on the dose rate and temperature can be seen, the trend with aging time is not strong. Similar consideration can be made for trap controlled mobility.

Further investigations are needed clarify better the phenomena involved in insulation aging due to radiation and temperature at different dose rates. Correlations with mechanical results will be used as reference for further studies aiming at finding the best CM methods.
Many hopes are pinned on charge/discharge current measurements which are able to obtain dielectric response for very low frequencies and to confirm what we have observed in this work. Moreover, infrared spectroscopy (IR) results are now in progress in order to investigate if accelerated aging was homogenous and if diffusion limited oxidation was avoided.
In the next steps of the project these results will be compared to those from naturally aged cables in nuclear power plants. Field tests could verify the presence of cable degradation and, thanks to the comparison with these laboratory tests, assess the degree of degradation and estimate the residual lifetime.

Abbreviations

AMP	ageing management program
ASTM	American Society for Testing of Materials
BR	butyl rubber
BWR	boiling water reactor
CI	condition indicator
CM	condition monitoring
CSPE	chlorosulphonated polyethylene (Hypalon)
C/D	charge/discharge current method
DBE	design basis event (e.g. LOCA or MSLB) sometimes referred to as DBA
DED	dose to equivalent damage
DLO	diffusion limited oxidation
DMA	dynamic mechanical analysis
DS	dielectric spectroscopy
DSC	differential scanning calorimeter
EaB	elongation at break
EPR/EPDM	ethylene propylene based materials
EPRI	Electric Power Research Institute
EQ	environmental qualification
ETFE	ethylene trifluoroethylene
ESR	electron spin resonance
EVA	ethylene vinyl acetate
FR	fire retardant
FTIR	Fourier transform infrared spectroscopy
HELB	high energy line break
I&C	instrumentation and control
IEC	International Electrotechnical Commission
IEEE	Institute of Electric and Electronic Engineers
IM	indenter modulus
ISO	International Standards Organisation
LCM	life cycle management
LDPE	low density polyethylene
LOCA	loss of coolant accident
LR	license renewal
LV	low voltage
MSLB	main steam link break
NPP	nuclear power plant
OIT/OITP	oxidation induction time/temperature
PD	partial discharge
PE	polyethylene
PEA	pulsed electroacoustic method
PEEK	polyether ether ketone
XLPE	cross-linked polyethylene

References

[1] T. De Schoutheete, ADVANCE Project – State of the art of ageing mechanisms of materials in low voltage cables, Review article, Laborelec (2011)

[2] D. Corbin, Etude de l'oxydation et de la tenue d'élastomères irradiés : conséquences sur l'intégrité des câbles électriques lors d'une situation accidentelle d'un réacteur à eau pressurisée, Université de Caen/Basse-Normandie (2005)

[3] R.L. Sindelar, Nuclear Radiation, Savannah River National Laboratory (2009)

[4] T. J. Lewis, Charge transport in polymers, IEEE Proc. Electr. Insul. And Diel. Ph., pp. 533-561, 1976

[5] L.A. Dissado, J.C. Fothergill, Electrical degradation and breakdown in polymers, Peter Peregrinus Ltd., 1992

[6] J P. Runt, J.J. Fitzgerald, Dielectric Spectroscopy of Polymeric Materials, American Chemical Society, 1997

[7] G.C. Montanari, D. Fabiani, "Evaluation of dc insulation performance based on space charge measurements and accelerated life tests", IEEE Trans. on Dielectrics and Electrical Insulation, Vol. 7, n. 3, pp. 322-328, June 2000.

[8] G.C. Montanari, "Extraction of information from space charge measurements and correlation with insulation ageing ", CSC 2001.

[9] A. Cavallini, D. Fabiani, G. Mazzanti and G.C. Montanari, "A general model for life estimation of cables under dc stress with voltage-polarity inversions accounting for space-charge effects ", ISEIM 2001

[10] T. Maeno, T. Futami, H. Kusibe, T. Takada and C. M. Cooke, "Measurement of spatial charge distribution in thick dielectrics using the pulsed electroacoustic method", IEEE Trans. on Dielectrics and Electrical Insulation, Vol. 23, n. 3, pp. 433-439, June 1988.

[11] D.W. Clegg & A.A. Collyer, “Irradiation Effects on Polymers”, *Elsevier Applied Science*, London 1991.

[12] L. Simoni, “Fundamentals of Endurance of Electrical Insulating Materials”, *CLUEB*, Bologna 1983.

[13] K. T. Gillen, R. L. Clough, “Predictive Aging Results for Cable Materials in Nuclear Power Plants”, Sandia National Laboratories, Albuquerque, November 1990.

[14] K. T. Gillen, R. L. Clough, “Time-temperature-dose rate superposition : a methodology for extrapolating accelerated radiation aging data to low dose rate conditions”, Sandia National Laboratories, Albuquerque, 1988.

[15] G. V. Gordon, C. Shen, M. T. Shaw, “A Method for Correlating Natural Aging Data and its Application to Insulation Aging in Nuclear Power Plants”, *CEIDP, Annual Report*, 1992.

[16] J. M. Braun, “Condition Assessment of Unshielded Aged Power and Control Cables by Electrical Techniques”, *IEEE Electrical Insulation Magazine, Vol. 8, No.5,* Sept./Oct. 1992.

[17] H. M. Banford, R. A. Fouracre, S. J. MacGregor, M. Judd, “An Investigation of Radiation-Induced Aging in Cable Insulation via Loss Measurements at High and Low Frequencies”, *Conference Record of the IEEE ISEI*, Arlington, 1998.

[18] M. Ekelund, P.F. Fantoni, U.W. Gedde, “Thermal ageing assessment of EPDM-chlorosulfonated polyethylene insulated cables using line resonance analysis (LIRA)”, *Polymer Testing 30, pp. 86-93*, 2011

[19] M. Kahle, R. Prozel and R. Ruhlicke, “Investigation of Ins Properties by Means of Very Low Frequencies”, International Symposium on High Voltage Engineering, 21

[20] M. Tavlet, S. Ilie, “Behaviour of organic materials in radiation environment”, Radiation and Its Effects on Components and Systems, RADECS 99 (1999) 210-215.

[21] T. Segughi, K. Tamura, T. Ohshima, A. Shimada, H. Kudoh , “Degradation mechanisms of cable insulation materials during radiation-thermal ageing in radiation environment”, Radiation physics and chemistry 80 (2011) 268-273, Elsevier.

[22] Radiation damage to organic materials in nuclear reactors and radiation environments, IAEA-TECDOC-551, Vienna (1990)

[23] Assessment and management of ageing of major nuclear power plant components important to safety: In-containment instrumentation and control cables, INTERNATIONAL ATOMIC ENERGY AGENCY, IAEA-TECDOC-1188, Vienna (2000)

[24] L. Sanche, IEEE Trans. Dielectr. Electr. Insul. 4, 507 (1997)

[25] G. Mazzanti, G. C. Montanari, F. Palmieri, and J. Alison, Apparent trap-controlled mobility evaluation in insulating polymers through depolarization characteristics derived by space charge measurements, J. Appl. Phys. 94, 5997 (2003)

[26] G. Mazzanti, G.C. Montanari, J. M. Alison, "A space-charge based method for the estimation of apparent mobility and trap depth as markers for insulation degradation. Theoretical basis and experimental validation", IEEE Trans. on Diel. El. Insul., Vol. 10, pp. 187-197, 2003.

[27] A. K. Jonscher, Dielectric relaxations in solids, Chelsea Dielectric Press, London, UK, 1983.

[28] G. Williams, D.K. Thomas, "Phenomenological and molecular theories of dielectric and electrical relaxation of materials", Department of Chemistry, University of Wales Swansea, UK

[29] G. Mazzanti, G.C. Montanari, F. Palmieri, "Quantities extracted from space-charge measurements as markers for insulation aging," IEEE Transactions on Dielectrics and Electrical Insulation, Vol. 10, no. 2, pp. 198- 203, 2003.

[30] G.C. Montanari, D. Fabiani, M. Melloni, F. Palmieri, "Diagnostic markers for ac power cable insulation aging based on space charge measurements", IEEE ISEI, pp. 464-467, Boston, USA, 2002.

[31] J. M. Alison, "The pulsed electro-acoustic method for the measurement of the dynamic space charge profile within insulators", in Space Charge in Solid Dielectrics, 93-121, The Dielectric Society, UK, 1998.

[32] K. Gillen, R. A. Assink & R Bernstein, "Nuclear energy pant optimisation (NEPO): final report on ageing and condition monitoring of low-voltage cable materials", SAND2005-7331, Sandia Laboratories, USA (2005) [available as EPRI 1011873]

[33] The final report of the project of "Assessment of cable ageing for nuclear power plants", Japan Nuclear Energy Safety Organisation, JNES-SS-0903, July 2009

[34] IEC 61244-2, Determination of long term radiation ageing in polymers, part 2: Procedures for predicting ageing at low dose rates

[35] K.T. Gillen, J. Wise & G. M. Malone, Explanation of enhanced mechanical degradation rate for radiation-aged polyolefins as the ageing temperature is decreased, 208th ACS National Meeting, Washington DC, USA, p.1491; Polymer Preprints 35 (1994), 911–912.

[36] M. Celina, K.T. Gillen, J. Wise & R.L. Clough, 1998, Anomalous ageing phenomena in a crosslinked polyolefin cable insulation, Rad.Phys & Chem. - in press,

[37] S. G. Burnay, & J. Dawson, Reverse temperature effect during radiation ageing of XLPE cable insulation, Proceedings of International Conference on “Ageing studies and life extension of materials”, 12-14 July 1999, Oxford, UK, Kluwer/Plenum Press

[38] IEC 216-1,1990: Guide for the Determination of Thermal Endurance Properties of Electrical Insulating Materials. [several parts]

[39] K. Spang, Methodology for artificial ageing of electrical components in nuclear power plants. Results of experimental studies, SKI Technical Report 93:39, 1993, Swedish Nuclear Power Inspectorate, Stockholm, Sweden

[40] K. Spang, Ageing of electrical components in nuclear power plants: relationships between mechanical and chemical degradation after artificial ageing and dielectric behaviour during LOCA, SKI Technical Report 97:40, 1997, Swedish Nuclear Power Inspectorate, Stockholm, Sweden

[41] Y. Morita, T. Yagi, T. Seguchi, “Temperature and dose monitoring of surroundings and accelerated ageing of electrical cables in nuclear power plants” Twenty-sixth Water Reactor Safety Information Meeting (Proc. of the U. S. Nuclear Regulatory Commission, Bethesda, 1998)

[42] K. Pielichowski, J. Njuguna: Thermal Degradation of Polymeric Materials, Rapra Technology, 2005

[43] SANDIA REPORT (SAND 2010-7266) "Review of Nuclear Power Plant Safety Cable Aging Studies with Recommendations for Improved Approaches and for Future Work", Kenneth T. Gillen and Robert Bernstein (November 2010)